WARSAW UNIVERSITY OF TECHNOLOGY

Faculty of Electronics and Information Technology

Ph.D THESIS

Grzegorz Kasprowicz, M.Sc.

Determination of Beam Intensity and Position in a Particle Accelerator

Supervisor

Professor Ryszard Romaniuk, Ph.D, D.Sc.

Warsaw, 2010

POLITECHNIKA WARSZAWSKA

Wydział Elektroniki i Technik Informacyjnych

ROZPRAWA DOKTORSKA

mgr.inż. Grzegorz Kasprowicz

Metody i algorytmy pomiaru natężenia i położenia wiązki w akceleratorze cząstek

Promotor

Prof. Dr hab. Ryszard Romaniuk,

Warsaw, 2010

To Jeroen, Uli, CERN

The system was developed in the context of the EU Framework Program 2006 (FP6), as part of the FAIR DIRAC secondary beams project.

Abstract

The Proton Synchrotron* accelerator (PS), installed at CERN † , although commissioned in 1959, still plays a central role in the production of beams for the Antiproton Decelerator, Super Proton Synchrotron, various experimental areas and for the Large Hadron Collider (LHC)‡.

The PS produces beams of different types of particles, mainly protons, but also various species of ions. Almost all these particle beams pass through the PS. The quality of the beams delivered to the LHC has a direct impact on the effective luminosity, and therefore the performance of the instrumentation of the PS is of great importance. The old trajectory and orbit measurement system of the PS dated back to 1988 and no longer fulfilled present day requirements. It used 40 beam position monitors (BPMs) and an analogue signal processing chain to acquire the trajectory of one single particle bunch out of many, over two consecutive turns at a maximum rate of once every 5ms. The BPMs were in good condition, however the electronics was aging and increasingly difficult to maintain.

The new system digitizes the BPM signals using 125MS/s, 12 bit ADCs. The digitized sample stream are processed on the fly into individual bunch positions, using numerical algorithms implemented on fast programmable

*synchrotron - a particular type of cyclic particle accelerator in which the magnetic field (to turn the particles so they circulate) and the electric field (to accelerate the particles) are carefully synchronized with the traveling particle beam

†European Organization for Nuclear Research, Geneva

‡Large Hadron Collider (CERN)

logic (FPGA). The system stores the positions of all bunches in the machine over the full duration of an acceleration cycle, requiring large memories. Post processing can be applied to the data in order to extract orbits (averaged positions over many turns), mean radial position, phase space images or machine tune data. Client orbit display programs running on operator consoles can then concurrently request measurements from any interesting part of the cycle.

The ADCs digitize their input signals at a constant rate, whereas the revolution frequency of the particle bunches varies along the acceleration cycle. The increase of this frequency depends on the increase of particle velocity, and varies over more than an octave for heavy ions. The system is able to keep track of each individual bunch from injection all through to ejection using tracking and synchronization algorithm.

In essence, its task is to decide which of the ADC samples belong to each particle bunch. The new system uses an entirely numerical synchronization algorithm, implemented in the FPGA and running at the ADC sampling rate. Synchronization is made more complicated by the possibility of the PS machine to change the harmonic number of the machine (the number of possible bunches in the machine) during acceleration. These operations are used, among others, to split bunches into two or three bunchlets, in order to better match the beam to the properties of the subsequent accelerators. The system must be able to keep track of the beam throughout.

Development of effective algorithm which enables precise trajectory tracking of individual particle bunches with sub-mm precision was aim of this thesis. Moreover, using similar, already verified algorithm, new

absolute beam intensity measurement system was developed as well. The scope included hardware development, algorithm adaptation and tests.

Streszczenie

Mieszczący się w CERN Synchrotron Protonowy (PS), pomimo iż oddany do użytku w 1959r, wciąż odgrywa główną rolę w produkcji wiązek dla spowalniacza antyprotonów (Antiproton Decelerator), Super-synchrotronu Protonowego (SPS), wielu różnych obszarów eksperymentalnych na potrzeby Wielkiego Zderzacza hadronowego (LHC).

PS produkuje wiązki różnych typów cząstek, głównie protonów, ale także wielu odmian jonów. Prawie wszystkie te wiązki przechodzą przez PS. Jakość wiązek dostarczanych do LHC ma bezpośredni wpływ na efektywną intensywność, a zatem wydajność i jakość systemów pomiarowych PS-a ma istotne znaczenie. Dawny system pomiaru trajektorii i orbity cząstek w akceleratorze PS powstał w 1988r i nie spełniał już wymagań dnia obecnego. Używał on 40 elektrostatycznych monitorów pozycji wiązki (BPM) oraz analogowego systemu przetwarzania sygnałów w celu akwizycji trajektorii jednego z wielu pakietów (bunch, zgęstka) cząstek. Akwizycja odbywała sie w zakresie 2 następujących po sobie okrążeń w maksymalnym zakresie raz na 5ms. Jest to wartość obecnie niewystarczająca. BPMy są wciąż w dobrym stanie technicznym, lecz elektronika przetwarzająca sygnał starzała się i była coraz trudniejsza w utrzymaniu.

Nowy system pomiarowy kwantuje sygnały BPM używając 125MS/s, 12 bit przetworników ADC. Przekonwertowany na postać cyfrową strumień jest przetwarzany w czasie rzeczywistym na indywidualne pozy-

cje pakietów cząstek, przy użyciu numerycznego algorytmu zaimplementowanego w logice programowalnej (FPGA). System gromadzi pozycję i intensywność wszystkich pakietów wiązek w akceleratorze pokrywając zakres całego cyklu przyspieszania, używając do tego odpowiednio dużych ilości pamięci. Przetwarzanie offline może być zastosowane do tych danych w celu ekstrakcji średniej pozycji z wielu okrążeń, średniej pozycji wzdłuż akceleratora, intensywności wiązki, obrazów przestrzenno-fazowych lub dostrojenia maszyny (tune). Programy wizualizujące orbitę wiązki na stacjach roboczych mogą jednocześnie odwoływać się pomiarów z jakiejkolwiek interesującej części cyklu, co nie był możliwe w starym systemie.

Przetworniki dokonują kwantyzacji sygnału wejściowego ze stałą częstotliwością, podczas gdy częstotliwość obiegu pakietów cząstek zmienia się wraz z cyklem przyśpieszającym. Wzrost częstotliwości zależy od wzrostu prędkości cząstek i zmienia się ponad 1 oktawę dla ciężkich jonów. System jest w stanie śledzić tor każdego pojedynczego pakietu cząstek począwszy od wstrzyknięcia aż do jego ekstrakcji.

W istocie, zadaniem algorytmu jest klasyfikacja która próbka z ADC należy do którego pakietu wiązki. Nowy system używa całkowicie numerycznego algorytmu synchronizującego, zaimplementowanego w FPGA i pracującego na częstotliwości próbkowania ADC. Osiągniecie synchronizacji jest trudniejsze poprzez fakt, iż PS ma możliwość zmiany numeru harmonicznego maszyny (liczby możliwych pakietów w akceleratorze) podczas przyspieszania. Te operacje są używane, jako jedne spośród wielu, aby podzielić pakiety na dwa lub trzy czesci, w celu lepszego dopasowania wiązki do kolejnych akceleratorów. System jest w stanie śledzić trajektorię

wiązki na wskroś całego akceleratora.

Opracowanie efektywnego algorytmu który umożliwia bezbłędne śledzenie toru każdego pakietu cząstek z precyzja ułamka mm było celem niniejszej pracy. Oprócz tego, używając sprawdzonego w przypadku pomiaru trajektorii algorytmu, opracowano od podstaw system pomiaru bezwzględnej wartości intensywności wiązki. Zakres prac obejmuje konstrukcję sprzętową, adaptację algorytmu oraz testy.

Contents

Chapter 1

Introduction

1.1 The meaning of fundamental research

Some areas of scientific research, such as particle physics and cosmology, seem remote from everyday life and unlikely to bring immediate practical applications. From the beginning of the civilization, people wanted to know more about the Universe. The aim was knowledge, practical applications came later.

This research may take us far away from the conditions of everyday life, but because it continually pushes boundaries of thinking and of technology it is a springboard for many new developments.

Fundamental science is where new ideas and methods begin that later become commonplace - from the electric light, which originated in 19-century curiosity about electricity, to the World Wide Web, invented at CERN to allow international teams of particle physicists to communicate more easily. No work of applied research on the candle would have brought us the electric light; no R&D on the telephone would have brought about the Web. Science needs the space for curiosity and imagination.[20]

An example of practical application of scientific discovery are accelerators. Their first constructors didn't even dream how widely their invention will be used in everyday life. An ordinary CRT television set is a simple form of accelerator.

The fundamental research laboratories like CERN (European Organization for Nuclear Research), Brookhaven National Laboratory, DESY , , SLAC use complicated very expensive accelerator complexes to study matter properties and structure. The accel-

erator consists of several building blocks like: particle source, deflecting and focusing, accelerating structures, particle detectors ,diagnostic and measurement devices. The last ones are the scope of this thesis which was realized at CERN.

1.2 Research area of the thesis - the accelerator science and applications

Beams of high-energy particles are useful for both fundamental and applied research in science. For the most basic research into the dynamics and structure of matter, space, and time, physicists seek the simplest kinds of interactions at the highest possible energies[11].

High-energy physics needs very sophisticated instruments using technologies that often exceed the available industrial know-how. Many of these technologies have made our daily lives more efficient, practical and comfortable.

Although the accelerators were primarily invented for research in physics, thousands of them are being used in another areas of science, as well as in industry and medicine. Most of them are small linear accelerators used in factories to polymerase the plastics, waste utilization and food sterilization, in hospitals for miscellaneous therapies. In medicine there are also cyclotrons used mainly to produce isotopes, which are used in hospitals for PET (Positron emission tomography).

Industry is a prime user of accelerators. The market, consisting of constructing accelerators, with their associated peripheral equipment, is estimated to be more than US $1000 million a year. Unlike the disciplines described above, industrial use of accelerators has not led to the development of new types of accelerators or even to the many developments of accelerator technology that have allowed advances. However, industrial use has stimulated nontrivial, ever-more sophisticated forms of conventional machines and, of course, has depended on the community of accelerator scientists that are needed to make this happen. The primary use of accelerators is in the semiconductor industry, where doping silicon with boron or phosphorus (forming p or n junctions) requires a range of energies from 100 keV to 1.5MeV. In the high energy portion of this range, linacs and tandem Van de Graffs are used; electrostatic machines cover the mid-energy range (tens of keV) and the low energy range (hundreds of eV). These machines are commercially pro-

duced and sold primarily in the US, Europe, Malaysia, Singapore, China, South Korea, Japan, and Taiwan.

There are many other industrial applications of accelerators. In common use is enhancement of the brilliance of gemstones. A special application is in the treatment of sugar being transformed into ethanol (such as in Brazil). Accelerators make x-rays for studying the continued integrity of airplane wings, bridges, and other structures. For this application, at least one company has designed a compact, portable betatron, which it is producing and selling commercially.

The medical advantage of high energy x-rays as an external beam for cancer therapy has driven the development of x-ray-producing linacs. At first these were rather large spatially fixed machines operating below the energy for producing radioactivity, i.e. below about 10MeV. Now there are compact linacs (still operating below 10MeV), which are reliable and mounted directly on a gantry, so they may be rotated about the patient. The protons or ions with sub-millimeter precision deposit most of their energy at specified depth under the tissue, minimally affecting neighboring regions. A great many of these machines are in hospitals around the world. One large commercial supplier is manufacturing two or three such machines every day.

The special constructions called Free Electron Laser are used in medicine and industry as a very intense, precision and coherent light sources. Current FELs cover wavelengths from nanometer to visible and are nudging into the ultraviolet. New facilities designed specifically to produce x rays are under construction The x ray versions enable extremely precise imaging in medical applications.

Synchrotron radiation sources, such as the ones provided by ESRF in Grenoble, have mushroomed all over the world, and their narrow beams and turnable radiation are put to a huge variety of applications. In research, X ray diffraction techniques reveal the structure of proteins and enzymes and the crystal lattices of exciting new materials such as high temperature superconductors.

Beams of high-energy particles are useful for both fundamental and applied research in the sciences. For the most basic inquiries into the dynamics and structure of matter, space, and time, physicists seek the simplest kinds of interactions at the highest possible energies. These typically entail particle energies of many GeV, and the interactions of

the simplest kinds of particles: leptons (e.g. electrons and positrons) and quarks for the matter, or photons and gluons for the field quanta. Since isolated quarks are experimentally unavailable due to color confinement, the simplest available experiments involve the interactions of, first, leptons with each other, and second, of leptons with nucleons, which are composed of quarks and gluons. To study the collisions of quarks with each other, scientists resort to collisions of nucleons, which at high energy may be usefully considered as essentially 2-body interactions of the quarks and gluons of which they are composed. Thus elementary particle physicists tend to use machines creating beams of electrons, positrons, protons, and anti-protons, interacting with each other or with the simplest nuclei (eg, hydrogen or deuterium) at the highest possible energies, generally hundreds of GeV or more.

The highest, TeV range energy accelerators are built mainly for fundamental research application. The largest of such complex exists at CERN (fig. 1.1). It consists of two injectors - proton and ion linear accelerators followed by a set of synchrotron machines. The accelerated particles then end up in the collision points being collided together. The collision products are then analyzed by the detectors *.

The central accelerator at CERN is Proton Synchrotron (PS) through which all particle beams pass. The PS, although commissioned in 1959, still plays a central role in the production of beams for the Antiproton Decelerator , LEIR † Super Proton Synchrotron, various experimental areas and for the Large Hadron Collider (LHC) . The PS accelerates beams of protons and lead ions.

The PS is equipped with a beam position measurement system. However, the existing measurement system has several limitations and does not meet the requirements for the beam quality for the LHC. The construction of a novel PS position and intensity measurement system based on existing sensors is the scope of this thesis.

The position (trajectory) measurement system was initially developed in cooperation with GSI ‡, Germany. The European Union supported the project in the framework of

*particle detector - also known as a radiation detector, is a device used to detect, track, and identify high-energy particles. Modern detectors are also used as calorimeters to measure the energy of the detected radiation. They may also be used to measure other attributes such as momentum, spin, charge etc. of the particles.

†LEIR - Low Energy Ion Ring is a central part of the injector chain to supply lead ions to the LHC. It will transform long pulses from Linac 3 into short and dense bunches for the LHC.

‡ The GSI Helmholtz Centre for Heavy Ion Research GmbH in the Arheilgen suburb of Darmstadt,

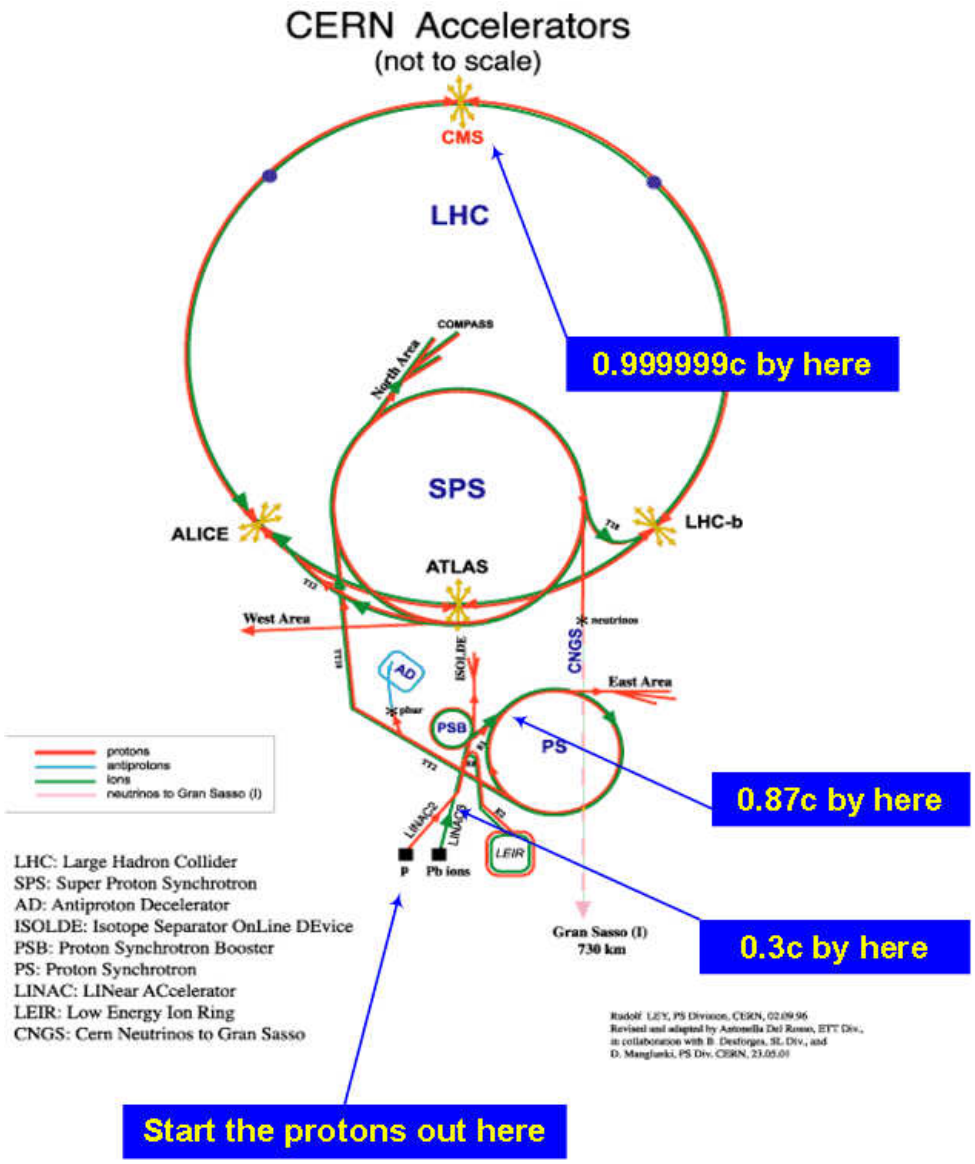

Figure 1.1: CERN accelerators complex [5]

the FAIR project (DIRAC secondary beams).

Germany is a federally and state co-funded heavy ion research center. The laboratory performs basic and applied research in physics and related natural science disciplines. Main fields of study include plasma physics, atomic physics, nuclear structure and reactions research, biophysics and medical research. The chief tool is the heavy ion accelerator facility consisting of UNILAC, the Universal Linear Accelerator (energy of 2 - 11.4 MeV per nucleon), SIS 18, the heavy-ion synchrotron (1 - 2 GeV/u) and ESR, the experimental storage ring (0.5 - 1 GeV/u) and FRS. The UNILAC was commissioned in 1975, the SIS 18 and the ESR were added in 1990 boosting the ion acceleration from 10% of light speed to 90% [14]

Chapter 2

Particle accelerators

2.1 Definitions, basic concepts

A particle accelerator is a device that uses electric fields to propel electrically-charged particles to high energies and to confine them. An ordinary CRT television set is a simple form of accelerator. There are two basic types: linear accelerators and circular accelerators.

In a linear accelerator (linac), particles are accelerated in a straight line with a target of interest at the end. Linacs are very widely used - every cathode ray tube contains one. They are also used to provide an initial low-energy kick to particles before they are injected into circular accelerators. The longest linac in the world is the Stanford Linear Accelerator, SLAC, which is 3 km (2 miles) long. SLAC is an electron-positron collider.

Linear high-energy accelerators use a linear array of drift tubes(or standing wave cavities *) to which an alternating high-energy field is applied (fig. 2.1) . As the particles approach a tube they are accelerated towards it by an opposite polarity charge applied to the tube. As they pass through a hole in the tube, the polarity is switched so that the tube now repels them and they are now accelerated by it towards the next tube. Normally a stream of "bunches" of particles are accelerated, so a carefully controlled AC voltage is applied to each tube to continuously repeat this process for each bunch.

*A cavity resonator is a hollow conductor blocked at both ends and along which an electromagnetic wave can be supported. It can be viewed as a waveguide short-circuited at both ends. In case of electron linacs, so called disc loaded structures are used.

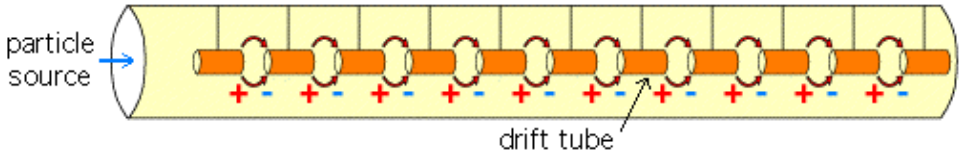

Figure 2.1: Drift Tube Linac (DTL) principle [39]

As the particles approach the speed of light the switching rate of the electric fields becomes so high that they operate at microwave frequencies, and so RF cavity resonators are used in higher energy machines instead of tubes. The linear accelerators are very often used as injectors to the circular ones.

In the circular accelerator, particles are circled back to a cavity until they reach sufficient energy. The particle track is typically bent into a circle using electromagnets. The advantage of circular accelerators over linear accelerators (linacs) is that the ring topology allows continuous acceleration, as the particle can transit indefinitely. Another advantage is that a circular accelerator is relatively smaller than a linear accelerator of comparable power (i.e. a linac would have to be extremely long to have the equivalent power of a circular accelerator or use higher accelerating gradients).

Depending on the energy and the particle being accelerated, circular accelerators suffer a disadvantage in that the particles emit synchrotron radiation. When any charged particle is accelerated, it emits electromagnetic radiation. As a particle traveling in a circle is always accelerating towards the center of the circle, it continuously radiates towards the tangent of the circle. This radiation is called synchrotron light and depends highly on the mass of the accelerating particle. For this reason, many high energy electron accelerators are linacs. Certain accelerators (synchrotrons) are however built specially for producing synchrotron light (i.e. X-rays Free Electron Lasers).

Since the special theory of relativity requires that matter always travels slower than the speed of light in a vacuum, in high-energy accelerators, as the energy increases the particle speed approaches the speed of light as a limit, never quite attained. Therefore particle physicists do not generally think in terms of speed, but rather in terms of a particle's energy or momentum, usually measured in electron volts (eV). An important principle for circular accelerators, and particle beams in general, is that the curvature of the particle trajectory is proportional to the particle charge and to the magnetic field,

but inversely proportional to the (typically relativistic) momentum.

To reach still higher energies, with relativistic mass approaching or exceeding the rest mass of the particles (for protons, billions of electron volts GeV), it is necessary to use a synchrotron. This is an accelerator in which the particles are accelerated in a ring of constant radius. An immediate advantage over cyclotrons [†] is that the magnetic field need only be present over the actual region of the particle orbits, which is very much narrower than the diameter of the ring. (The largest cyclotron built in the US had a 184 in dia magnet pole, whereas the diameter of the LEP [‡] and LHC built at CERN is nearly 10 km. The aperture of the beam of the latter is of the order of centimeters.)

However, since the particle momentum increases during acceleration, it is necessary to turn up the magnetic field B in proportion to maintain constant curvature of the orbit. In consequence synchrotrons cannot accelerate particles continuously, as cyclotrons can, but must operate cyclically, supplying particles in bunches, which are delivered to a target or an external beam in beam"spill" typically every few seconds.

Since highest energy synchrotrons (like SPS [§] & LHC) do most of their work on particles that are already traveling at nearly the speed of light c, the time to complete one orbit of the ring is nearly constant, as is the frequency of the RF cavity resonators used to drive the acceleration.

Note also a further point about modern synchrotrons: because the beam aperture is small and the magnetic field does not cover the entire area of the particle orbit as it does for a cyclotron, several necessary functions can be separated. Instead of one huge magnet, one has a line of hundreds of bending magnets, enclosing vacuum connecting pipes. The focusing of the beam is handled independently by specialized quadrupole magnets, while the acceleration itself is accomplished in separate RF sections, rather similar to short linear accelerators. Also, there is no necessity that cyclic machines be circular, but rather the beam pipe may have straight sections between magnets where beams may collide, be cooled, measured etc.

[†]Cyclotrons accelerate charged particles using a high-frequency, alternating voltage. A perpendicular magnetic field causes the particles to spiral almost in a circle so that they re-encounter the accelerating voltage many times [13]

[‡]Large Electron Positron Collider (CERN)

[§] SPS - The Super Proton Synchrotron is the second largest machine in CERNs accelerator complex. Measuring nearly 7 km in circumference, it takes particles from the PS and accelerates them to provide beams for the LHC, the COMPASS experiment and the CNGS project[21]

More complex modern synchrotrons such as the Tevatron [¶], LEP, and LHC (fig.2.2) deliver the particle bunches into storage rings of magnets with constant B, where they can continue to orbit for long periods for experimentation or further acceleration. The highest-energy machines such as the Tevatron and LHC are actually accelerator complexes, with a cascade of specialized elements in series, including linear accelerators for initial beam creation, one or more low energy synchrotrons to reach intermediate energy, storage rings where beams can be accumulated or "cooled" (reducing the magnet aperture required and permitting tighter focusing), and a last large ring for final acceleration and experimentation.

Figure 2.2: Large Hadron Collider [20]

The output of a particle accelerator can generally be directed towards multiple lines of experiments, one at a given time, by means of a deviating electromagnet. This makes it possible to operate multiple experiments without needing to move things around or shutting down the entire accelerator beam. Except for synchrotron radiation sources, the purpose of an accelerator is to generate high-energy particles for interaction with matter.

[¶]Tevatron is a circular particle accelerator at the Fermi National Accelerator Laboratory in Batavia, Illinois and is the second highest energy particle collider in the world after the (LHC)

This is usually a fixed target, such as the phosphor coating on the back of the screen in the case of a television tube; a piece of uranium in an accelerator designed as a neutron source; or a tungsten target for an X-ray generator. In a linac, the target is simply fitted to the end of the accelerator. The particle track in a cyclotron is a spiral outwards from the centre of the circular machine, so the accelerated particles emerge from a fixed point as for a linear accelerator.

For synchrotrons, the situation is more complex. Particles are accelerated to the desired energy. Then, a fast acting dipole magnet is used to switch the particles out of the circular synchrotron tube and towards the target.

A variation commonly used for particle physics research is a collider, also called a storage ring collider. An example is LHC. Two circular synchrotrons are built in close proximity - usually on top of each other and using the same magnets (which are then of more complicated design to accommodate both beam tubes). Bunches of particles travel in opposite directions around the two accelerators and collide at intersections between them. This can increase the energy significantly. Whereas in a fixed-target experiment the energy available to produce new particles is proportional to the square root of the beam energy, in a collider the available energy is linear[11].

2.2 Particle beam parameters and their importance to the experiments

In order to precisely describe collider accelerator properties, several parameters are used. The most important is luminosity. The luminosity is the number of charges (or particles) per unit area per unit time times the opacity of the target, usually expressed in either the cgs units $cm^{-1}s^{-1}$ or $b^{-1}s^{-1}$ (2.1). The integrated luminosity is the integral of the luminosity with respect to time. The luminosity determines the number of collisions seen by experiment and characterize the performance of an accelerator[15]. For an intersecting storage ring collider:

$$L = f \cdot n \frac{N_1 \cdot N_2}{A} \tag{2.1}$$

Where: f is the revolution frequency, n is the number of bunches in one beam in the storage ring, N_i is the number of particles in each bunch, A is the cross section of the beam.

The equation above shows that measurement of the number of charges (beam intensity) in each bunch has a very high importance to precise estimation of main accelerator parameters. The beam intensity measurement is a scope of this thesis. One type of the sensor which is used to measure beam intensity is called Beam Current Transformer (BCT) described precisely in chapter 2.3.

Another important parameter of accelerator is the beam emittance. It is the extent occupied by the particles of the beam in space and momentum phase space as it travels. A low emittance particle beam is a beam where the particles are confined to a small distance and have nearly the same momentum. A beam transport system will only allow particles that are close to its design momentum, and of course they have to fit through the beam pipe and magnets that make up the system. In a colliding beam accelerator, keeping the emittance small means that the likelihood of particle interactions will be greater resulting in higher luminosity.

Emittance has units of length, but is usually referred to as "length/angle", for example, "millimeter/milli-radians". It can be measured in all three spatial dimensions. The dimension parallel to the motion of the particle is called the longitudinal emittance. The other two dimensions are referred to as the transverse emittances[12].

The acceptance is the maximum emittance that a beam transport system or analyzing system is able to transmit.

The emittance is somehow related to the betatron oscillations. The effects to the magnets and the transport system caused by high emittance and betatron oscillations could be similar.

Betatron oscillation are the oscillations of particles about their equilibrium orbits. At the accelerator, usually the bending and magnets are connected in series and have the same current. A particle with the correct energy and alignment will circulate around the ring on the central orbit of the Bending Magnets and will pass through the center of each one. Protons with the wrong alignment (position or angle) are forced to oscillate about this central orbit by the focusing forces produced by the magnets.The number of

oscillations performed by a proton in one turn of the synchrotron is called the Q-value or betatron tune. Thus a proton will not retrace the same path through the synchrotron ring on subsequent turns unless the Q-values are integers. Integer Q-values must be avoided or the small errors in the magnetic fields will make the Betatron Oscillations grow rapidly and the particles will hit the vacuum chamber.

One of the applications of the beam orbit measurements system, which is the scope of this thesis, is to detect betatron oscillations and measurement of the beam position in order to kepp the emittance minimal. The position of the beam is measured using special devices called Beam Position Monitors (BPM) or Position Pickup Unit (PU) . They are described more precisely in chapter 2.3.

The measurement of precise position of the beam in the vacuum pipe is critical. A set of BPMs forms part of a feedback system responsible for beam steering which ensures that beam is placed optimally in the pipe. Large displacement of the beam, specially at very high energies, may destroy the vacuum system.

The beam in accelerators is usually packetized. These small packets of particles are called bunches. There can be one or more bunches circulating in the accelerator. The place in the accelerator foreseen and allowed for bunch to exist is called bucket. The bucket can be filled with bunch or not. The fig 2.3 presents relationship between bunch and bucket. The bucket area is called longitudinal acceptance, while the bunch area is longitudinal beam emittance.

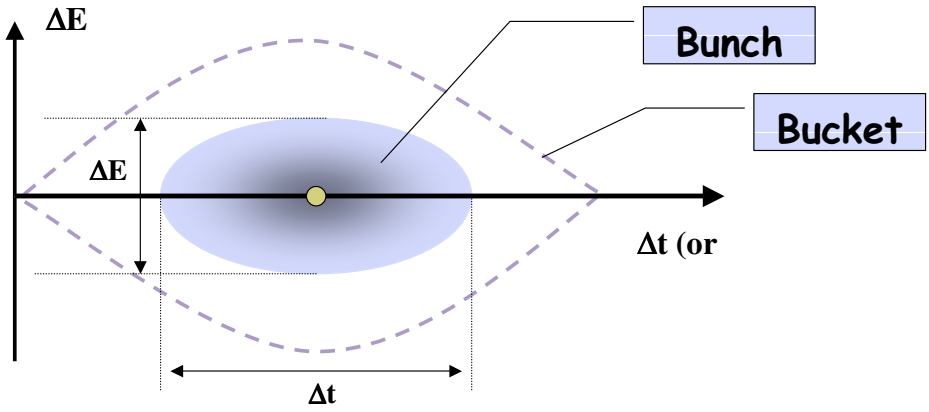

Figure 2.3: Bunches and buckets [7]

The number of RF buckets (stationary or accelerating) in accelerator is called harmonic

number. High harmonic number is used for high energy machines which require high voltage for acceleration and short bunches are more suitable to achieve high luminosity. Low harmonic number is used for low energy machines to reduce space-charge effects, enable high revolution frequency range, large acceptance.

Space-charge effect is caused by interaction between the particles caused by Coulomb repulsion and magnetic attraction. In a real beam (or bunch), with many particles, each particle will suffer the repulsive forces from the others since they have the same electrical charge. This intrinsic effect is however important only at low energies and vanishes for ultra-relativistic beams where magnetic forces compensate electric forces. The space charge forces affect the longitudinal dynamics (as well as the transverse one). Since request for higher and higher intensities, at low and medium energies, is driving the next future the space charge phenomenon needs particular attention.

The beam intensity measurement system can detect Synchrotron oscillation as well. Synchrotron oscillation are small periodic variations of the particles about the equilibrium values of phase and energy. Synchrotron tune Q_z is a number of synchrotron oscillations per machine revolution.

The measurement of the parameters described above and many others is a scope of this thesis. However, due to the complexity of the beam manipulation in the PS, implementation of the measurement system was not trivial.

2.3 Instrumentation for intensity and position measurement

Among a rich set of different apparatus used to monitor beam parameters, the position and intensity is analyzed mainly using three of them: Beam Current transformer, Wall Current Monitor, electrostatic and electromagnetic position pickup. First three of them are the source of measurement signal for algorithms and hardware described in this thesis.

The BCT consists of toroidal core mounted over a vacuum chamber of the transfer line into which an insulating gap is inserted. The pulsed beam current I_B and its image (wall) current form a single turn primary winding, inducing a magnetic flux F in the core and a voltage V_S across the secondary winding. The wall current is conduced outside the core,

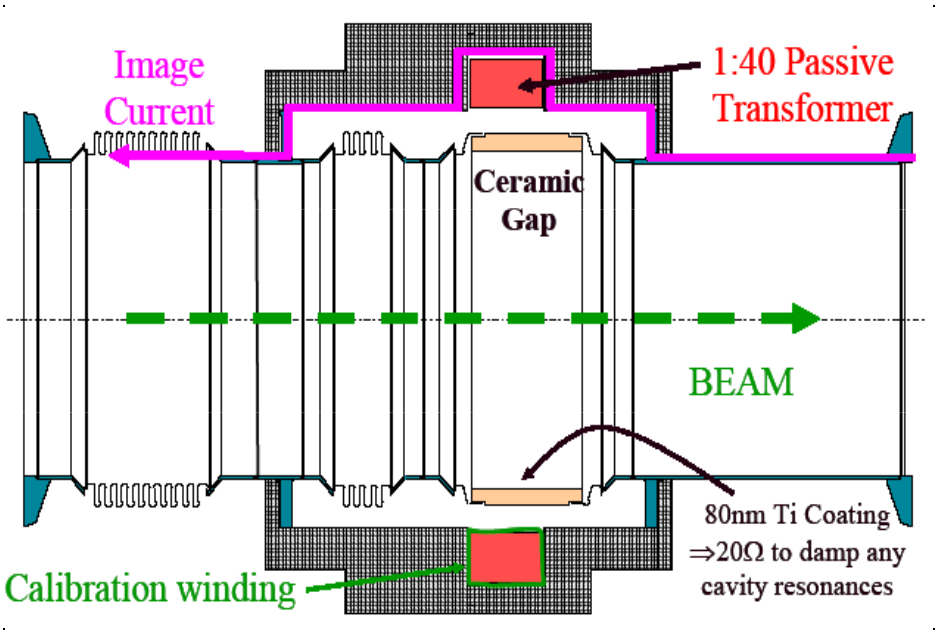

Figure 2.4: Beam Current Transformer (BCT) construction [34]

the beam inside. The high permeability core ensures tight magnetic coupling ($k = 1$) between the primary and secondary windings, where (2.2): $I_P = I_B$ and L_0 represents the single turn inductance, L_S the total secondary inductance, and N the number of secondary turns [2].

$$V_S = -k \cdot N \cdot \Phi = -k \cdot N \cdot L_0 \cdot I_P = \frac{-k \cdot L_S \cdot I_P}{N} \tag{2.2}$$

In practice, analysis of BCT is more complex. The equation above does not include parasitic components. Fig. 2.5 presents simplified equivalent electrical diagram of a BCT.

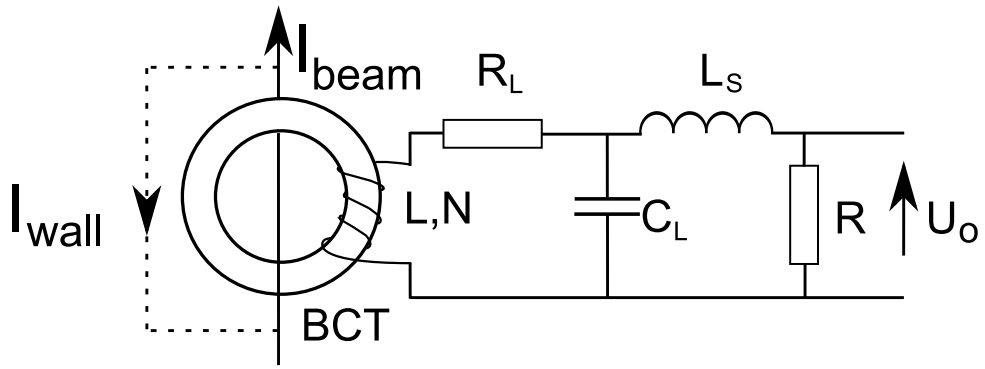

Figure 2.5: Simplified equivalent schematic of a beam current transformer [2]

where: L - the transformer inductance, N - the number of secondary windings, R - the

load resistance of the system, R_L - the resistance of the secondary winding, C_L - the stray capacitance between the components (cables, core, windings), L_S - the stray inductance between components.

The transfer function $f(s)$ with s as the Laplace variable

$$U_a(s) \rightarrow f(s) \cdot I_{beam}(s) \tag{2.3}$$

and the corresponding solution

$$U_a(s) \rightarrow F(s) \cdot I_{beam}(s) \tag{2.4}$$

become rather complex. On the other hand, the most important features of a passive transformer, such as the sensitivity $S = U_a/I_{beam}$ and droop time constant τ can be determined neglecting the small values of L_s and C_L. Thus, in a first approximation, the transfer function simplifies to:

$$U_a(s) = -I_{beam}(s) \cdot \frac{sRL}{N} \cdot \frac{1}{sL + R_L + R} \tag{2.5}$$

Assuming $I_{beam} = i_p/s$, which idealizes the beam current to a step function, the solution of 2.5 is

$$U_a(t) = i_p \frac{R}{N} e^{[-\frac{R+R_L}{L}t]} \tag{2.6}$$

The sensitivity is

$$S = \frac{U_a(0)}{i_p} = \frac{R}{N} \tag{2.7}$$

And the droop time constant τ of the exponential droop is given by

$$\tau = \frac{L}{L + R_L} \approx \frac{L}{R} \tag{2.8}$$

Considering (2.6), a conflict arises with respect to the selection of N since the output voltage is proportional to $1/N$ and therefore requires a low N. On the other hand, the BCT inductance is proportional to N^2 and should be high enough for a low cut-off frequency value which very often needs to be as low as possible to limit the signal droop (baseline effect) [41].

The upper cut-off frequency is limited by the stray capacitances and inductances and mainly by the core material losses. In case of commercially available BCTs (i.e. Bergoz), the core technology is kept secret. To achieve better bandwidth, in some BCT constructions, 2 or more cores working in tandem are used with an appropriate filter circuit attached to them. This idea allows independent shaping of low and high frequency response of the BCT [23].

The BCT measures the current formed by N particles of charge state q per unit of time t or unit of length l and velocity $\beta = v/c$.

$$I_{beam} = \frac{qeN}{t} = \frac{qen}{l} \cdot \beta c \tag{2.9}$$

with e being the elementary charge.

The BCTs can be calibrated by passing a precisely generated current pulse through the special calibration winding which simulates the current generated by the particle beam [24].

The BCTs are widely used in particle accelerators and also in many industrial installations to measure high currents where resistive shunts cannot be used. One of the problems with BCT is its limited upper cut-off frequency, usually it does not exceed a few hundreds of MHz. There are applications, where higher frequencies are required. In such cases, Wall Current Monitors are often used.

In Linear accelerators, where bunch frequency is in order of hundred MHz, BCTs are often replaced by Wall Current Monitor (WCM) . Unlike the transformers, the WCM does not have a secondary winding - the output voltage is proportional to the wall image current induced by the relativistic particle bunch. The vacuum tube has a gap of few mm over which a low inductance resistor is installed on which the voltage proportional to the beam current is developed. To improve the high frequency response, around the beam pipe a ferrite core is installed which isolates the high frequencies active part of the tube from the rest of the circuit. A screening box filled with magnetic material, usually ferrite, is electrically connected on the two sides to force the image current to pass through the resistor (fig.2.6).The dependence of the observed signal on the beam radial position is minimised by collecting and summing the image current in 8 places around the gap circumference using 8 feedthroughs and an external combiner [40].

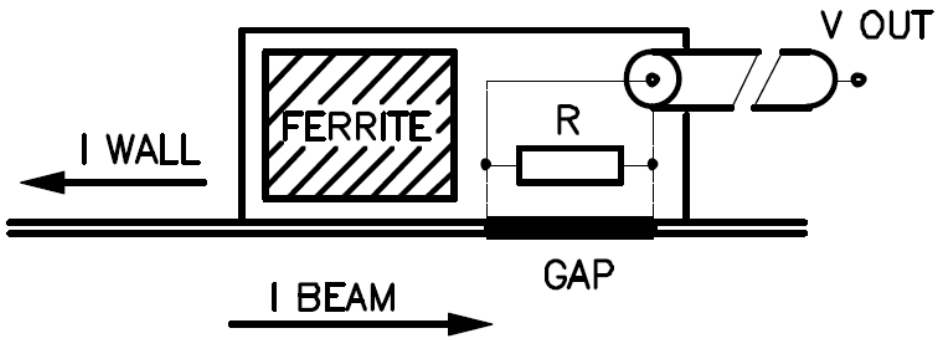

Figure 2.6: The Wall Current Monitor principle [40] [42]

The WCM equivalent circuit is presented in fig.2.7 The high frequency cut-off depends on C_gap and on R.The low frequency cut-off depends on R, already mentioned, and on L the inductance of the screening box.

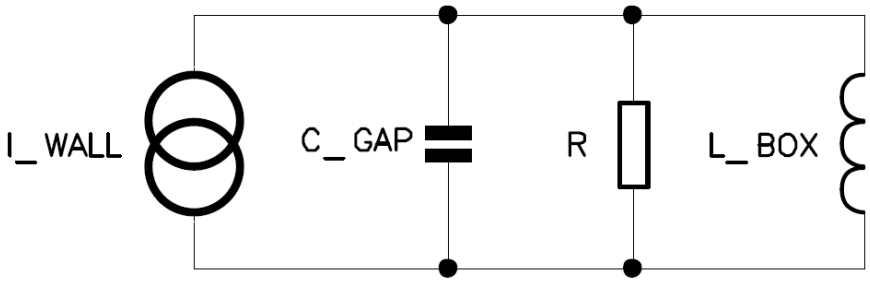

Figure 2.7: The Wall Current Monitor equivalent schematic [40]

From the equivalent circuit of the wall current monitor (2.7) we can get:

$$\begin{cases} i_r \cdot R = L\frac{di}{dt} \\ i_w = i_R + i_L (when t = 0, i_L = 0) \end{cases} \tag{2.10}$$

Where i_w - Wall current, R- Sampling resistor, L - inductance between sampling point and ground.

The example mechanical construcion of the WCM is presented in fig.2.8

The WCM due to the lack of the calibration winding cannot be calibrated on-line, during measurement. The only way of calibrating WCM is laboratory test bench or cross-calibration with the BCT.

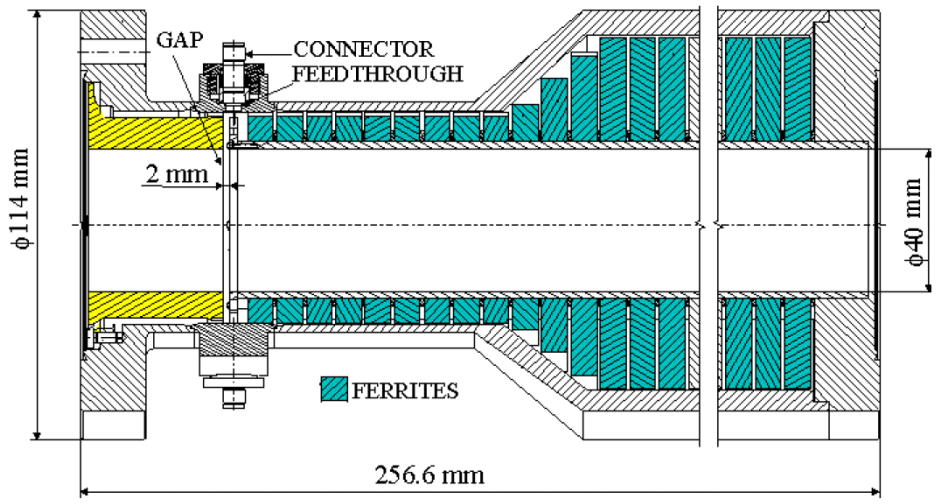

Figure 2.8: The Wall Current Monitor cross section [40]

The most common method of monitoring the position of a charged-particle beam is to couple to the electromagnetic field of the beam. The beam is a current, and it is therefore accompanied by both a magnetic and an electric field. In the limit of very high beam energy, the fields are pure transverse electric and magnetic. If the beam is displaced from the center of a hollow conducting enclosure, the magnetic and electric fields are modified accordingly. Precision knowledge of the magnetic and electric field distribution allow accurate beam position determination. Pickup electrodes, in general cannot sense DC electric or magnetic fields. The signal is induced by variable component of the beam signal, usually beam current modulation [1]. We first consider the response of electrostatic (capacitive) pickups. Two opposing electrodes of length l and azimuthal width ϕ are placed in a pipe of radius b. If the current of a centered pencil beam is $I_b(t)$ and the beam has velocity $V_b = \beta_b \cdot c$, the charge density of the beam is

$$q_b(t) = \frac{I_b(t)}{\beta_b c} \tag{2.11}$$

Equal magnitude, opposite-polarity charge appears on the inside surface of the electrodes. For an electrode of length l and azimuthal width ϕ this charge is

$$Q_s(t) = \frac{-\phi l}{2\pi} \frac{I_b(t)}{\beta_b c} \tag{2.12}$$

Assuming there is a capacitance between the electrode and ground given by C, the signal current flowing onto the capacitance is equal to the time derivative of the charge

on the electrode:

$$i_s(t) = \frac{-dQ_s(t)}{dt} = \frac{\phi l}{2\pi}\frac{1}{\beta_b c}\frac{dI_b(t)}{dt} \tag{2.13}$$

There is no DC component of charge on the capacitance. The capacitance of the electrode integrates this current, producing an output voltage

$$V_c(t) = \frac{\phi l}{2\pi C}\frac{I_b(t)}{\beta_b c} - V_0 \tag{2.14}$$

where V_0 is constant of integration. This integrating capacitance may be directly between the electrode and the beam pipe, or it can be added externally. The equivalent circuit is shown in fig 2.9

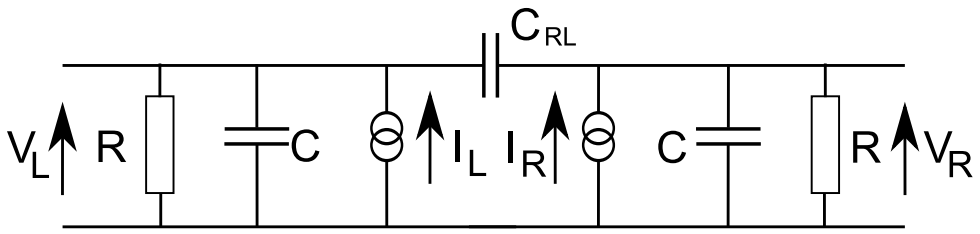

Figure 2.9: Simplified equivalent schematic of an electrostatic pickup [1]

The C_{RL} represent inter-electrode capacitance. R is a protection resistor used to prevent excessive charge build-up in the circuit which could cause dangerous discharges. The resistor also causes the average voltage to be close to zero. Usually in electrostatic pickups circuits the shunt capacitance is the dominant conductance path at the important frequencies, and the voltage across it then represents the beam bunch temporal profile [1]. The electrostatic pickups require high impedance electronics to cope with. This means that long transmission cable cannot be used. The amplifier must be placed as close as possible to the pickup. Often radiation-hard amplifiers are installed just at the terminals of the pickup. The pickup is a high pass filter with cut-off frequency $f_{cut} = 1/(2\pi RC)$ The low cut-off frequency depends on the R value. For high impedance amplifiers with R equeal to hundreds of kOhm, the frequency is in order of tens of kHz, while for $R = 50Ohm$ this gives frequency in order of a few tens of MHz. A pickup has to match the interesting frequency range, which is given by the accelerating frequency and the bunch length. In a proton synchrotron typical values of the accelerating frequency are in the range from 1-10

MHz, while for LINACs and electron synchrotrons typically 100 MHz to 3 GHz are used [32]. The pickup type used in CERN PS is a "shoe box" one, which could be used due to relatively long bunches (In case of LHC, button pickups are used). A box-like device is used normally, to get a precise linear dependence with respect to the beam displacement (fig 2.10).

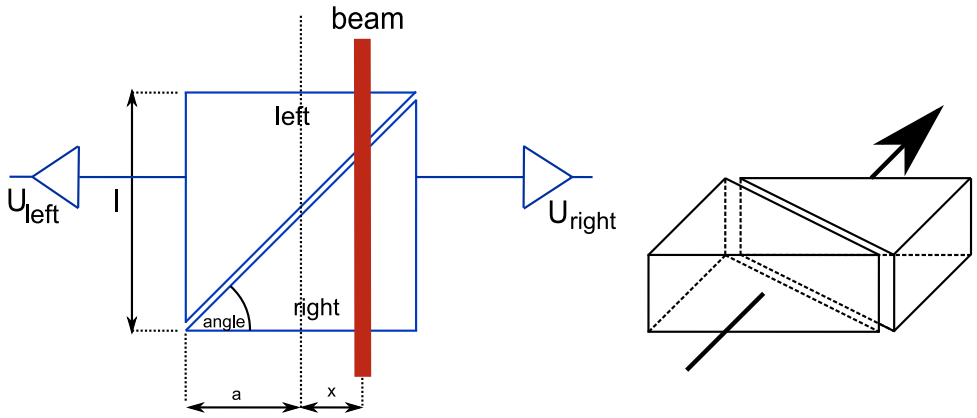

Figure 2.10: The position measurement and an example of electrode arrangement [32]

In case of the shoe-box pickups the influenced signal is proportional to the actual plate length at the beam center position. For a given beam displacement x the electrode's image voltage Uim is proportional to the length l of the beam projected on the electrode surface as shown for the horizontal direction in fig. 2.10, left. For triangle electrodes with half-aperture a one can write:

$$l_{right} = (a+x)\cdot tan\alpha, \quad l_{right} = (a-x)\cdot tan\alpha \quad \mapsto \quad x = a\cdot \frac{l_{right} - l_{left}}{l_{right} + l_{left}} \tag{2.15}$$

The position reading is linear and can be expressed by the image voltages as

$$x = a\cdot \frac{l_{right} - l_{left}}{l_{right} + l_{left}} \equiv \frac{1}{S_x}\cdot \frac{\Delta U_x}{\Sigma U_x} \quad \mapsto \quad S_x = \frac{1}{a} \tag{2.16}$$

which shows that the position sensitivity for this ideal case is simply given by the inverse of the half-aperture. Compared to other types of pickups, the position sensitivity is constant for nearly the full range of displacements, i.e. nearly no corrections due to non-linearities have to be applied [32]. To get the position of the beam, the signals from the electrodes have to be compared. For this comparison, the signal shape (differentiation

or proportional behavior) is of minor importance. For the position resolution, the signal-to-noise ratio is important. Beside the stray fields from the rf cavities, the broadband amplifier noise, as well as the electronic noise of the following devices contribute. Therefore a minimum bunch current is needed for a reliable position measurement. In many applications the sum and difference voltages are analogously generated by a 180° hybrid or a differential transformer. Because they are pure passive devices, they can be mounted quite close to the BPM plates even in case of high radiation. The difference signal, which is normally lower by at least a factor of 10, can be amplified by a higher amount than the sum signal to exploit the full ADC range [32].

2.4 The challenges of beam parameters determination in PS

The PS is a circular accelerator with a diameter of 200m. It accelerates protons injected from Linac 2 or lead ions from Linac 3. The vacuum chamber is of elliptical cross-section, 140mm wide and 70mm high. One hundred combined function magnets focus and bend the beam to guide it around the machine. One hundred straight sections in between the magnets contain auxiliary equipment, such as vacuum pumps, injection and ejection kickers, correction magnets and various kinds of instrumentation.

The machine sections are numbered from 0 to 99. A straight section carries the same number as the bending magnet following it (Fig 2.11). Forty pickups (PU) of the trajectory measurement system are installed in straight sections with numbers ending in 0, 3, 5 and 7. Each PU is identified by the straight section in which it resides, even though it is actually installed in the pumping manifold of the preceding bending magnet. The PU locations are shown as dots on fig 2.13. Each pickup measures the horizontal and the vertical positions simultaneously.

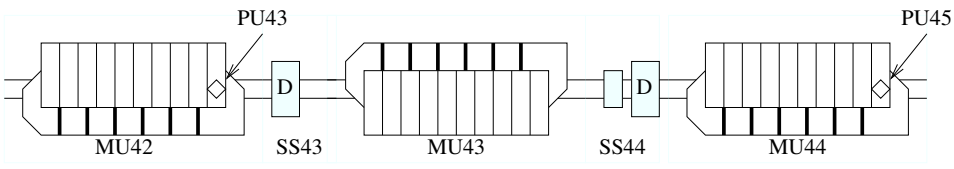

Figure 2.11: Some magnets and straight sections in the PS ring

The accelerator operates in basic periods, each lasting 1.2s. From one to sixteen bunches of particles are injected near the beginning of the cycle at energy of 1.4 GeV. Radio frequency cavities accelerate the beam. Some acceleration operations may span up to three basic periods. After acceleration to up to 27 GeV, the beam is ejected towards an experiment in a target area, or to the next accelerator in the chain. During acceleration, bunches of particles can be split into several bunchlets, or moved closer together or farther apart using what is colloquially known as 'RF gymnastics'. During the accelerating process, the revolution frequency Frev of the beam varies from 437 to 477 kHz for p+. The revolution frequency for ions can be much lower: down to 177 kHz at injection [10].

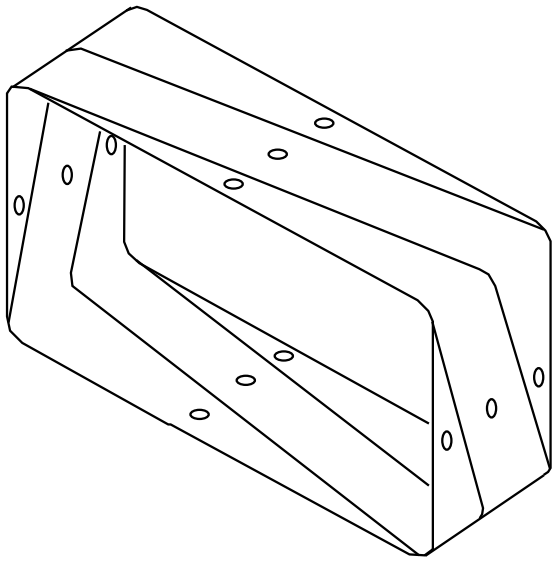

Figure 2.12: The PU

The Pickups (PU) are composed of four electrode plates fixed inside the vacuum chamber (Fig 2.12). The PU aperture is 166 x 80 mm. The passage of a particle bunch induces image charges on the plates, resulting in a measurable voltage pulse. The signals are combined into a sum signal (Σ) and horizontal and vertical difference signals (Δx, Δy) using passive hybrid transformers which are radiation resistant. The signal levels are raised to about 1 Vp by variable-gain amplifiers installed near to each PU in special area under the accelerator where radiation is reduced. The signal bandwidth is from 150 kHz up to 35 MHz. The upper cut off frequency has an Bessel roll-off characteristic

to preserve the pulse shape. A computer in the Central Building (CB) (see Fig 2.13) remotely controls the amplifier gain, based on the expected beam intensity. All CERN computers use a common technical network but critical timings and instrumentation data are distributed by a separate timing network.

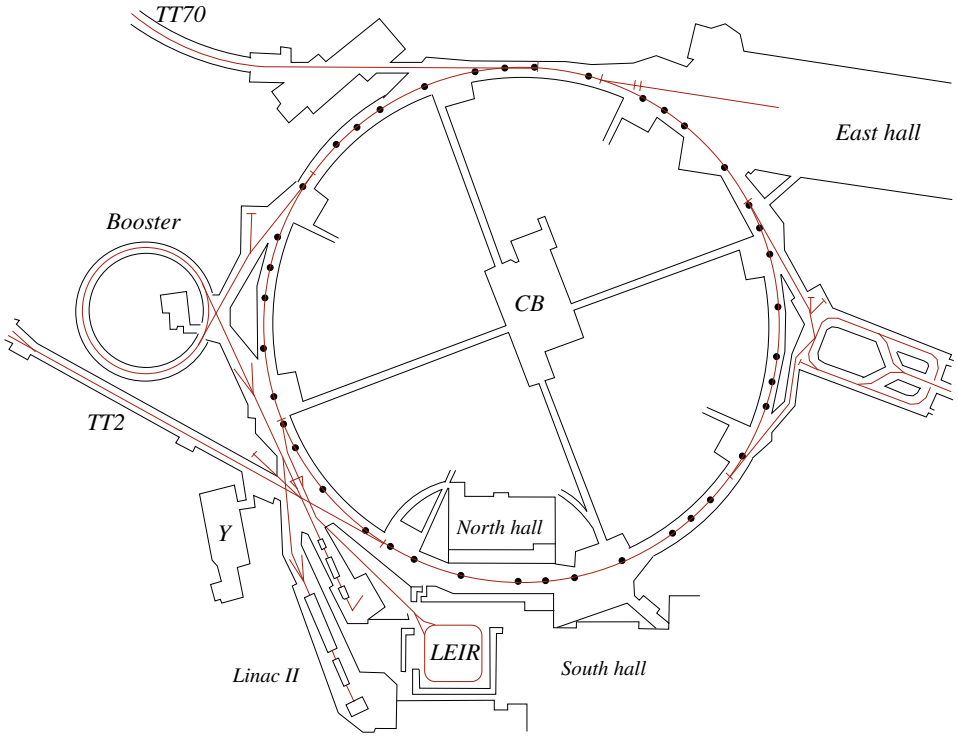

Figure 2.13: The PS complex and placement of the PU

The plot shows an example of a typical beam signal (Fig 2.14). The beam is an example of a p+ beam that will be common in the LHC era. Four bunches are injected into the PS and kept circulating there at constant energy for 1 s while the injectors (Linac II + Booster) prepare a second batch of two bunches. The picture shows the instant this second batch arrives in the PS. The new bunches can be identified by their large negative displacement during the first turn, near sample 700.

A normal acceleration cycle takes 1.2 s(Fig 2.15). During the first 100 ms, there is time for calibration and other setup operations. At 100 ms after the start, the magnetic field is ramped up to its injection value. One or more bunches of particles are injected at C170 (C is 1 ms timing signal). A timing signal marks the exact instant of injection. This signal is synchronized to 8Frev, even if the machine harmonic (the number of accelerating RF periods per turn) is different from eight.

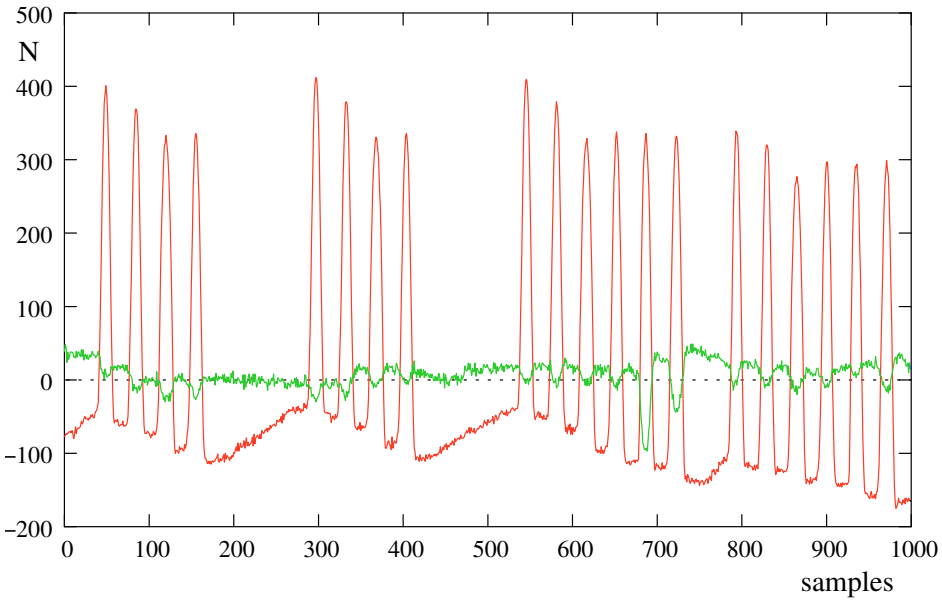

Figure 2.14: The Σ and Δ signals of the LHC beam

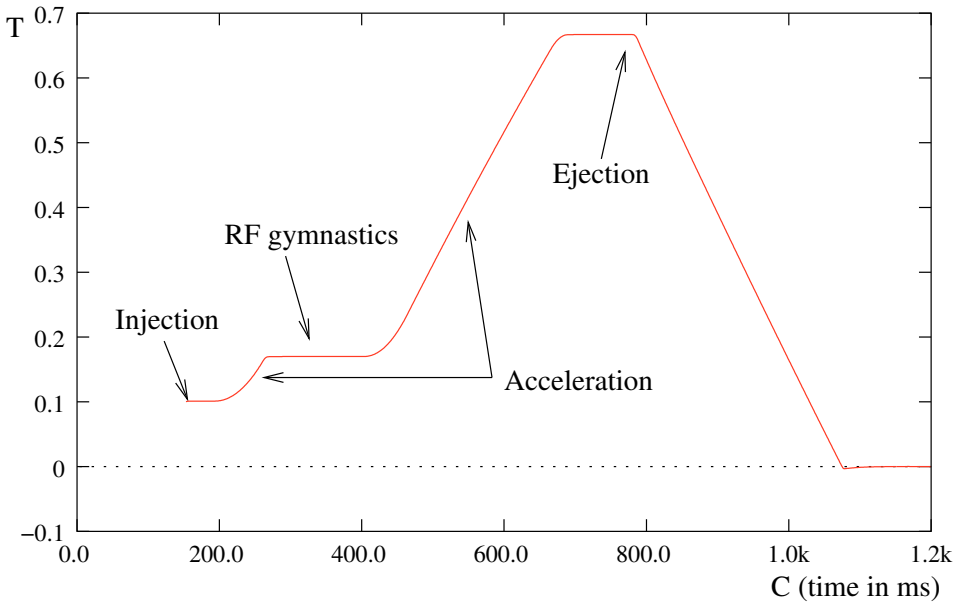

Figure 2.15: Example magnetic cycles in PS (SFTPRO)

The RF gymnastics (i.e. bunch splitting, harmonic number change) may take place at any time. They are always done on a constant-energy (and therefore constant B-field) plateau, and take from 20 to 300ms, depending on the specific operation. At the beam's final energy, some operations may debunch the beam, or raise its harmonic number beyond the bandwidth of the PUs, in which case further trajectory measurements become

impossible. If the beam remains bunched up until ejection, the EJ signal marks the last possible instant at which a valid trajectory exists. It is possible to eject the beam over several turns, or to eject one bunch, while another stays in the machine to be subjected to further acceleration before being ejected in turn.

Beams are injected at a magnetic field of 102 mT. Acceleration can then take place up to a maximum field of 1.26 T. While p+ undergo only a small variation of their revolution frequency due to the particle speed increase when accelerated from 1.4 to 26 GeV, Pb ions see their revolution frequency change by more than one octave.

With reference to Fig 2.16, Rm=70.0789 m is the bending radius of the main magnet, R0=100 m is the machine radius, Q [C] is the particle charge, m [kg] the particle mass and B [T] the magnetic flux density. The peak dB/dt is about 2.3 T/s, yielding a peak dF/dt of 1.6 MHz/s near the start of acceleration for protons.

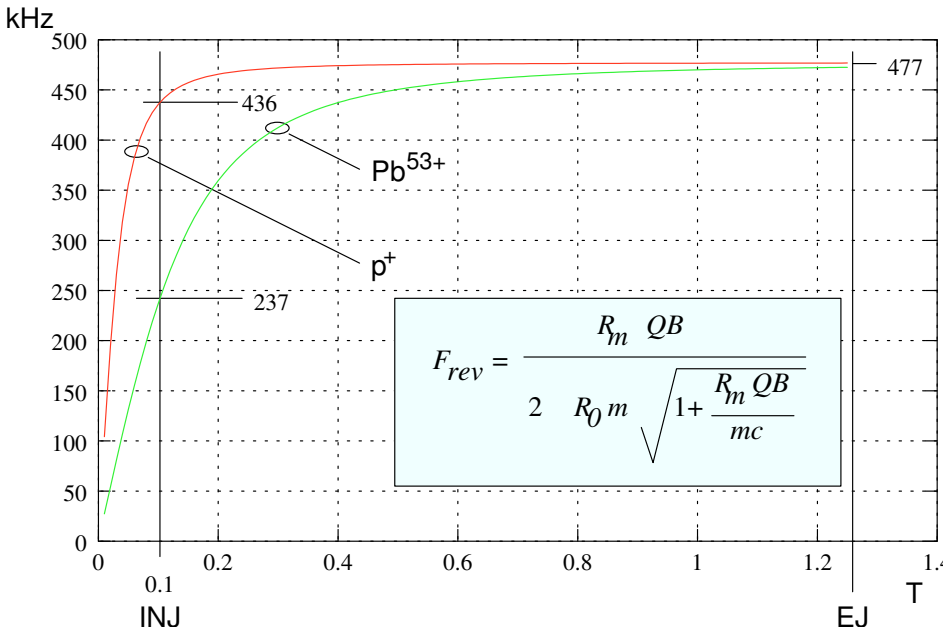

Figure 2.16: Revolution frequency vs B field)

The beam orbit measurement system must be able to measure the position of the centre of charge of each bunch as it passes through each PU, during the time there is beam in the machine. The projected resolution of the measurement is 0.1 mm (vacuum chamber size is 70mm). The principle of position measurement is as follows: For each of the three signals Σ, Δx and Δy, the signal is integrated over the duration of one bunch. The x position can then be found by applying

$$x = S_x \frac{\Delta x}{\Sigma} + E_x \tag{2.17}$$

where x is the horizontal bunch position, S_x is a proportionality constant and E_x is an additive error correction. The resulting value is the horizontal position of the centre of charge of the passing bunch. S_x and E_x are found as the result of a calibration procedure. The same calculation applies to the vertical axis. In order to measure the position, we envisage a system where the 120 PU signals are digitised using 12 bit ADCs running at a rate of at least 125 MS/s. Commercially available 12 bit ADCs ensure at least 10.5 effective number of bits (ENOB) which is more than required measurement accuracy. Integration of the samples further reduces requirements for the accuracy of the ADCs. Due to the large amount of raw ADC data ($40PUs \cdot 3channels \cdot 125MS/s \cdot 2s \cdot 2 = 60 \cdot 10^9 Bytes$), the samples must be pre-processed on the fly into per bunch integrals before being stored in memory. The pre-processing reduces the data storage rate per channel to the bunch frequency. It also simplifies handling of the measurement data reducing the need for further processing and transfers of a large data blocks. The required memory size depends on the time the beam resides in the machine (up to 2 s), the number of bunches in the machine (up to 21) and the beam revolution frequency Frev (up to 477 kHz). This yields 20 millions of acquisition per channel, corresponding to 128 MB per PU (16 bit results). (Rounded up to the nearest power of two).

For some types of cycle, the beam undergoes manipulations that change the number of bunches, or the spacing between them. Typically, these operations span several tens of microseconds on a constant energy plateau. An example is the triple splitting of LHC bunches (Fig 2.17): before splitting, there are six bunches at harmonic number h=7, and after splitting there are 18 at h=21.

The position PU provides only a calibrated beam position signal. The $\sum$ signal, although proportional to the number of charges, does not contain absolute intensity information because the PU cannot be calibrated in absolute values. For this reason, comparison with a BCT is used (cross-calibration method).

The beam intensity measurement system must also be able to cope with varying beam frequency, high dynamic range and lack of DC coupling. Unlike the PU, the BCT measures the current of the beam directly. The beam is treated as a primary turn of the transformer

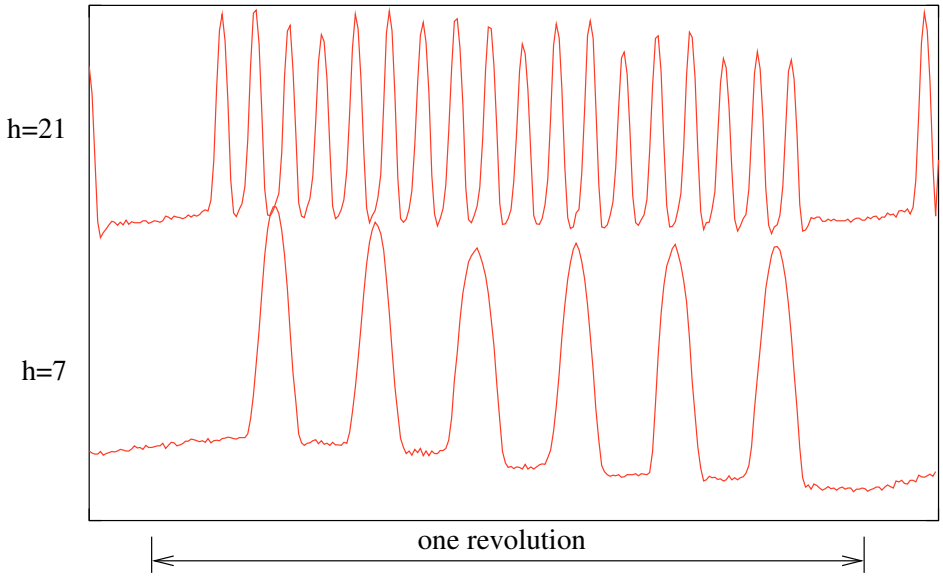

Figure 2.17: The bunch splitting on LHC beams

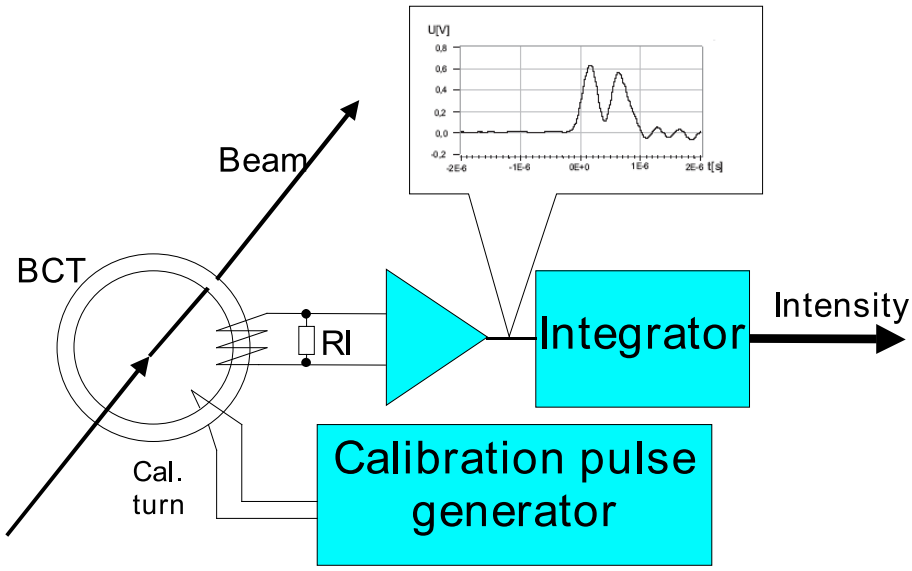

Figure 2.18: The beam current transformer principle [24]

whereas on the secondary turns the measurement voltage is developed. Figure 2.18 shows the BCT principle.The current flowing through Rl is n-times smaller then beam current, where n is a number of secondary turns.

This type of the measurement device enables absolute and high precision calibration. An additional single calibration turn into which a known charge can be injected is treated

by the transformer in the same way as the beam. This is one of the reasons why BCTs are usually used to measure the beam intensity instead of the electrostatic pickups.

Chapter 3

The Aim and the scope of the work

The Proton Synchrotron (PS) produces beams of different particle types, mainly protons, but also lead ions. Almost all these particle beams pass through the PS. The quality of the beams delivered to the LHC has a direct impact on the effective luminosity, and therefore the performance of the instrumentation of the PS is of great importance.

The extremely flexible RF accelerating system of the PS manipulates the beam in many different and complicated ways. Several types of beam are produced for various users. The PS is equipped with a trajectory measurement system, based on 40 electrostatic pickups (PUs), which measures the beam trajectory of any selected particle bunch over two consecutive revolutions anywhere during the acceleration cycle. However, measurements done by the existing system cannot be spaced closer than 5 ms apart and it does not handle bunch splitting and merging operations very gracefully. Due to the operation of the LHC , there is higher quality of the beam produced by the PS required. The present system cannot satisfy this requirements.

The present trajectory and orbit measurement system of the PS dates back to 1988 and no longer fulfills present day requirements. The BPMs are in good condition and will be kept, however the electronics are aging and increasingly difficult to maintain.

The newly developed Trajectory Measurement System (TMS) must be able to keep track of each individual bunch from injection all through to ejection (unlike 2 consecutive like in the existing system), imposing the use of a tracking or synchronization system. The ADCs digitize their input signals at a constant rate, whereas the revolution frequency

of the particle bunches varies along the acceleration cycle. The increase of this frequency depends on the increase of particle velocity, and varies over more than an octave for heavy ions. The new system uses an entirely numerical synchronization algorithm, implemented in the FPGA and runs at the ADC sampling rate.

Synchronization is made more complicated by the possibility of the PS machine to change its harmonic number (the number of possible bunches in the machine) during acceleration. These operations are used, among others, to split bunches into two or three bunchlets, in order to better match the beam to the properties of the subsequent accelerators. The system must be able to keep track of the beam throughout.

It must be integrated with the accelerator timing system and a memory layout must be designed, allowing the data pertaining to a given instant of the machine cycle to be identified. A hub computer will control the forty acquisition stations, accept measurement requests from operator consoles, collect and post-process the data and communicate the results for display.

The Intensity of the beam in PS cannot be precisely determined from the sum signal of the position pickup. This is caused due to the fact that PUs are designed to handle relative measurements of the beam position. The calibration system embedded to the PUs does not give an absolute accuracy in terms of number of particle detected, but the relative displacement.

Due to the limitation of the PUs, another sensor is installed. It is a Beam Current Transformer (BCT). It allows absolute beam intensity measurement. Moreover, it is equipped with special calibration turn which enables continuous calibration of the system.

The existing beam intensity measurement system allows measurement of the intensity of individual bunches only during first six turns of the beam after the injection to the PS. The upgrade of the PS transformer requires to measure at least the first 1000 turns after injection. It is critical to monitor beam losses at injection into the PS. There is also DC Transformer installed which enables very precision measurement of the average beam intensity, but does not give information about absolute intensity of individual bunches. Due to its very low bandwidth, it delivers precision readouts after several ms (due to a feedback system which needs a time to stabilize) after the injection which does not give useful information about the intensity of the beam during critical phase just after the

injection.

So the new, bunch by bunch, beam intensity system need be proposed as well.

There exists a particular method that is able to synchronize to the beam and follow the changes of its frequency in order to precisely estimate its intensity and position.The method bases on extension of the measerument circuits and digital analysis of the measurement results with the usage of advanced FPGA hardware and relevant algorithms.

Chapter 4

The methods and algorithms for beam position (trajectory) estimation

4.1 Requirements of the beam trajectory measurement for PS

The Trajectory Measurement System (TMS) is required to measure the trajectory of particle beams within the CERN Proton Synchrotron. It measures the amplitude and x/y displacement of the individual particle bunches as they pass each of the 40 analogue sensors in the ring. The system integrates the data received for each particle bunch and stores the results in memory for later data access. In order to accurately measure the particle bunches the system needs to synchronize the data capture to the incoming data. Due to the large amount of data sampled by 125MHz ADCs in 120 analogue channels, the signal processing must be done in real-time, in order to determine information on the position of particle bunches as they orbit at around 437kHz. The precision of measurements required is below 500μm. Moreover, the system must deliver following types of measurements [26]

- TRAJECTORY bunch by bunch both horizontal and vertical - the position of selected bunch(es), on selected pickup(s), over a number of turns.

- ORBIT: horizontal and vertical - same as trajectory but averaged over several hundred turns.

- MEAN horizontal and vertical - the mean value of the orbit over all pickups.

- ORBIT bunch by bunch horizontal and vertical - the mean position of selected bunch on all the pickups over few hundreds of turns published every 1ms.

- MEAN bunch by bunch horizontal and vertical - the mean value of the orbit bunch by bunch over all the pickups.

- MEAN Radial Position (MRP) - arithmetic mean radial position of the beam all around the machine

4.2 Existing solutions and limitations

The Closed Orbit Digital Display (CODD) - existing PS Trajectory measurement system is based on set of analogue integrators ,Gate & BLR pulse generators, VME digitizers and a synchronization block which generates a reference frequency synchronous to the beam. The Gate and BLR generator is a VME module which, associated with another module -the RF-MUX and Synchroniser, generates accurate timing signals for the control of the integrators of the CERN Proton Synchrotron's closed orbit measurement system, CODD. The module accepts a reference frequency and start triggers, via front panel inputs, and produces appropriate timing pulses on its outputs, as directed by the settings of its internal registers. The length and phase of the outputs with respect to the reference frequency are programmable over a wide range

Referring to 4.1, a phase locked loop circuit produces a frequency equal to sixteen times the bunch repetition frequency. A counter, dividing by sixteen and then by h, the harmonic number, traverses a full cycle at a rate equal to the revolution frequency of the particles in the accelerator. Eight comparators watch the counter and trigger an output signal when the counter reaches their respective comparison values. The comparators can be made to ignore one or more of the harmonic counter bits, allowing the generation of

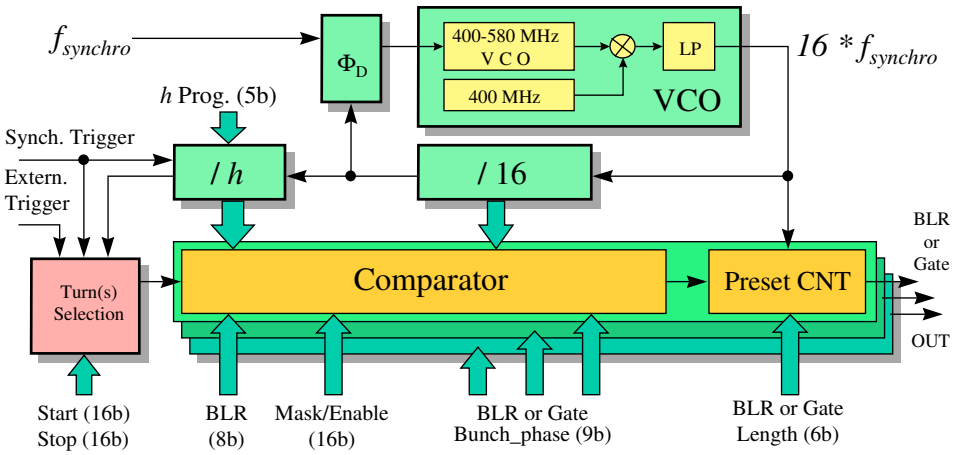

Figure 4.1: Block-diagram of the Gate and BLR generator

multiple pulses per turn. An individual length counter for each channel terminates the output after a pre-set number of counts, thus setting the length of the generated pulse. Another counter keeps track of the number of turns since the last trigger. Its value is compared with the settings of a start and a stop register. The outputs are normally enabled only while the turn number falls between the start and stop values. All timings are scaled linearly with the period of the Fsynchro input[35].

The RF-MUX and Synchroniser is a VMEbus module to generate timing signals for the closed orbit display (CODD) of the CERN PS machine. Based on the machine revolution frequency, a pick-up signal and timing inputs, it produces a beam-synchronous reference frequency and a number of acquisition triggers, as needed by the remainder part of the CODD system. In combination with a separate DDS PLL, a few TG8 * timing modules and 10 BLR & Gate Generators, it produces all timing and RF signals needed for orbit acquisitions and calibration. CODD is initially synchronized with the reference frequency of the injecting machine. After injection, it uses a pick-up signal to derive its timing. During the calibration, a local calibration source is used. The RF-MUX selects the appropriate frequency source, according to the measurement mode, and provides synchronization and acquisition triggers, whenever necessary during the PS acceleration

*The TG8 is a multipurpose VMEbus Timing receiver and pulse generator module. It receives all the messages distributed over the dedicated serial multi-drop line. These messages include Timing information, event, clock, telegram and calendar, are compared with a set of pre-loaded parameters contained in a portion of the on-board memory. If a comparison is valid the requested action, relevant to that particular condition, is initiated. Normally the action will be to interrupt the VMEbus and/or to transmit a trigger pulse to some external equipment. This action can be delayed from the trigger occurrence using one of the eight on-board counters and one of the four different clocks [22]

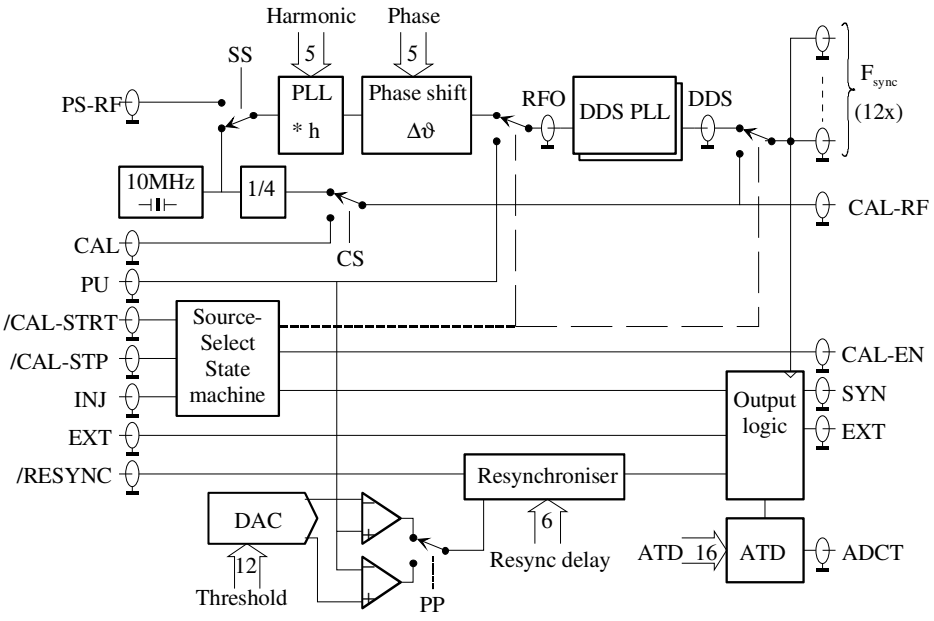

Figure 4.2: Block diagram of the VME RF-MUX and Synchronizer

cycle. The PS-RF input (Fig 4.2), normally the revolution frequency, is multiplied by the machine harmonic number to create a signal at the RF bucket rate, which must lie between 2 and 10 MHz. It is followed by a programmable phase shifter, to align the bucket clock with the PU signal and allow a smooth transition. The block labeled DDS PLL is not part of the RF-MUX and consists of a set of NIM modules in a nearby crate. Its function is to produce a clean version of the PS machine's RF frequency, based on a look-up table plus a correction derived from its input.

The output signal, Fsync, which can be either the DDS signal or a calibration clock, is distributed over 12 outputs to the BLR & Gate Generators [2], which in turn produce the appropriate gating signals for the analogue orbit acquisition hardware.

The RF-MUX and Synchronizer uses externally generated timing information to select the source signals: calibration-RF between Calibration Start and Calibration Stop, PS-RF thereafter, and the PU signal following injection. The re-synchronizer is used for harmonic number changes. During such operations, the system momentarily looses synchronism. When the situation has stabilised on the new harmonic, the RESYNC trigger initiates a sequence which aims to lock on the first non-empty RF bucket detected. A pulse on RESYNC marks the end of RF-Gymnastics. The re-synchroniser must be loaded with time delay information related to the final harmonic number, prior to reception of the

RESYNC trigger.

The RF-MUX and Synchroniser can be roughly divided into three functionally distinct sections. The first is a state machine, driven by three of the input triggers, which switches one of three RF sources to a common output. The second section, in the top half of the block diagram, is the RF switchyard. The third section synchronizes the triggers with the appropriate RF and passes the result on to the appropriate outputs.

During bunch merging or splitting operations, or during harmonic number changes, colloquially known as 'RF gymnastics', the tracking of the first bunch fails. The RESYNC input informs the RF-MUX to accept any bunch to pass through the PU it's looking at as being the first and to convey this information to the BLR & Gate generators by means of the SYN output. No acquisition is desired in this case, hence the absence of ADCT[36].

Due to the limitations of the analogue integrators and the ADC module, in order to measure 2 consecutive bunches, two sets of integrators were used per each PU signal.

4.3 Usage of numerical Phase Lock Loop for tracking of the beam revolution frequency

4.3.1 The synchronization algorithm

Due to the fact that orbit measurement system requires precise adaptation of the algorithm to the beam frequency, and each revolution of each bunch must be undoubtfully identified after the measurements, this implies a method with recovery of the bunch frequency.

Other possible methods based on generation of the integration gates from the signal itself cannot be used in this case, because they don't ensure proper layout of the measurements in the result memory allowing later identification of individual bunches. This limitation is visible especially in case of malfunction of the accelerator system, where some bunches have to small energy to be registered or bunch splitting occurs. Such bunch - based system would not notice them and the system would not detect that malfunction. In case of very often practiced operation of the PS with harmonic number grater than one and not all the bunches filled, that type of algorithm would easily loose the synchro-

nization. Such method was developed for the SIS-18 accelerator in GSI [28] [27] [29].

One of the most widely used methods of synchronization of the local generator to an external varying signal source is a Phase Locked Loop (PLL) . Its operation is based on continuous comparison of the phase of the local oscillator (LO) to the phase of the external signal, and such control of the LO frequency to keep the phase difference between them as small as possible.

Usage of the PLL principle to estimate the bunch frequency requires several adaptations to be made and imposes some special requirements. One of the problems is the dynamic range of such loop. The bunch energy varies in a very wide range. Different types of the beam, different harmonic numbers and energies create very high range of possible levels of the input signal. So the PLL algorithm must not be sensitive to changes in beam energy. The useful input signal range can be narrowed by setting the initial gain of the loop. During acceleration of certain type of beam its energy does not change more than decade. Since the next acceleration cycle is known before, the measurement system can be prepared for the expected type of the beam to ensure that the signal range will be acceptable by the algorithm.

One of the methods which can be applied to improve the immunity of the PLL to the dynamic range of the input signal is a logarithmic amplifier which compresses the signal. But such operation produces lots of harmonics which may decrease the ability to lock to the signal. Additionally such operation requires proper DC level of the signal. But proper restoration of the DC requires synchronization of the PLL in order to create valid gating signals. So the logarithm approach cannot be used in this case.

Attempts were made to use the numerical version of a Constant Fraction Discriminator [16]. Such circuit should theoretically be insensitive to the input pulse amplitude and produce the square pulses at the half of the input signal height. However, tests with the real beam signal showed that the CFD circuit introduces additional jitter to the gating signals which increased the measurement noise. It was also demonstrated that PLL loop without any signal preprocessing is able to synchronize and keep locked during all the acceleration cycles for bunch intensities varying more than 20dB.

The standard PLL loop consists of a Voltage Controlled Oscillator (VCO) , phase detector and regulator (low pass filter). Since the algorithm needs to be entirely digi-

tal, a classical VCO cannot be used. The digital equivalent of the VCO is Numerically Controlled Oscillator [18] and Direct Digital Synthesizer[17]. Since the synchronization algorithm is required to deliver a pattern of control signals, the DDS-based version of the PLL was used.

Usually some kind of multiplier is used as the phase detector in PLL systems. In digital signals domain this can be replaced by the XNOR gate. In case of the discrete version of analog input signal, the signed multiplier will be sufficient. It has also the advantage of simple hardware implementation. Instead of implementing a full multiplier logic, a single multiplexer and arithmetic inverter can be used instead.

Figure 4.3 presents the conception of such system. The DDS block generates a local oscillator (LO) square wave signal, which is then mixed with the PU sum signal. The product, after low pass filtering, controls the DDS frequency. The filter time constant, pole/zero arrangement and loop gain need to be chosen as a compromise between loop stability and lock-in time.

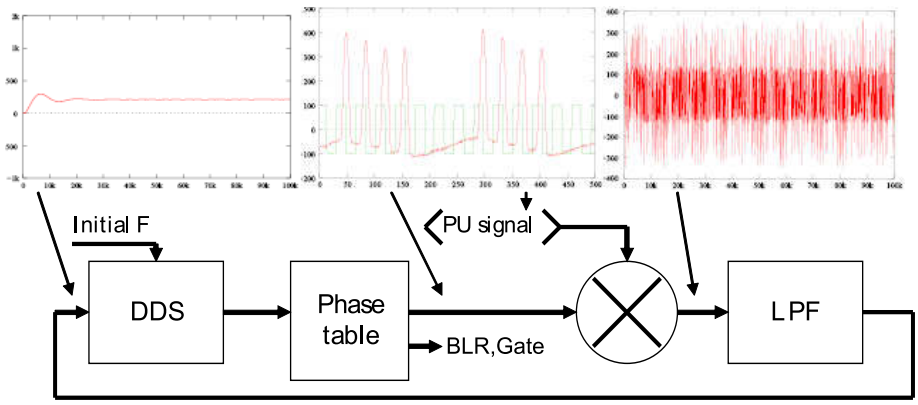

Figure 4.3: The PLL [33]

The PLL ensures a fixed phase relation between the DDS and the beam thanks to the phase detector. The phase detector multiplies the input signal with the reference produced by the DDS. During PLL lock-in state, the transition of the DDS LO signal occurs in the middle of the beam pulse (PU) in such a way, that its integrals for both high and low level of reference signal are the same (see fig.4.4).

The low pass filter placed after the detector removes the beam frequency and its

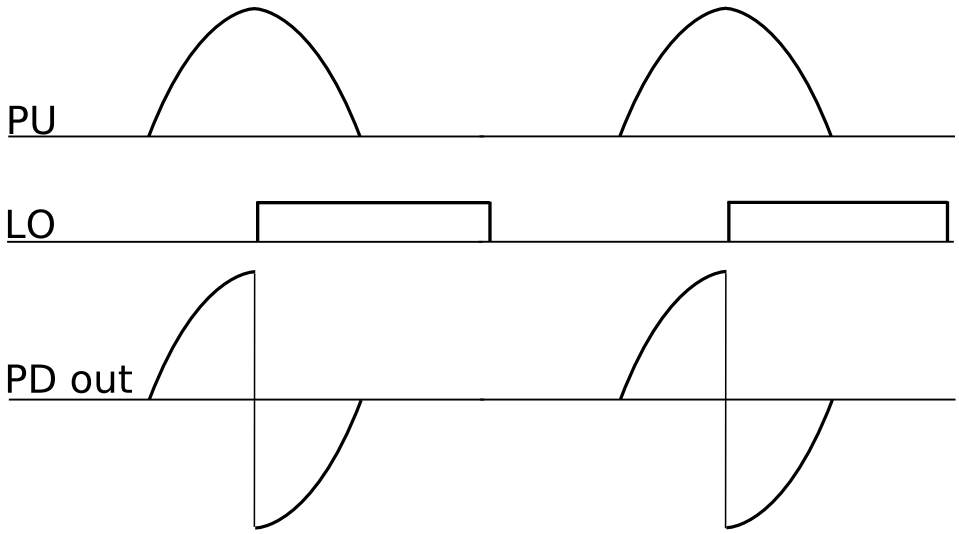

Figure 4.4: the phase detector signals

harmonics leaving only low frequency components responsible for DDS frequency control. Before the input PU signal can be applied to the DDS controlled integrator, it needs additional processing in order to restore the DC component and correct its baseline. The signal DC component is removed due to the AC coupling of the PU and BCT. An additional DC component is created in analog chain before the ADC. For this reasons the signal chain proceeding the integrator must be DC insensitive.

4.3.2 The PU signal treatment

The PU, with its load resistance, yields a high-pass filtered version of the instantaneous beam current(Fig 4.5).

This leads to distortion of the PU signal baseline. Figure 4.6 presents an example beam current as it is passing through the PU. Since it is usually non-periodical, its DC components varies significantly compared to the pulse amplitude.

Figure 4.7 presents the influence of the PU to the signal. Integration of such a signal without the correction would cause unacceptable error.

Several approaches to solve this problem have been tested. One of them was based on full rectification of the input signal and low-pass filtering to regenerate the baseline. Then the baseline was subtracted from the signal. But this approach affected the corrected

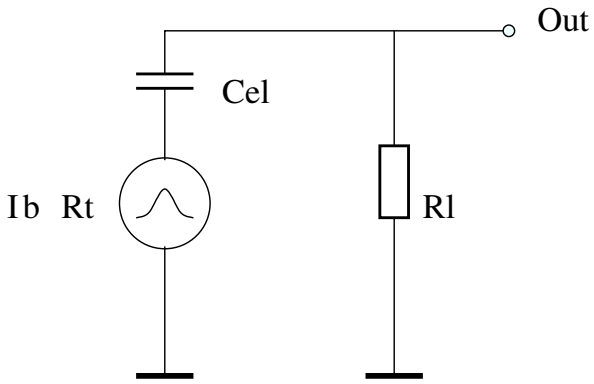

Figure 4.5: PU substitute schematic

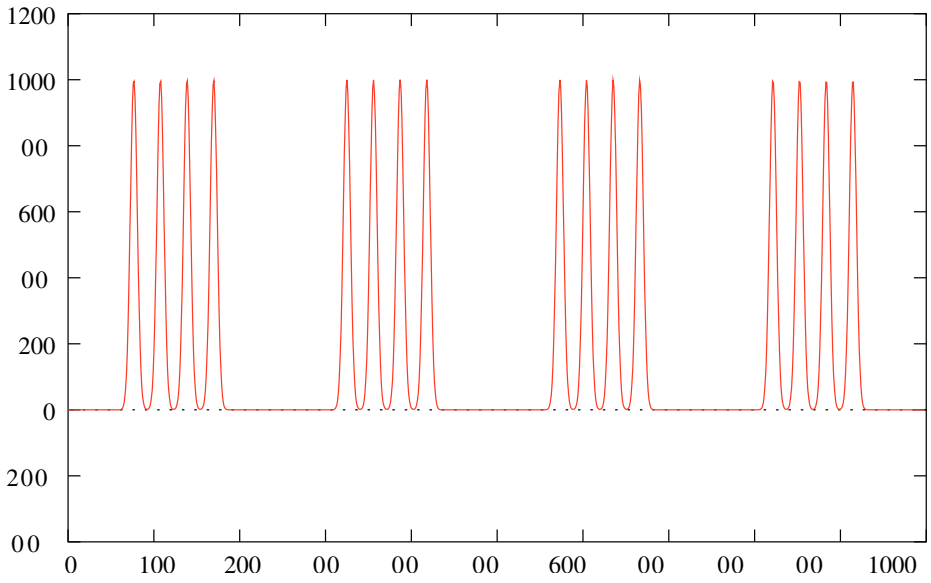

Figure 4.6: Instantaneous beam current

signal shape and the amplitude.

Since the baseline effect is caused by the high pass character of the PU, the correction can be done using the complementary low-pass filter which would compensate the signal distortion for lower frequencies. The PU has a pole at the region of 150kHz. Below that frequency the gain drops 20dB/decade. So the first-order low pass filter of transmittance 4.1 will do the job.

$$H_F = \frac{z^{-1}}{1 - 0.992z^{-1}} \tag{4.1}$$

Due to the fact that the information about the DC level of the signal was lost, the

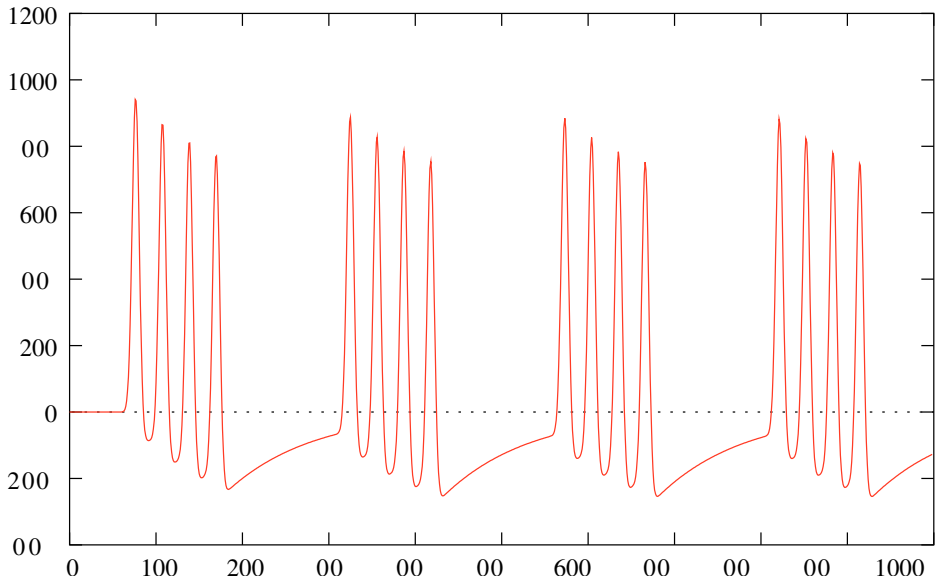

Figure 4.7: Simulated PU output signal

low-pass correction filter will introduce at the output the DC component of the average value of the input signal. To accurately measure the integral of the pulse, it must be DC-corrected. There are several possible implementations of the DC restoration algorithm. The simplest one is known from analogue solutions and is called signal clipping. It requires a reference signal which gives an information to the restorer circuit about a valid level "zero" to which the signal is to be clipped. The same idea may be used in digital world. The level "zero" in this case is defined between the pulses, and to achieve it, an additional signal called Base Line Restitution (BLR) is required.

The proper DC value may be generated at least in two ways:

- As a feedback loop with regulator which ensures that the output value of the restorer is zero at the time indicated by the BLR pulse (Fig 4.8). It also protects the digital correction filter against saturation.

- As a forward circuit which measures input offset at the time indicated by the BLR pulse and subtracts it from the signal.

The first method is more complicated, slower but seems to be more precise due to the fact that the DC value is taken from averaged several pulses. The second one gives immediate update of the DC value but may introduce additional noise due to smaller

number of samples which are used to generate the DC value. Further tests will evaluate usefulness of both methods.The same treatment must is applied to all three signals, Σ, Δ_x and Δ_y

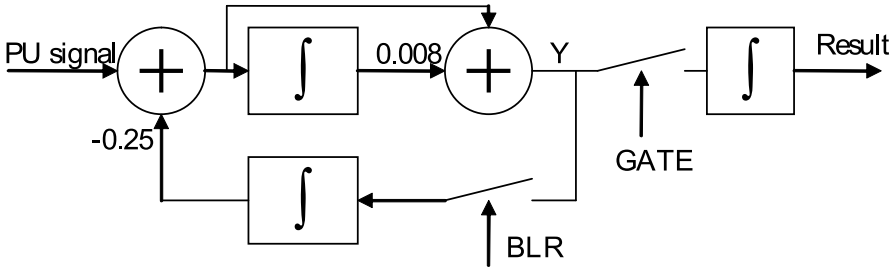

Figure 4.8: The Base Line Restoration block, correction filter and integrator

Similar problems exist in the case of the intensity measurement, with signal distortion caused by the Beam Current Transformer. The main difference is the cut-off frequency which is lower. The same baseline correction algorithm may be applied as in case of PU signal processing, the only change is a value of the coefficient in the low pass filter.

Proper operation of both the integrator and DC offset compensation circuit, require precision reference pulses, which are generated by the numerical PLL block.

4.3.3 Implementation of numerical Phase Lock Loop for tracking of the beam revolution frequency

The algorithm is actually independent on the target hardware used. It has been implemented on 3 different hardware platforms, all of them providing fast 12..14bit ADCs, large field programmable gate arrays (FPGAs) and fast memory.

The first platform, Libera (Fig 4.9) available on the market from Instrumentation Technologies was used mainly for laboratory tests and was actually a candidate for the final system implementation. Due to several limitations finally was not chosen as a TMS hardware. Anyway it was very useful for raw data acquisitions, implementation and tests of the PLL algorithm.

The original FPGA firmware developed by Instrumentation Technologies was removed due to several limitations and bottlenecks. The code was developed from scratch and

Figure 4.9: The Libera bunch position processor [6]

integrated with the Single Board Computer (SBC) ARM processor based module available in Libera, simple control software was written as well.

Figure 4.10 presents the block schematic of FPGA and hardware of the Libera used to implement a single channel beam position measurement system.It consists of the Virtex II Pro FPGA circuit, a set of four 125MS/s 14 bit analog to digital converters driven by low-jitter clock generator, SDRAM memory and a single board computer running the Linux operating system and providing network connection. In addition to the PLL algorithm, an embedded dual channel signal analyzer was implemented inside the FPGA, which was used for diagnostic purposes as well as first position data acquisitions.

The second tested hardware platform was developed by Alpha Data. It is a custom Compact PCI board designed specially for the TMS system (fig 4.11).

The card implements nine 14 bits, 125MS/s ADCs, large Xilinx Virtex IV FPGA, several DDR II SDRAM memories, PCI-X bridge and clock generator. Due to its compactness, low cost per channel and flexibility it was chosen as a final hardware platform for the TMS(4.12).

In order to enable easy migration of the algorithm between different hardware platforms, the signal processing was implemented in VHDL[†] using general adders/ register, without using vendor dedicated FPGA resources like multipliers, shifters or DSP blocks. The ADCs and all the processing logic run at 106..125MHz clock rate and the FPGA

[†] Hardware Description Language

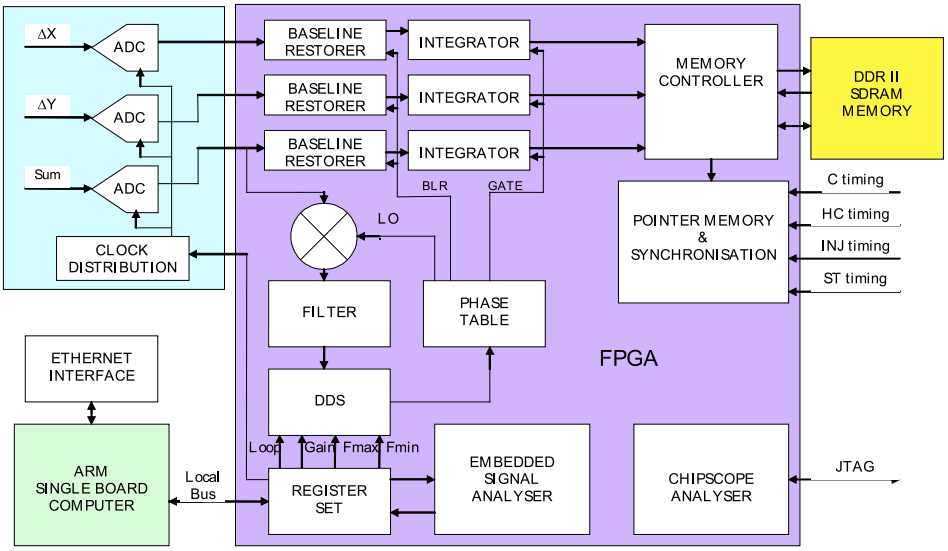

Figure 4.10: The Libera based PLL system

internal data bus is 24..32 bits wide. They are driven by a low-jitter clock generator. High-speed applications using fast data converters in their design require an extremely clean clock signal to make sure an external clock source does not contribute undesired noise to the overal dynamic performance of the system. It is therefore crucial to select suitable system components, which help generate a low phase-jitter clock .

Jitter generated by a clock source can cause the ADC's internal circuitry to falsely trigger the sampling time. As shown in Figure 4.13 , uncertainty in sampling time Δt

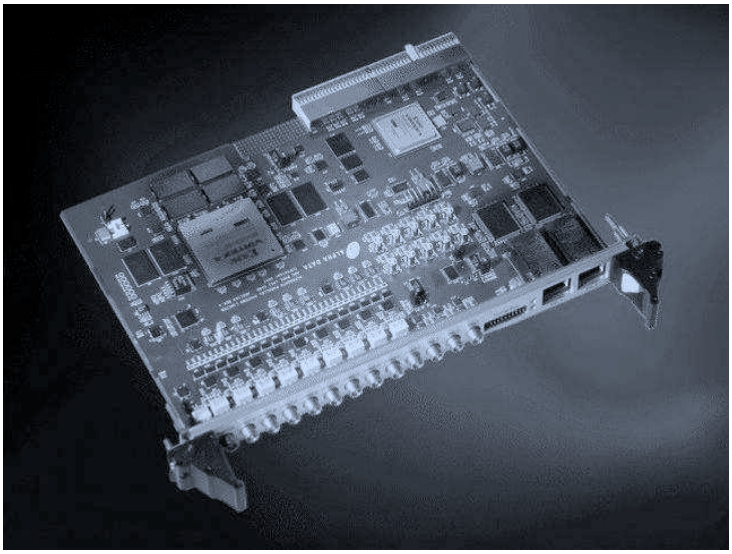

Figure 4.11: The Alpha Data ACP-FX-N2/125 capture card [4]

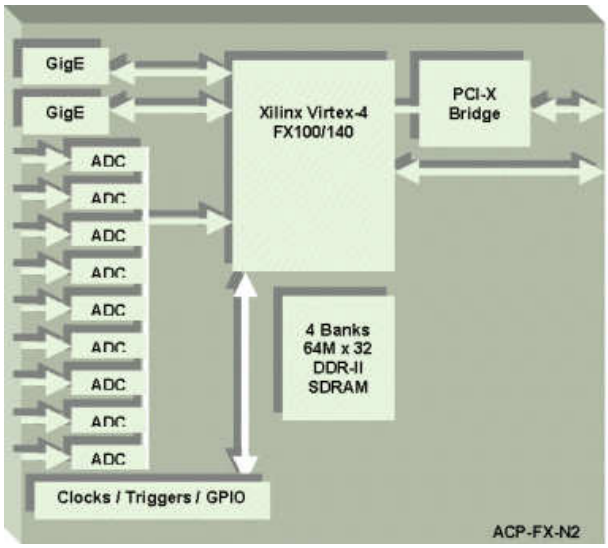

Figure 4.12: ACP-FX-N2/125 capture card block schematic [4]

equates to uncertainty in amplitude ΔA . This results in false sampling of the analog input amplitude, thus degrading the Signal to Noise Ratio (SNR) of the ADC.

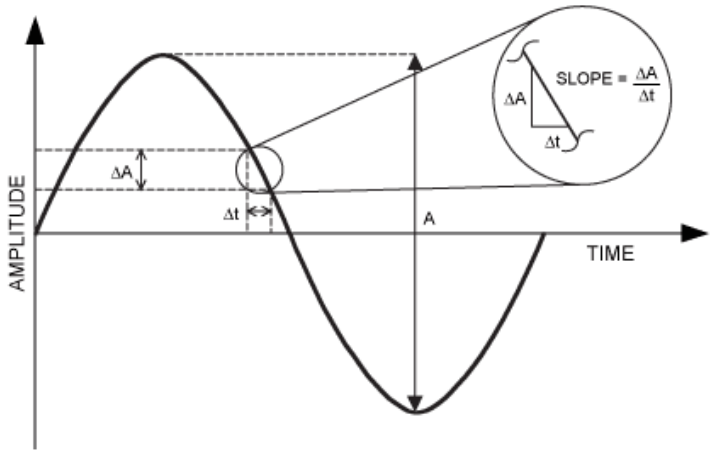

Figure 4.13: An SNR model obtained using the sampling time uncertainty

With the following equations, the maximum SNR of a data converter can be calculated for a given amount of clock jitter:

$$\frac{\Delta A}{\Delta t} = slope = A\omega cos(\omega t) \tag{4.2}$$

The slope is at its maximum when the term $cos(\omega t) = 1$ Therefore

$$\frac{\Delta A}{\Delta t} = A\omega \tag{4.3}$$

$$\frac{A}{\Delta A} = \frac{1}{\Delta t \omega} \tag{4.4}$$

By definition, $A/(\Delta A)$ is the signal-to-noise ratio, and Δt is the root-mean-square (RMS) value of the jitter. Equation 4.4 can be rewritten as[8]:

$$SNR_{ADC} = \frac{1}{2\pi f \sigma_{RMS}} \tag{4.5}$$

Provided that the bandwidth of the analogue signal is limited to 30MHz, and the ADC with effective number of 12bits is used, which has theoretical SNR of 75dB (5600x), the clock jitter must be less than 0.9ps RMS.

The jitter introduced to the clock source by the FPGA PLL blocks is in order of a few hundreds of ps RMS. The FPGA PLL circuit outputs are sometimes used by unconscious designers to drive high speed ADCs. This affects their performance drastically. Due to that fact, the primary version of the acquisition system offered by Alpha Data for the TMS system had to be modified to fulfill the jitter requirements. The TRIC card (chapter5.3.3) is equipped with low jitter clock generator as well.

A timing reference to produce the Gate and BLR signals must be derived from the Σ signal by locking to it with a locally produced frequency, using a numerical Phase Locked Loop (PLL). Referring to Fig 4.14, a phase accumulator Θ is advanced by f every period of the sampling frequency Fs, such that Θ overflows at the rate of the revolution frequency $Frev$. The phase accumulator is used to address a phase table that contains h periods of the Local Oscillator (LO) signal. The LO frequency is thus $hFrev$.

The centre of charge of a bunch is found by integration over the bunch length. The LO is mixed with the incoming PU signal and the product is low-pass filtered to extract a phase error (e). This phase error is then fed back through a suitable regulator to correct the value of f. The regulator keeps the phase relation between the PU and LO signals, and consequently the phase accumulator, constant.

The length of the phase table, which results in a number of most significant bits of the phase accumulator, must be such as to allow setting of the Gate and BLR signal with the precision of 1 clock cycle. Further increasing of the table length will not improve the precision because the number of clock cycles of the Fs during one accelerator turn

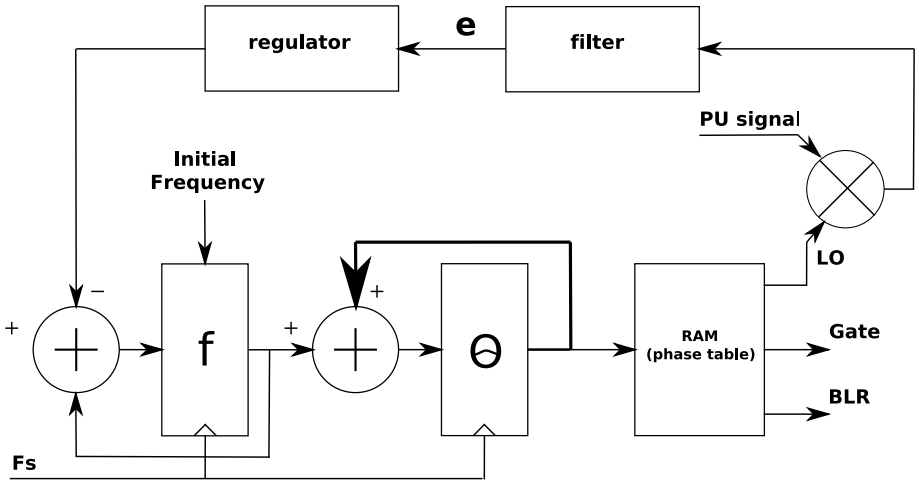

Figure 4.14: Reference frequency generation principle

is limited. Thus, at minimal revolution frequency of 437kHz at the injection gives the minimal length of the table :

$$n = Fs/Frev_{min} = 125MHz/437kHz = 286 \tag{4.6}$$

This number needs to be rounded to the closest power of 2 that is 512, which results in 9 most significant bits of the phase accumulator addressing the memory. One of the phase table columns is reserved for LO signal generation. The other columns are added to produce a Gate and a BLR signal, for the use of the integration and DC restoration algorithms. At the end of each gate period, i.e., at the end of each bunch, the integrals are stored into memory. As already stated, the actual position calculation can be deferred until data are requested for display.

The value of the initial frequency (Fig 4.14) represents the value of the revolution frequency Frev according to:

$$f = \frac{AF_{rev}}{F_s} \tag{4.7}$$

where A is the full-scale value of the phase accumulator (2^{32}). A suitable initial value for f is provided by the control register updated by the TMS software before the injection.

In case of the position measurement, the same gate length (and jitter) is applied to the Σ and Δ signals. So such generated noise in all the channels is correlated. Since the

position is derived:

$$x = S_x \frac{\Delta x}{\Sigma} + E_x \tag{4.8}$$

Due to the correlated character of the noise, its value in position result is suppressed.

The synchronization loop can be modeled as a discrete time feedback system [37] . Its transfer function can be expressed as polynomials in the 'z' domain.

$$H_o = H_{DDS} \cdot H_m \cdot H_F \cdot H_R \cdot z^{-n} \tag{4.9}$$

where H_{DDS} is a transmittance of the DDS, H_m is a mixer modeled as a pure gain, Hf - filter, Hr - regulator

The DDS can be modeled as a pure integrator

$$H_{DDS} = \frac{h}{2^{32}} \frac{z^{-1}}{1 - z^{-1}} \tag{4.10}$$

2^{32} is the full scale value of the phase accumulator and h is the accelerator harmonic number. The factor z^{-n} represents the pipeline delays of the FPGA implementation.

Low-pass filter that passes only the low frequency terms of the phase error. Its cut-off frequency is a compromise between rejection of F_{REF} and the loop setting time.

$$H_F = \frac{1}{256} \left(\frac{z^{-1}}{1 - 0.996 z^{-1}} \right)^3 \tag{4.11}$$

The task of the regulator is to keep the static phase error tending to zero. This implies usage of the integrator (with a pole at +1). In order to make the loop stable, two real poles needed to be added.

$$H_R = K_R z^{-3} \frac{(1 - 0.999 z^{-1})^2}{1 - z^{-1}} \tag{4.12}$$

For evaluation purposes of the loop stability, it is useful to express the closed-loop transfer function (4.13) :

$$H_c = \frac{H_o}{1 + K_R H_o} \tag{4.13}$$

K_R is the regulator gain. The stability of the loop can be verified by examining the root-locus of H_c with the regulator gain K_R as the independent variable. All poles must

lie within the unit circle for whole range of the input signals. The optimal setting of K_R depends on the beam intensity and through the mixer gain H_m and on the harmonic number h. The loop behaves acceptably over a variation of K_R of more than 20dB.

The filter coefficients have been chosen to reduce the multiplications to simple shift-and-add operations, in order to make them easy and efficient to implement in FPGA logic from different vendors: $0.996 = 1 - 2^{-8}$ and $0.999 = 1 - 2^{-10}$ [38] .

Prior to injection, while there is no beam signal yet to lock onto, an externally provided signal Fref at the revolution frequency serves to both lock the PLL and provide a bucket numbering reference. At injection, a timing pulse signals the arrival of the beam in the machine. The signal that is presently available for this purpose has a resolution of 1/8 of a revolution period, irrespective of the harmonic number of the accelerator. Switch changes are synchronized to the reconstructed Frev, because each PU has a different phase with respect to the common reference. At injection, the PLL reference is switched from the external Frev to the PU's sum signal. Coincident with that event, the LO frequency is switched from Frev (LO1) to hFrev(LO2), in such a way as to minimize the phase discontinuity. (The phase tables for these two frequencies must be correctly aligned.) The task of keeping the appropriate settings for switch and phase tables and distributing them to the acquisition hardware at the right times belongs to the system hub processor, the same that also collects the data and communicates with the PS control system.

The difficult task for the PLL algorithm occurs when there is a RF gymnastics. During this event, the single bunch can be split into 2 or more bunchlets. The bunch frequency changes in such a way, that it is not possible to determine its frequency at the duration of the splitting process. The revolution frequency of the accelerator does not change during RF gymnastics process, so it is possible to use it to support the PLL. Since it is not possible to determine valid integration boundaries during bunch splitting, the bunch position measurements are not valid during that process. In some cases, one can integrate over a single big bunch until the switch of the bunch frequency on the integrator over the bunchlets.

Injection and RF gymnastics are similar in a sense that the system must switch from one frequency reference to another without losing phase lock. The reference frequency generation block is extended as shown in fig 4.15. Switches select the reference frequency

source and phase error taps. The switches are controlled through a table that associates a set of switch settings with each relevant accelerator timing event (fig 4.16). While one branch of the duplicated signal path feeds the regulator in order to keep the loop locked, the parameters of the other are changed in anticipation of the next event. The switch table is freely programmable during system operation. Such approach with double filter paths reduces transients during switching. This allows to propagate the multiplier signal through the filter before switching takes place.

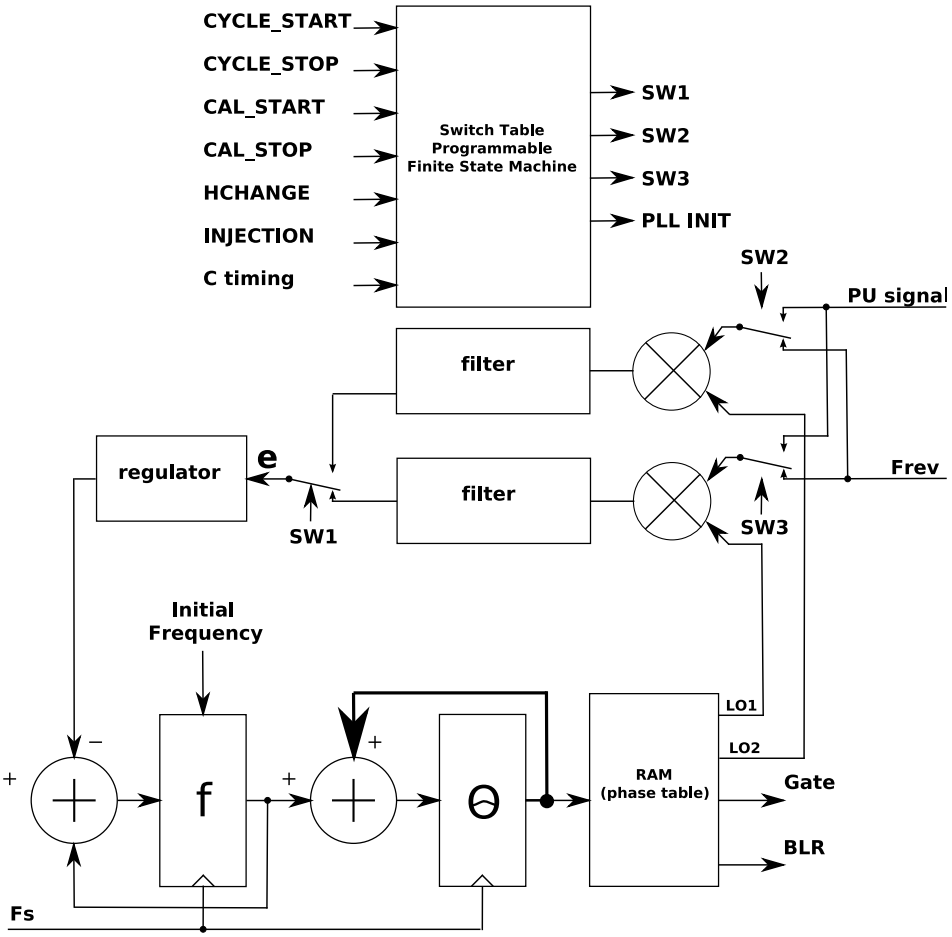

Figure 4.15: Dealing with injection and RF gymnastics

The Pickup Unit signal has a LF cut-off frequency of 150 kHz, resulting in a baseline that is not at zero potential. In order to get an accurate integral, the baseline must first be restored. This is done by passing the samples through a numerical low-pass filter with a characteristic that is complementary to the high-pass response of the analogue channel, extending the lower cut-off frequency down to DC. The signal treatment is described in

chapter 4.3.2.

The input signal, after baseline restoration, is fed into three numerical integrators which calculate sum and difference components (fig 4.16). The integration results are then stored into the 256MB SDRAM circular buffer.

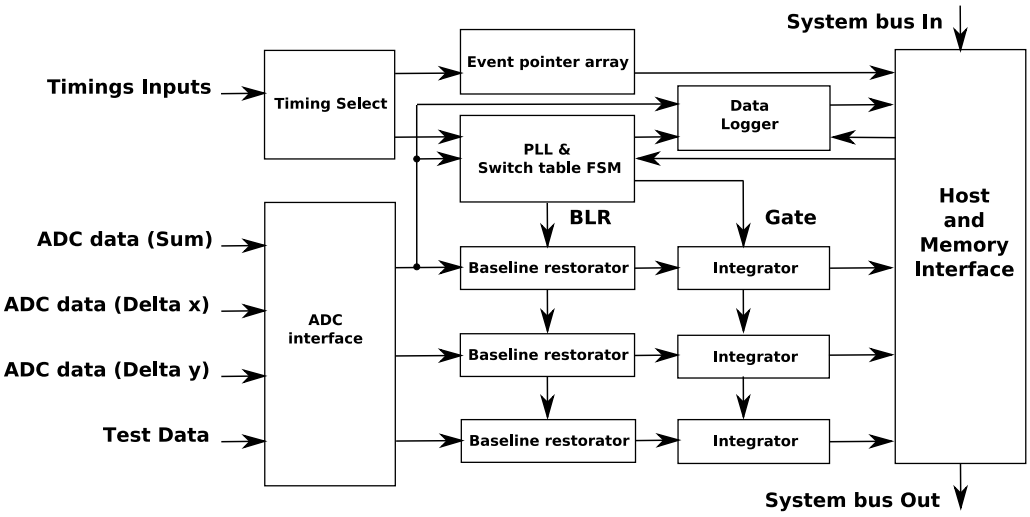

Figure 4.16: PU schematic

The depth of the buffer allows storing results for more than one full acceleration cycle which takes approximately 2 s. The speed of the SDRAM is not critical, since only the final integration results are stored. To make navigation over the buffer possible , there is a pointer array, implemented as separate embedded RAM memory, which points to specific events in the SDRAM memory, like harmonic changes, injection triggers and the 1 ms machine reference timing. Each time the external trigger or timing comes, an address of the SDRAM is stored in the pointer buffer to facilitate navigation over the SDRAM.

The results from the SDRAM buffer are then read out on user request and processed further in software running on a remote machine. There also are diagnostic facilities that provide remote access to recordings of critical algorithm signals. It has the form of a logical analyzer embedded in the main FPGA. Users can set triggers, choose delay times and signals to be recorded. It allows capturing the chosen signals on different time scales (fig 4.17). It is controlled by a small program that writes the recordings into text files on the remote machine.

The integral over the length of each bunch is found simply by adding together the sam-

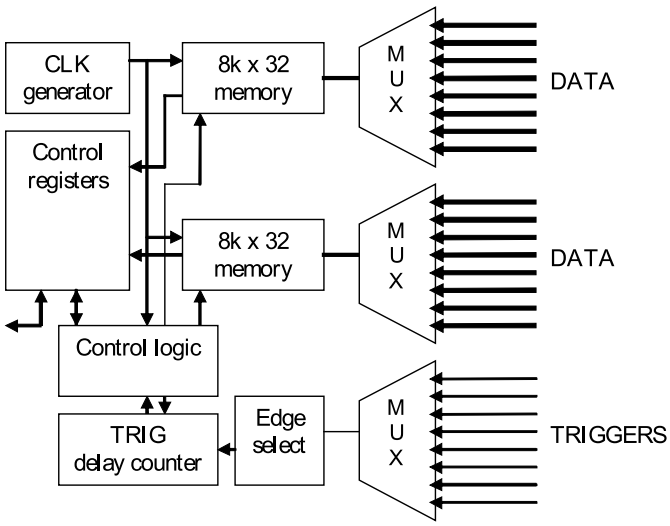

Figure 4.17: The Analyser

ples belonging to a given bunch. Attempts were made to implement a more sophisticated integration like the triangle method. But the difference of results in terms of accuracy and measurement noise were negligible. The synchronization system tells which samples are to be taken as part of a bunch, using a Gate signal. The length of the Gate signal is not very critical, because it starts and ends when the beam signals are near zero. Integration is also applied to all three signals. The three integrals are then stored in memory. All RF buckets are thus treated and stored, irrespective of whether there is beam in them or not. This is necessary to limit the complexity of locating a requested measurement in the memory.

The data coming out of the pre-processing stage consist of data triplets, representing the S, Dx and Dy integrals respectively. These are stored into consecutive memory locations. The memory is used as a circular buffer and can thus contain data pertaining to several acceleration cycles. At each occurrence of a C timing impulse, i.e., every ms, a tag, consisting of a small integer identifying the cycle, together with the current memory address pointer is stored in a table (The event pointer array). A measurement at a given C-timing can be then be found by looking up the address from the table and rounding that value to the nearest multiple of 3*h.

Timing events are almost all coincident with a C-timing. Exceptions are the injection and ejection timings, which are synchronised to 8Frev. These are stored as dedicated

entries in the event pointer array.

Associated with each timing event are actions that appropriately change the settings of the system. A dynamically re-programmable matrix controls the settings of switches that select appropriate reference frequency sources and LO, BLR and Gate columns during the acceleration cycle. Table 4.1 presents the typical actions that must be taken for each of the possible timing inputs (fig.4.18). Each column corresponds to a timing input and each row is an action[10].

	SCY	Cal_Start	Cal_Stop	Inj	H_change	ELFT	Spare
Set Switches	x		x			x	
Clear C Coutner	x						
Acquisition start		x		x			
Acquisition stop			x			x	
LO toggle			x	x	x		
Gate/BLR toggle			x		x		
RF toggle			x	x			

Table 4.1: Timing action matrix[10]

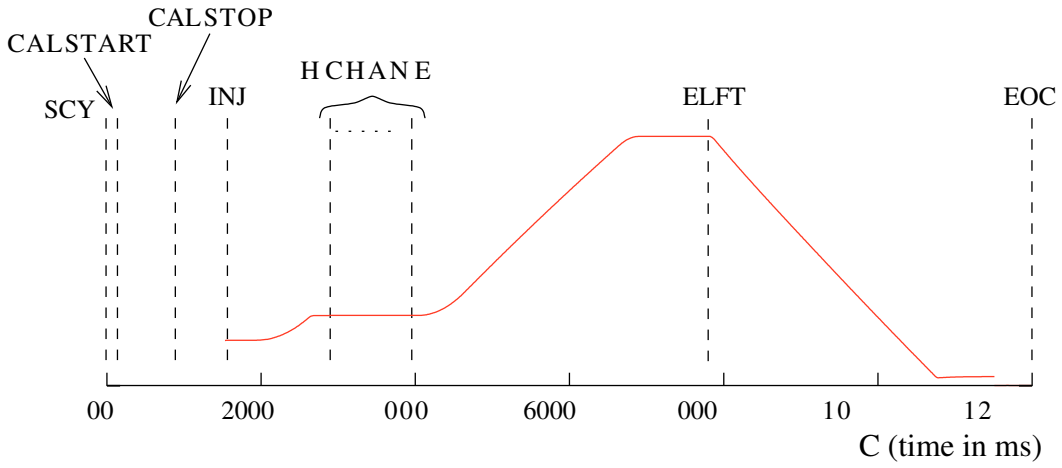

Figure 4.18: The timing events [10]

SCY is Start of Cycle (fig.4.18). It corresponds to $C0$, the zero millisecond mark. The local C-counter is then cleared. The applied $Fref$ at this time will normally be the 312.5 kHz calibration frequency. The phase table entries for LO, BLR and Gate are appropriate for the upcoming calibration. The system software fills the alternate LO, BLR and Gate tables to prepare for the Inj event.

$CAL-START$ is usually set at $C5$ (5 milliseconds after SCY). It causes the calibration system to simulate the injection of a single bunch beam. The acquisition of calibration data starts. Cal_Stop is usually set at $C95$. The calibration generator is stopped, and so is the acquisition. The system software provides new phase table contents and sets the initial loop frequency in anticipation of the INJ event. The system may then read out calibration data, if needed. An $Fref$ signal at the correct frequency and phase for injection will appear about 20 ms before actual injection[10].

Injection takes place near $C170$ (170 ms after SCY). The reference frequency source is switched from RF to PU (from externally delivered RF signal to the PU signal). LO is toggled because the $Fref$ frequency was at $Frev$ (accelerator revolution frequency), whereas the beam is at $h \cdot Frev$ (number of buckets times the revolution frequency). Software sets the inactive LO, BLR and $Gate$ columns of the phase table in anticipation of the first H-change event, if any. H-change events may or may not occur during a cycle. Harmonic changes imply a change of LO frequency and of $Gate$ and BLR timings, effected via the appropriate switching actions. Software then sets the inactive LO, BLR and $Gate$ columns of the phase table in anticipation of the next H-change event. $ELFT$ (End of Last Flat Top) signals that the magnetic field is going to be ramped down. Normally all beam has been ejected shortly before, and thus acquisition can be stopped and switches can be set in anticipation of the next calibration. The reference frequency source is CAL . The system software must set the proper initial loop frequency (312.50 kHz) and provide the correct LO, BLR and $Gate$ settings for the phase table. EOC is End Of Cycle . The next cycle starts about 30ms after EOC.

In order to be able to set up the system, and to verify its correct operation, it was necessary to be able to make short records of any two signals from the following list: S, Dx, Dy, $Gate$, BLR, LO, e, $Frev$, $Fref$, q, f, timing inputs and action switch bits. Since there is no way to pre-calculate the exact phasing of the beam signal with respect to the externally applied $Fref$, it is necessary to align the phases of the LO, the $Gate$ and BLR signals manually during system setup. It was also necessary to inspect the phase error and the frequency to make sure the loop locks reliably. This is a task for data logger (signal analyzer) (fig 4.16). The acquisition of the diagnostic data have a flexible triggering: It is possible to use any of the timing inputs as a trigger, and to delay the

recording by a programmable number of ticks at the sample rate selected.

Each of the Compact PCI PUPE modules (Pickup Unit Processing Engine) integrates 3 PU Processing Units (PUPU) and test data memory (fig 4.19).The system was also equipped with PU data simulation capability. The test data, i.e. recordings of raw PU signal can be fed into ADC interface which then delivers it into selected PUPU in order to proceed tests when PU signal is not available, for example during machine shutdown.

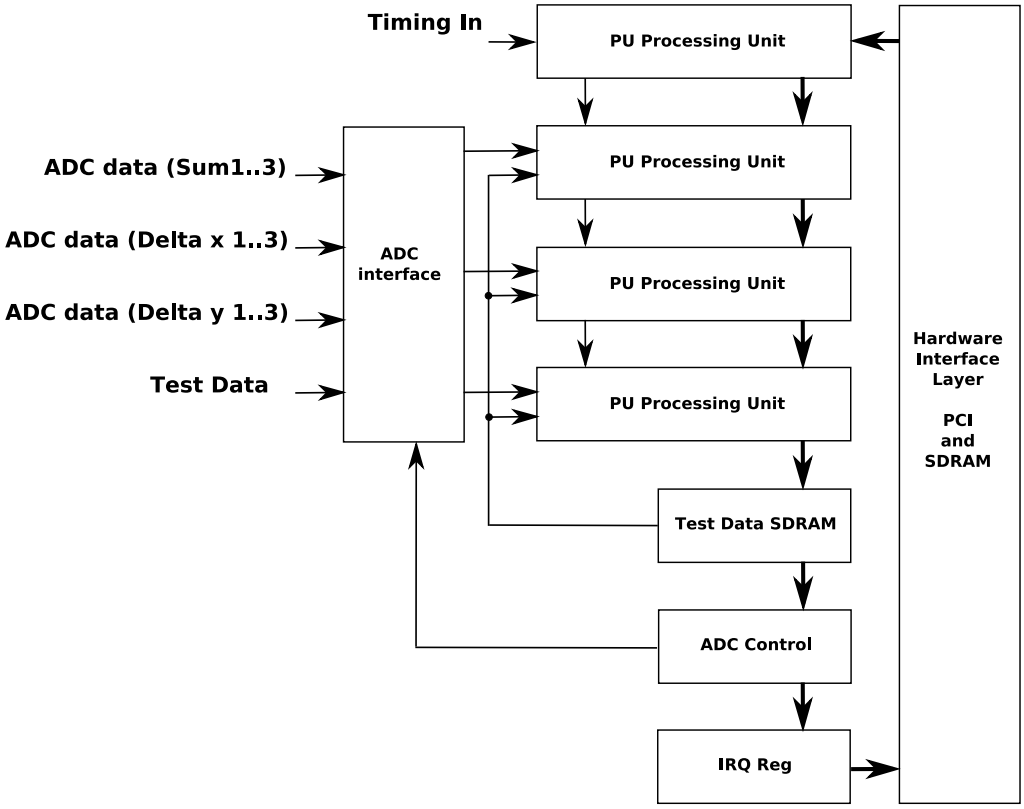

Figure 4.19: Top level PU schematic

4.3.4 Trajectory Measurement System Architecture

Implementation of system hardware and TMS control software was not part of this Thesis, although the author took part in its specification.

The system hardware design has been based, as much as possible, on common of the shelf (COTS) components available from Alpha Data and other sources. There is one, board level, component that has been specially designed and manufactured for the system:

the Pick Up processing Engine (PUPE). This compact PCI board is built around Alpha Datas ADM-XRC/FX100-10/1G FPGA PMC modules design.

It has a Vertex-4 FX100 FPGA together with 9 analogue to digital converters and digital timing/test signal interface circuitry. The system uses the industry standard compact PCI (cPCI) rack mounted bus system to house the main processing boards, power-supplies and provide fan cooling to the system's hardware.

The system design is focused on providing 24/7 service with minimal down-time in the event of a component failure. In order to achieve this and to ease system maintenance, system development time and testing the system has been designed in a modular way. The system consists of 3 identical processing modules and one reduced processing module as a spare. Each of these processing modules has its own power supply and an 8 slot cPCI backplane. The cPCI backplane has a PCI bus for board communications. Housed within each processing module is a conventional CPU based module controller and up to 5 PU processing engines. Each of the PU processing engines has 9 ADCs and 16 digital I/O lines connected to a Virtex-4 FX100 FPGA based processing engine. Thus each PU processing engine can acquire and process the data from 3 of the Proton Synchrotrons pick ups (PU's). This architecture was chosen to reduce system cost while providing FPGA processing power from one of the latest Xilinx FPGA generations available.

The PU processing engines are interconnected with an 8 signal, 16 wire timing bus. The first PUPE in a processing modules has an extra panel containing connectors for the external timing signals. This first PUPE engine is configured to transmit these timing signals to all PUPEs in the processing module over the timing bus. The timing signal bus consists of an IDC ribbon cable connected along the front panels of the PUPEs. There is also the future option for passing the digital timing signals using the J3 connector of the cPCI backplane (fig. 4.20).

The module controller is a COTS component. It has a conventional low power Intel x86 Core Duo CPU, some boot FLASH memory, 1 Gigabyte of RAM, a cPCI bus interface and triple Gigabit Ethernet ports. The actual unit to be used is the Concurrent Technologies PP 410/03x. The module controller boot's from the main system controller over the Ethernet interface and runs a small Linux based operating system. It is responsible for booting and managing the 5 PU processing engines (15 Proton Synchrotron PUs).

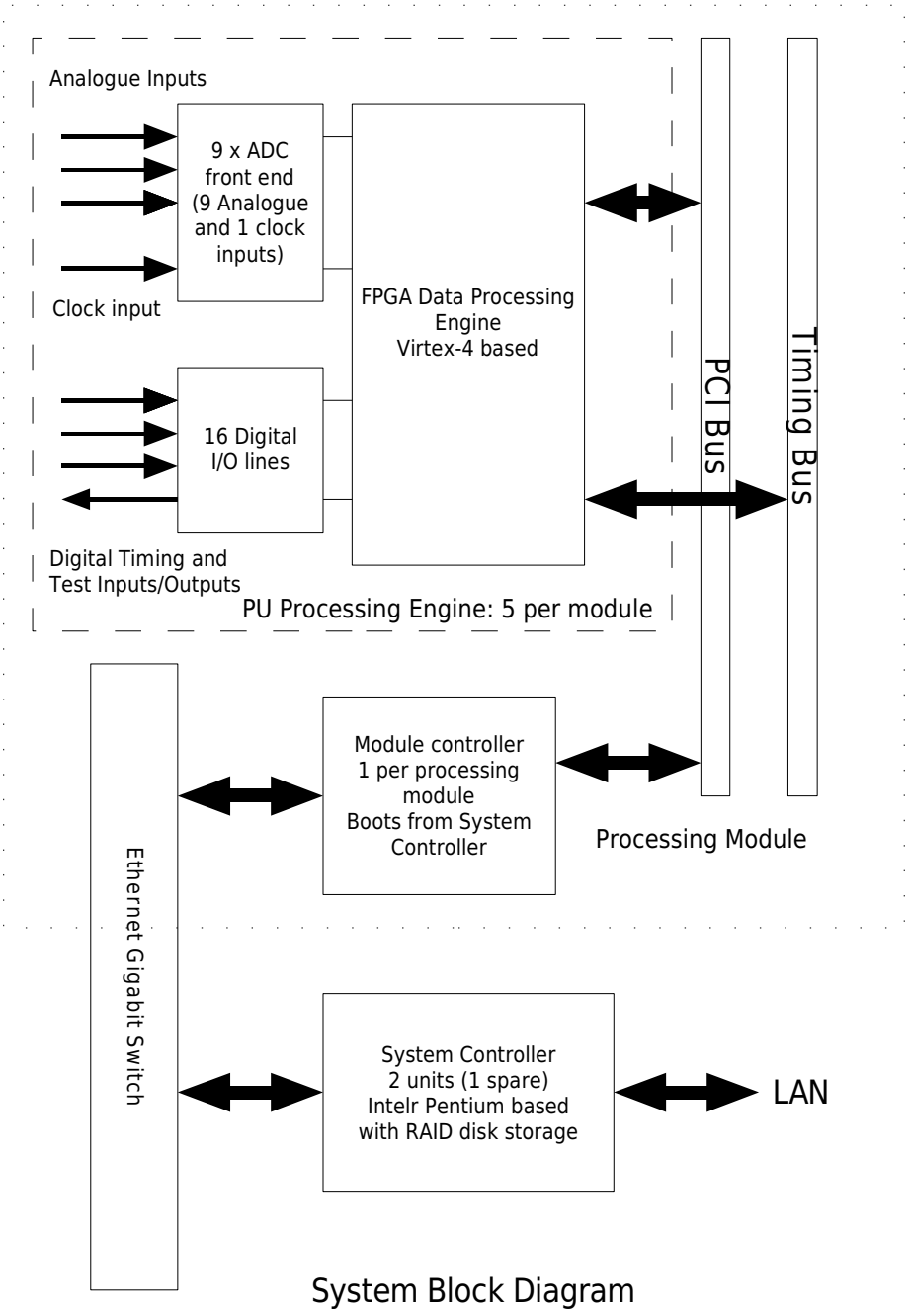

Figure 4.20: System architecture

Communications between the system controller and the individual PU processing engines is also handled.

The processing modules are controlled from a master system controller through a local Gigabit Ethernet switch. The system controller is used for booting the individual processing engines and overall system control, data access and management. There are

Figure 4.21: TMS photo

in fact two system controllers for system redundancy. Remote systems communicate with the system through the system controller, the individual processing modules are on a separate physical Ethernet based network[10].

The system controller is a standard Dual Intel Pentium Xeon based computer system. It is housed in a separate 4U 19 rack enclosure. The system controller has 2 Gigabytes of memory and dual SATA disk drives in a RAID configuration for disk redundancy. These disks contain all of the TMSs software, FPGA firmware and configuration information. The system controller has dual Gigabit Ethernet interfaces, one connected to the Gigabit switch that communicates with the processing modules controllers and one connected to

the sites LAN for remote access to the system. All system configuration and maintenance can be carried out over the Ethernet network. The system supports the IPMI over LAN control interface for managing low level BIOS access if needed for complete software re-installation (fig. 4.21).

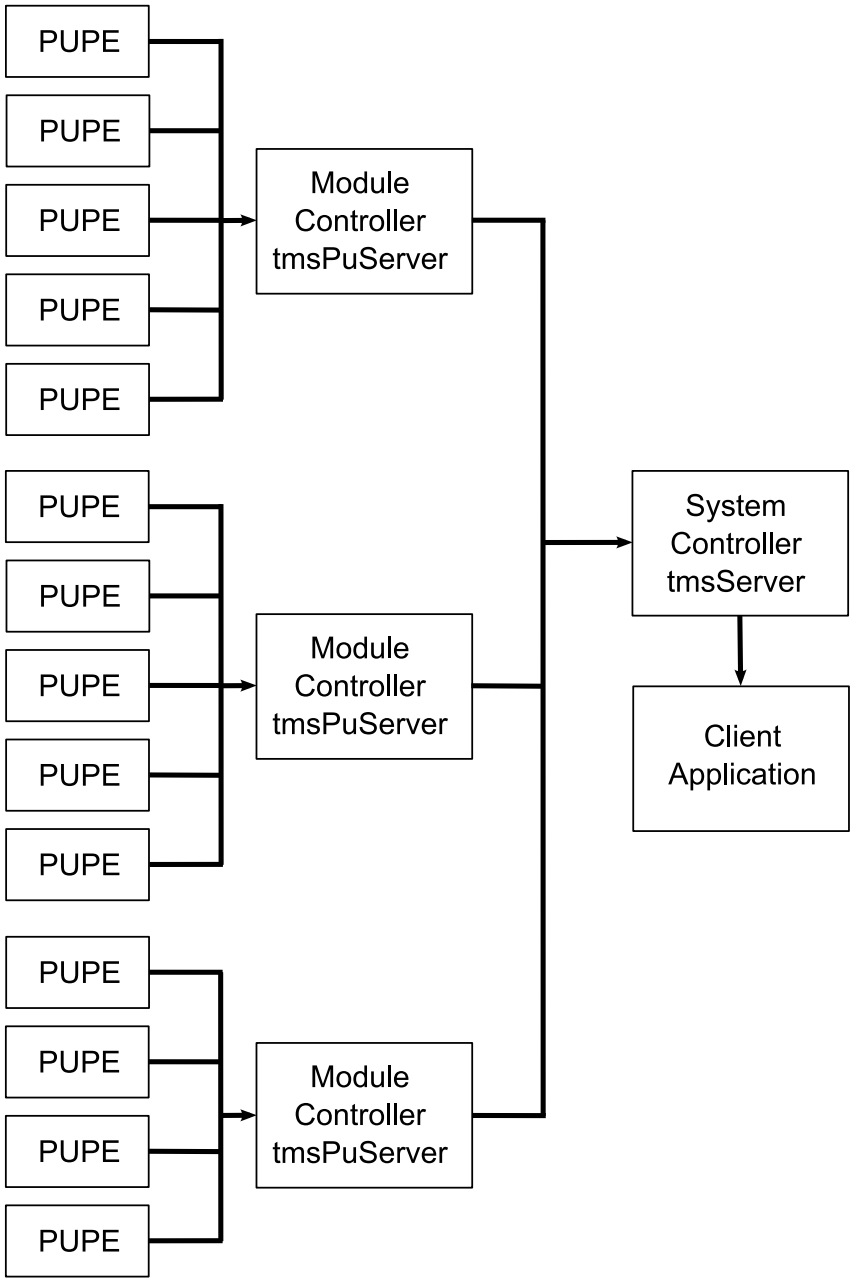

Figure 4.22: TMS Software

All of the system software is based on the Linux operating system. This provides a reliable and flexible system that can be easily maintained locally and remotely. All communications is through the system controller which supports a simple API to control

and gather data from the system. The system controller will interrogate the individual PU processing engines via the local Gigabit Ethernet network and the module controllers. CERN user interface software can control and acquire data across the network interface from a remote system via the network based API. The system controllers API accepts cycle information from CERNs system describing each Proton Synchrotrons machine cycle. This information allows the FPGA configuration to be correctly set and the data captured to be tagged with the appropriate cycle information. This information is distributed to all of the PU processing engines along with configuration data such as the position of the PU engine within the Proton Synchrotrons ring[10].

The TMSs API can be used across the network interface from a remote system or locally from applications running on the System Controller. The System Controller also supports a basic HTTP web interface for viewing system status and getting data. The software has been developed on the GNU/Linux operating system using the Open Source GNU toolset. The software is predominantly written in the C++ language[10].

From the softwares perspective there are four main modules in the system, the Pickup Processing Engine (PUPE), the Module Controller (MC), the System Controller (SC) and the Client Application (CLIENT) (fig. 4.22). The TMS has a private Gigabit Ethernet Network to which the Module Controllers and System Controllers are connected. The System Controllers have dual Gigabit Ethernet interfaces, one is connected to the TMSs private network and the second is connected to the CERN local area network.

The PUPE is the main module in the TMS system. It performs the analogue data capture and real-time data processing functions of the TMS. The PUPE is based on FPGA technology and is implemented as a cPCI board installed in a Compact PCI 19 inch rack. Each PUPE engine implements 3 pickup processing channels each having 3 ADCs. The PUPE is accessed via the cPCI bus from a cPCI Module Controller board.The PUPE FPGA boards are booted from the systems Module Controller (MC) using the standard Alpha Data FPGA boot protocol. Control and data access is implemented using the PUPE API across the 64 bit 33MHz cPCI bus.

The module controller is a conventional cPCI system controller. The Module Controller boots from the main System Controller (SC) over a Gigabit Ethernet interface and runs a small Linux based operating system. It is responsible for booting and managing the

5 PU processing engines (15 Proton Synchrotron PUs) on its cPCI bus. Communications between the SC and the individual PU processing engines is also be handled. The Module Controller runs the tmsPuServer program that implements a simple network based API, TmsPuApi, for control and access to the individual PUPE channels [3].

The client applications are CERNs system control and data gathering applications. These reside on different systems and communicate with the TMS through the CERN Control Network.

4.4 The limitations of used method, alternative solutions

The PLL- based approach of the beam frequency estimation copes well with slowly varying beam frequency, as well as high dynamic range of the input signal. But it still may have problems with locking to the signal when the initial frequency or phase is not set precisely. Another limitation is an excessive jitter caused by variation of the gate length when the frequency changes. The partial solution would be to increase the sampling frequency, at least twice. The 250MHz version of the measurement card is in under development (fig.4.23. The card will enable sampling at up to 1GS/s using 4 interleaved channels.

4.5 Usefulness for other accelerators of the method and hardware developed

The TMS system can be used to measure the position of the beam in virtually any circular accelerator. There were successful tests done with SIS18 machine in GSI.

The SIS18 is a fast cycling synchrotron that can be used for the acceleration of all kinds of ions. The accelerated ions can be delivered by fast extraction to the storage ring ESR (Experimental Storage Ring) or by slow extraction to the Target Hall (TH). The UNILAC serves as injector machine; in addition ESRbeams can be re-injected into SIS [9]. Compared to most accelerators, the SIS18 has some peculiarities a BPM system needs to address, like the large frequency span of the RF from 850kHz to 5Mhz, the high

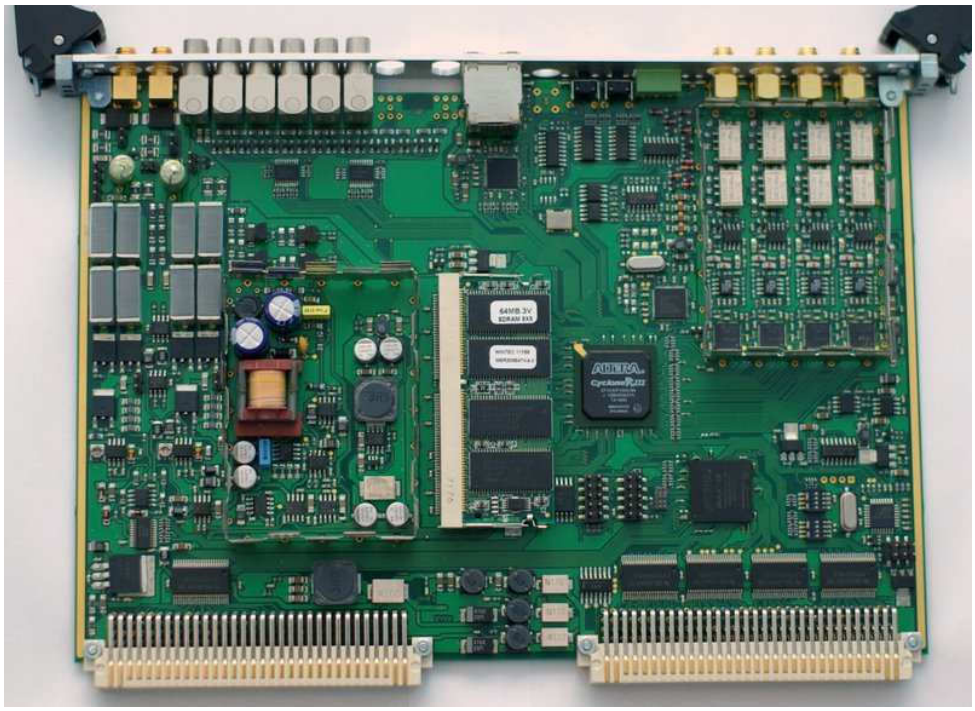

Figure 4.23: New, 4 channel acquisition card

signal dynamic, the injection of unbunched beams as well as the bunch length shortening of over one order of magnitude from some hundreds of ns down to 25ns[30]. The main difference in signal treatment is fact, that at the beginning of the acceleration cycle, the SIS18 does not have the bunch structure, therefore the bunch numbering is not possible. Moreover, in case of the SIS18, precision identification of the single bunch measurement result is not required. This simplifies the measurement process significantly.

4.6 Measurements and tests

4.6.1 Computer simulations with real data

The algorithm was tested by implementing it in the C-language and feeding it the raw data recorded using the prototype acquisition hardware.

Figure 4.24 shows a raw PU signal (EASTB beam) captured using Libera hardware, its baseline corrected version and the gating signal that was generated by the synchronization algorithm. The gate signal stays locked in phase with the beam pulses. The baseline restoration also works as expected.

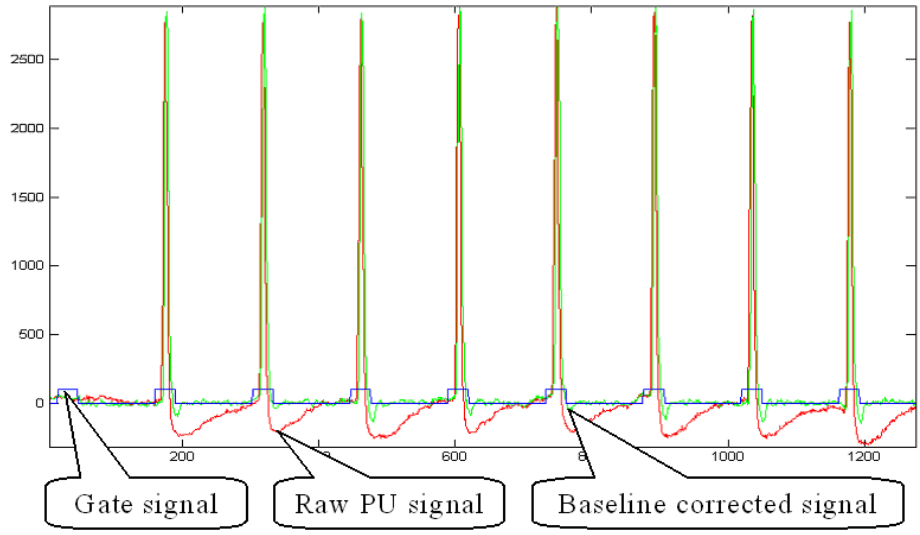

Figure 4.24: Real PU PLL signals

The position resolution of the system has been estimated by gathering some statistics on position measurements at a quiet spot in an EASTB cycle (single bunch, 10^11p+) (Fig 4.25). The true beam position was assumed not to vary over this roughly 250-turn interval.The RMS resolution is slightly better than 0.1mm.

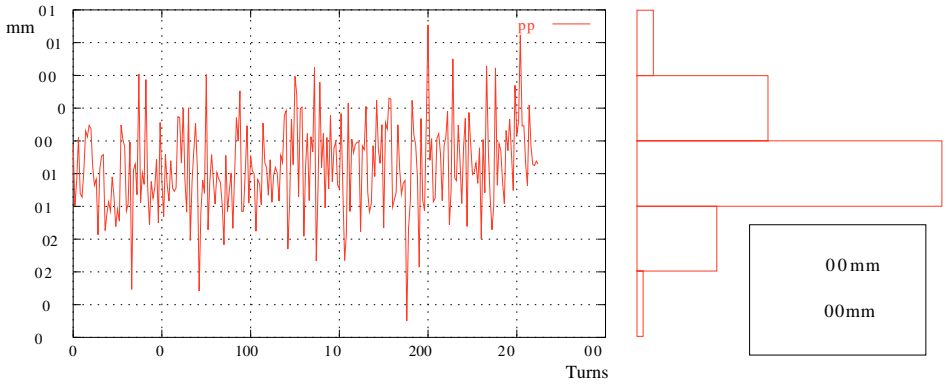

Figure 4.25: Positions and histogram over 250 turns on EASTB [19]

The algorithm after successful tests was implemented in VHDL language. Several simulation tests were performed with previously captured real PU data. The simulation was performed with Modelsim software. The fig 4.26 presents an example screen shot from the simulator. PLL lock-in state can be observed, the Local Oscillator signal is in phase with input signal (inverted). The signal below is the multiplier output.

In order to implement the algorithm in FPGA, several optimizations needed to be done. One of them was scaling of the data before and after the filter to avoid overflow. Another one was optimization of filter coefficients, so they were easily implementable in digital logics.

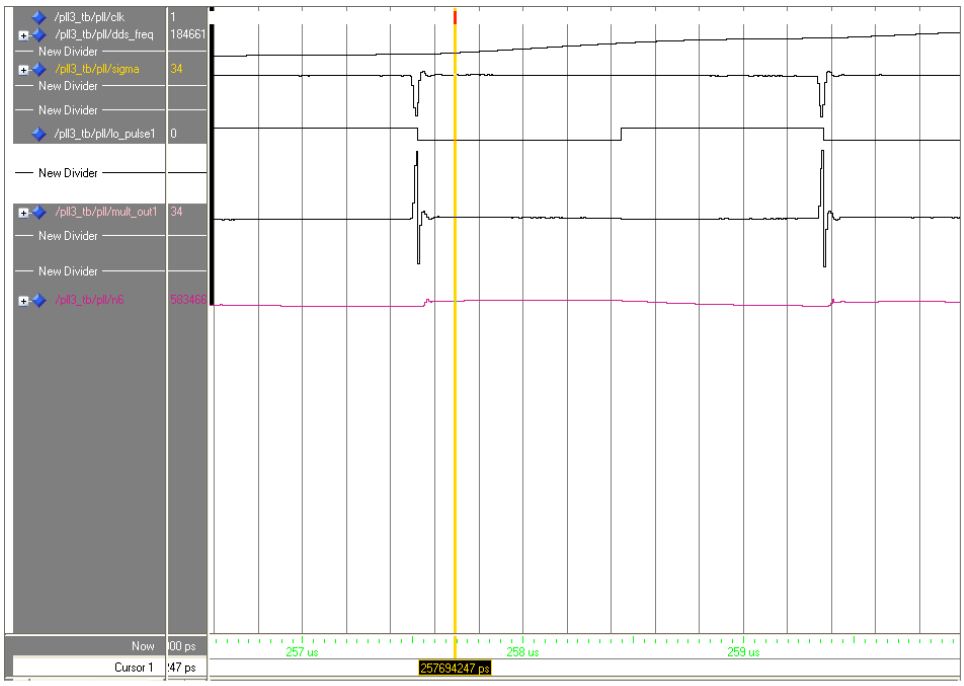

Figure 4.26: Modelsim simulations of the PLL

4.6.2 Laboratory tests

Before integrating with the accelerator infrastructure, several tests were processed in the laboratory. The Trajectory system was primarily implemented using Libera bunch processor and PCI test card from Alpha Data. Both solutions use Xilinx FPGA, so the same diagnostic utilities could be used. To quickly debug the algorithm with real hardware and beam signal simulated with generator, the Chipscope analyzer was used (fig. 4.27). The Chipscope analyzer utilizes FPGA resources to form a logic analyzer that communicates with FPGA through JTAG [‡] interface. The JTAG is connected with PC using Platform Cable USB II adapter.

[‡]Joint Test Action Group (JTAG) is the common name for what was later standarized as the IEEE 1149.1 Standard Test Access Port and Boundary-Scan Architecture. It was used initially for testing printed circuit boards using boundary scan. Today JTAG is also widely used for IC debug ports

Fig. 4.27 presents ChipScope analyzer window. Top section contains input sine wave signal produced by the generator and reconstructed Local Oscillator waveform. The LO signal is locked to the sine wave - each rising edge of LO resides in maximum of the sine wave. Bottom section contains DDS phase register - it overflows each time LO is generated. Triangle shape is caused by signed representation of signal that is unsigned in its nature. The ChipScope has also possibility to control a few registers inside FPGA. At the very early stage of the project, it was used to adjust the initial frequency of the PLL and start the acquisition. No other interface or software was required.

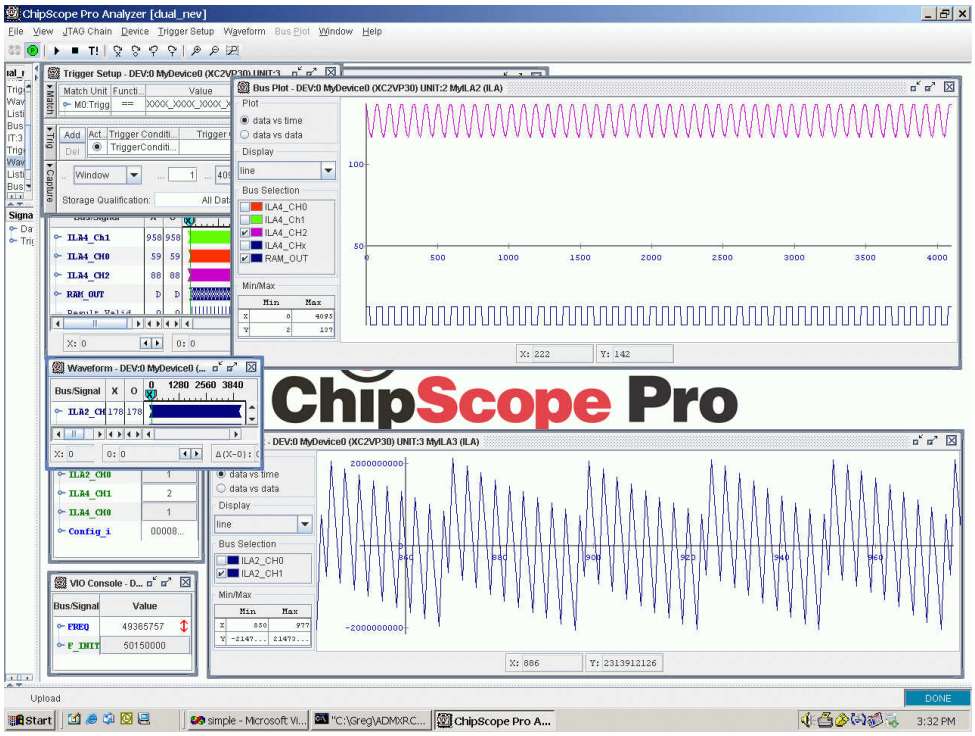

Figure 4.27: Chipscope analyzer signals

4.6.3 Real beam signal tests

Several tests with real signals from a single PU were performed in August 2006 on the CERN PS and in January 2007 on the GSI SIS-18. The results were captured using the embedded signal analyzer and simple control software running on embedded ARM9 processor with Linux operating system..

The evolution of the reconstructed revolution frequency (DDS frequency register content) during a full acceleration cycle was captured as well. Fig. 4.28 presents two slopes -

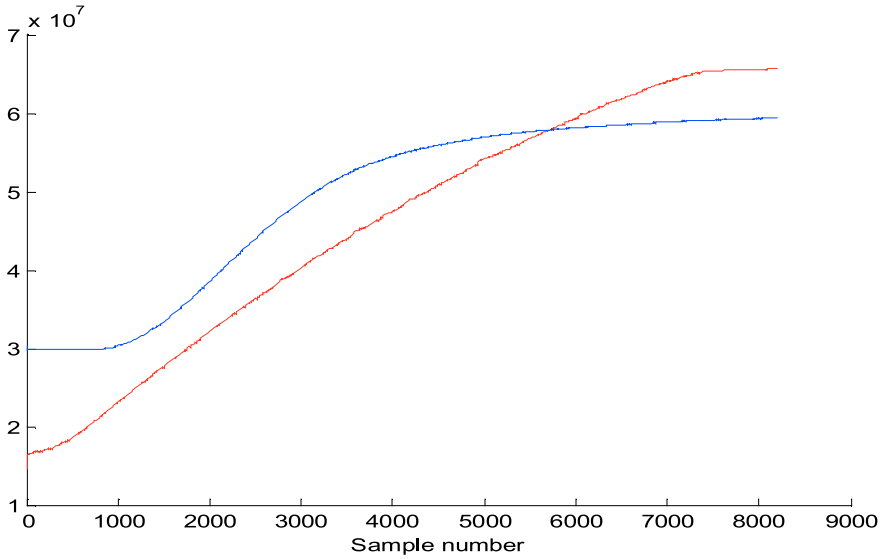

Figure 4.28: Acceleration slopes of SIS-18 and PS

the upper one is evolution of PS revolution frequency, the lower one - evolution of SIS-18 (GSI) accelerator frequency.

It clearly shows that the algorithm stays locked in case of both the PS and SIS-18 accelerator. At the PS the injected beam is already bunched by the preceding PS Booster and the algorithms locks to an external RF system until the beam is injected into the machine. As soon as the beam is circulating in the machine and PU signals are seen, the algorithm switches synchronization to the PU sum signals. In case of the SIS-18, the beam is injected from a Linac and is completely unbunched at the injection. The RF system bunches the beam shortly before starting acceleration. As soon as the bunch structure appears, the algorithm locks to the beam.

Figure 4.29 shows the measured sum (top) and horizontal difference (bottom) integration results, bunch per bunch. The position of the beam is then finally calculated off-line using these results. Enlarged part of the record is shown in fig 4.30 where betatron oscillations are observed at one of the PUs just after a kicker pulse. An off-line FFT can be used calculate the tune of the accelerator.

Next measurements were performed after successful installation and commissioning of the whole system in 2008 and 2009 year. Dedicated FESA [§]. software framework was

[§]FESA - Front-end Software Architecture developed by CERN for LHC and its injectors. The real-time front-end software architecture FESA is a framework used to fully integrate equipment such as power

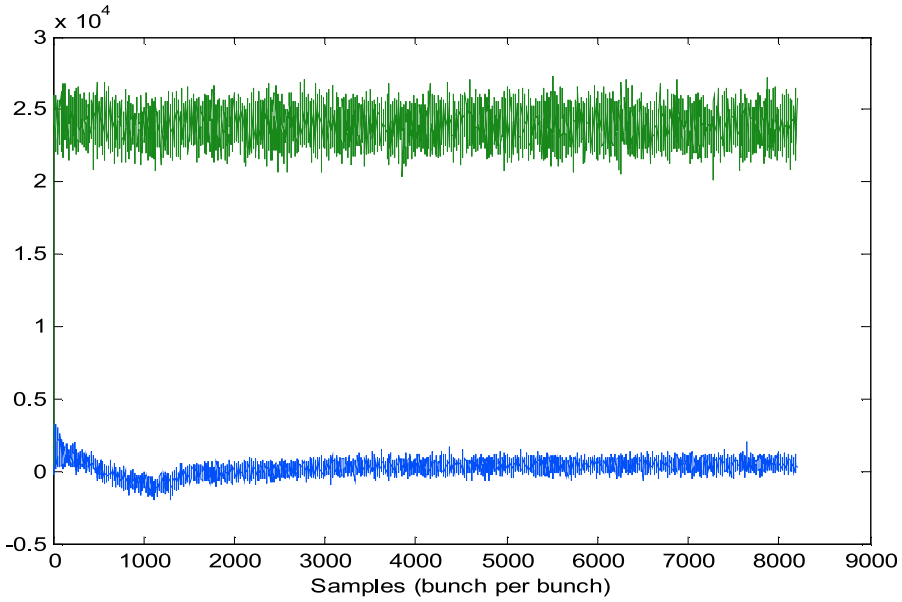

Figure 4.29: The sum and difference results

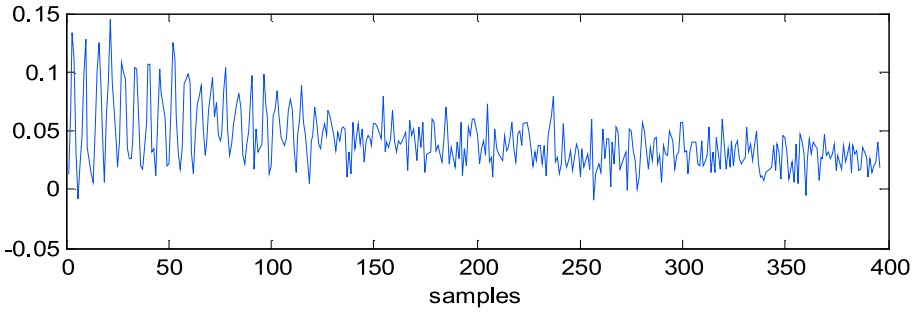

Figure 4.30: betatron oscillations

used to implement server application and Java based Graphical user interface. The FESA application allows many users to simultaneously access different measurements results from all the pickup. Before the results can be available, user has to select interesting beam type (beam user), subscribe to it and wait for next occurrence of the accelerator cycle.

The server based on CERNs FESA mediates between the TMS and control room applications. The FESA server is responsible for informing the TMS of the accelerating cycle

supplies, PLCs or beam diagnostic devices at the front-end level into the CS (Control System). The output product of this framework is a so-called equipment class. FESA provides JAVA based graphical user interfaces (GUI) to design, deploy, instantiate and test the equipment classes[31]

to be treated at the appropriate time, and for collecting and publishing data requested by the control room operators. It also controls BPM pre-amplifier settings, maintains and applies calibration data and provides access to diagnostic information. It runs on a processor installed in a separate VME crate, with network connections to both the TMS private segment and to the accelerator control network.

Figures 4.31 and 4.31 present horizontal and vertical mean radial position (averaged position from all PUs) until ejection. All the operations performed on the beam like injection, ejection,harmonic change, acceleration can be easily identified on horizontal. First positive bump reflect the moment of beam injection. Next, negative one - start of acceleration, where magnetic field is ramped up. Big positive peak at the end of the record is caused by the ejection of the beam - the kicker magnet is turned on and the beam is directed to the transfer line. Most of the position changes appear on the horizontal plane only - since all the beam transfer lines are aligned at the same level, no additional operations are performed on the beam in this direction. The monitoring of the vertical position has mainly diagnostic purposes in case of emergency.

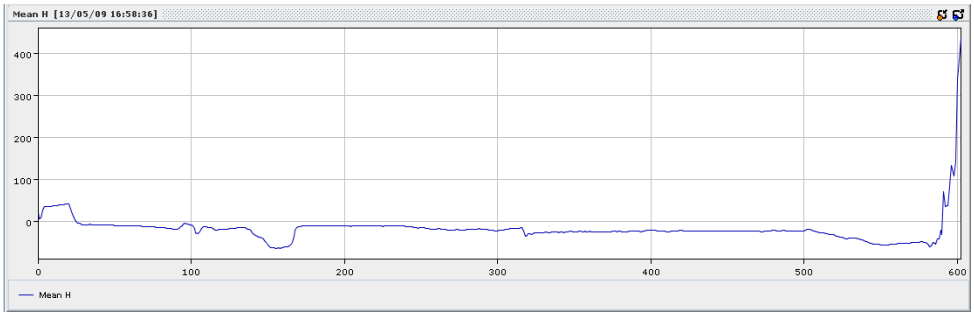

Figure 4.31: Horizontal Mean Radial Position

.

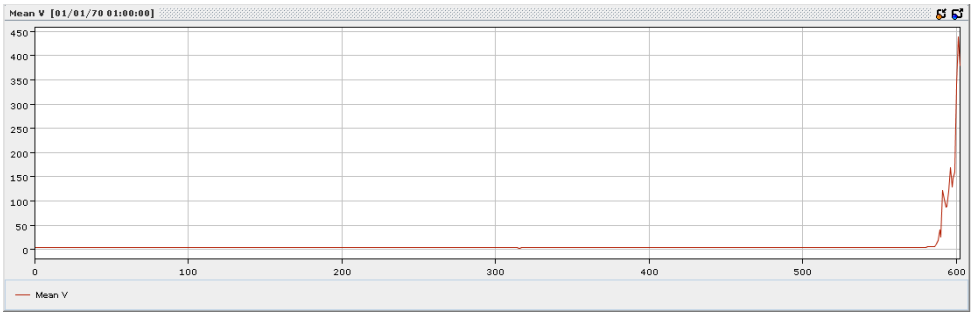

Figure 4.32: Vertical Mean Radial Position

Figure 4.33 presents horizontal trajectory (bunch per bunch mean position) for all the pickups during all the acceleration cycle until ejection. The same phases as in previous case are visible. Each PU is represented as separate color plot. This figure allows quickly diagnose status of the magnets, PUs since any serious fault causes large displacement on one of the PU plot.

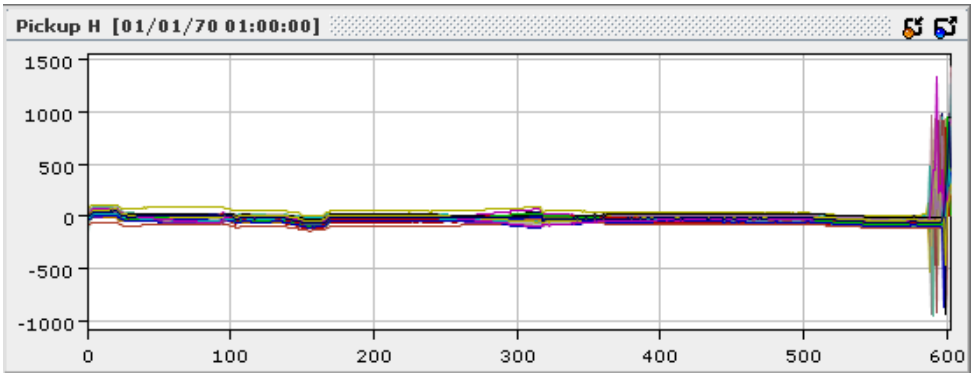

Figure 4.33: Trajectory along the cycle

Figures 4.34 and 4.35 present view of vertical and horizontal orbits for each of 5 filled bunches. It can be noticed, that variations of the beam in vertical direction are about 5x smaller than in horizontal direction. The displacements are caused mainly by the mechanical positions of the PUs. The 17-th PU is located close to the injection point, and big deflection is probably caused by the kicker action.

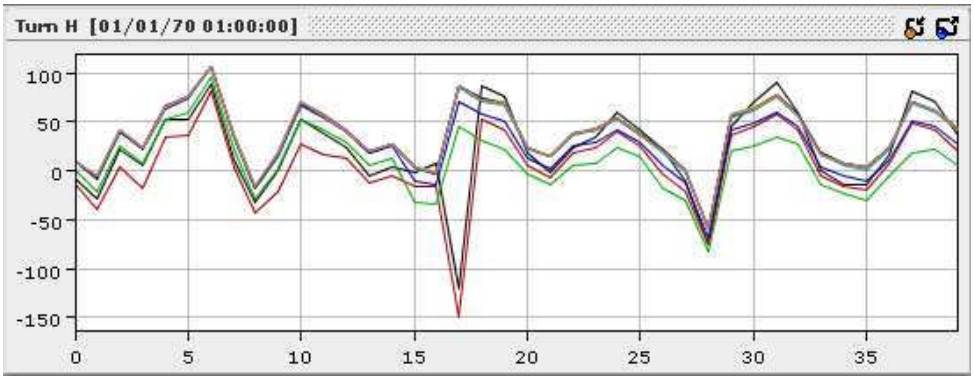

Figure 4.34: Horizontal orbit for 5 bunches

.

The kicker operation is visible precisely in figure 4.36 which presents orbit for first 20 turns, with visible injection at pickup 17. During first turn, the position of the bunch is

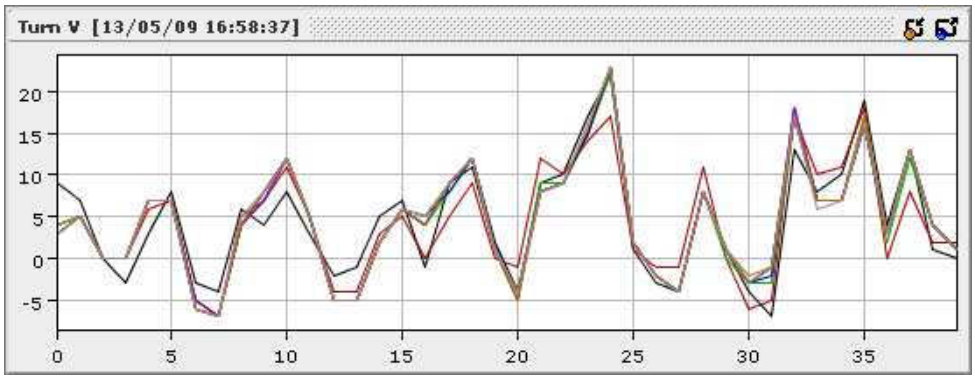

Figure 4.35: Vertical orbit for 5 bunches

displaced. The kicker also affect the bunches during next 19 turns turns. During the first few-hundred turns, it makes large excursions around its equilibrium orbit.

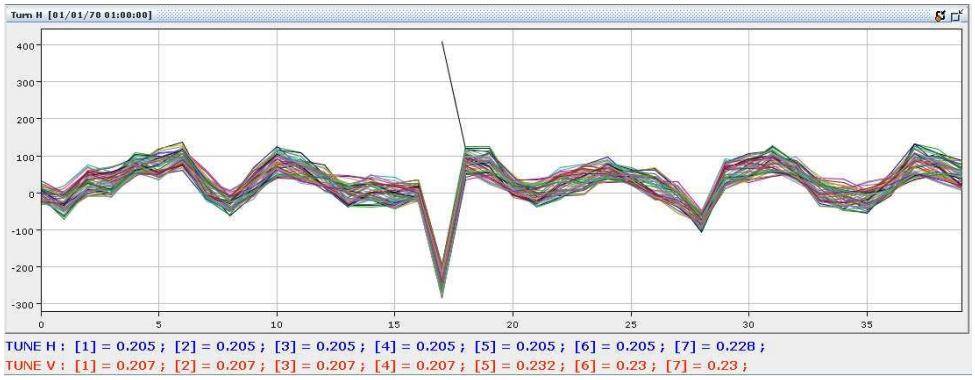

Figure 4.36: Horizontal orbit for the first 20 turns with the injection at pickup 17

Figure 4.36 presents horizontal orbit along the cycle with visible harmonic change (center of the plot). The operation of the algorithm is still imperfect during transition while harmonic changes. Where harmonic change starts, the more bunches split, the less gate signal covers them in the beam signal. This obviously leads to error in sum calculation and displacement of the measured position. At certain moment, the acquisition is stopped, PLL switches to RF as the synchronization signal and algorithm waits until end of harmonic change. When bunch structure can be identified with new harmonic number, acquisition is turned on and continues. This moment is visible at the position 310 where small jump occurs and displacement decreases.

The diagnostic capabilities of the TMS system were described in chapter 4.3 In fig 4.38 there is presented example screen shot of the diagnostic utility - the FESA application Expert GUI tab. There are visible following signals:

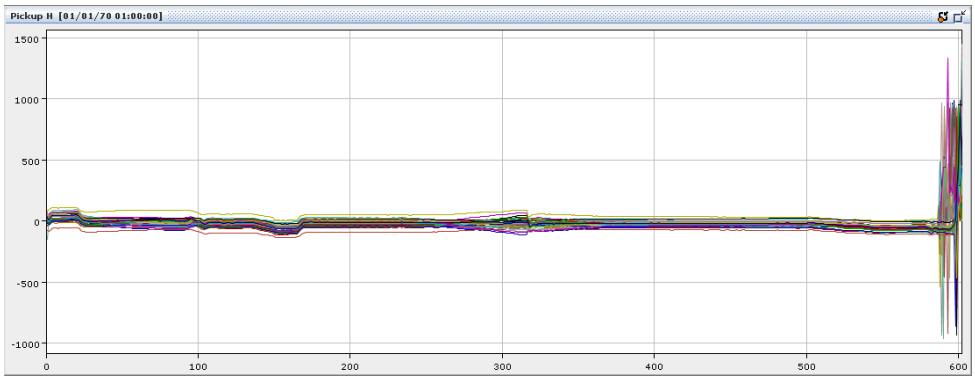

Figure 4.37: Horizontal trajectory along the cycle with visible harmonic changes

- LO,
- PU,
- BLR,
- GATE.

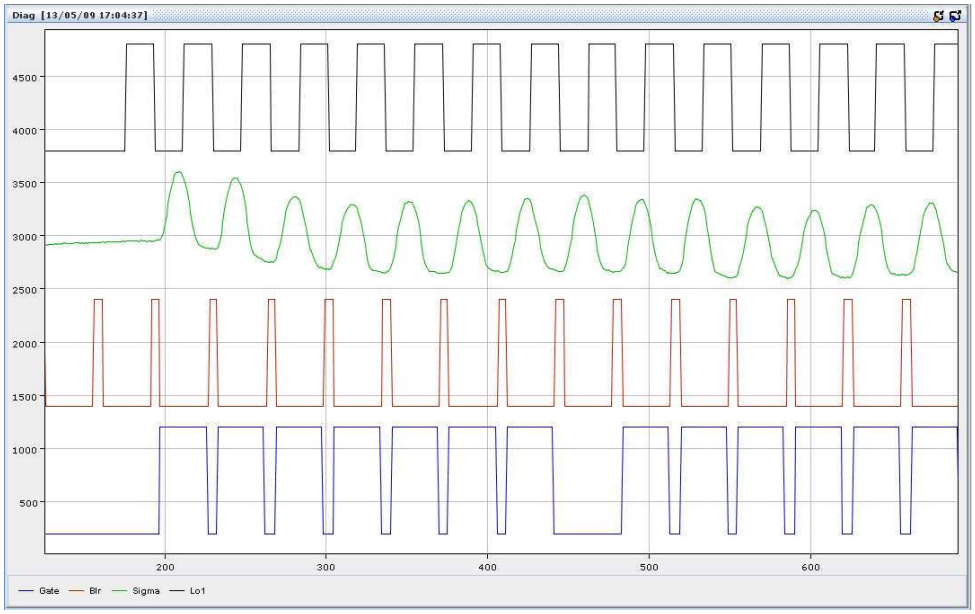

Figure 4.38: Diagnostic signals of the PLL for the SFTPRO beam

The PLL system Local Oscillator (LO) is properly synchronized to the beam - its rising edge occurs in a middle of the beam pulse. This diagnostic utility is used also during standard setup of the initial condition of the algorithm. Since it is part of user application, the proper operation of the system can be quickly verified and alignment of the gate and

BLR pulse corrected when necessary. Such correction is necessary after changes in timing or RF system of accelerator. Old trajectory measurement system system required in such cases physical presence at the place where acquisition hardware is installed and manual adjustment of the timings using connected oscilloscope and usually took several hours of work.

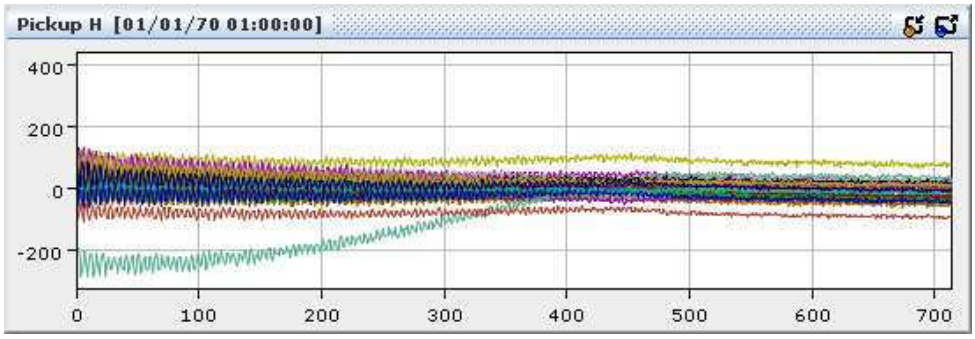

Figure 4.39: Horizontal trajectory for the SFTPRO beam

Figure 4.39 presents horizontal trajectory of a P+ bunch in PU43 for the all the buckets of the SFTPRO beam over 700 turns starting from injection, showing injection oscillations and the collapse of the injection bump.

Parameter	Old system (CODD)	New system (TMS)
Accuracy	0.3mm	0.3mm
Number of simultaneously tracked bunches	2	not limited
Trajectory measurement	1 user	not limited
Orbit measurement	1 user	not limited
Update rate	5ms	not limited
Harmonic change handling	limited	good
Occupied space	5 racks	1 rack
Calibration	yes	yes

Table 4.2: Trajectory measurement system summary

Short comparison of new and old systems is presented in table 4.2. The presented results only partially show robustness and performance of the new Trajectory Measurement system for CERN PS. The system has been demonstrated to have no trouble delivering over 700000 points of trajectory data, or full-cycle turn-by turn positions from selected PUs. Its multi-user oriented architecture and platform independent (Java) control interface cancels out all the limitation of the previous system. Utilization of programmable logic and opens possibility of further improvements.

Chapter 5

The methods and algorithms for beam intensity estimation

5.1 Requirements of the beam intensity measurement for PS

The intensity measurement system is required to measure intensity of all the individual bunches over first 1000 turns after the injection. There should be no limitation in using this system also for measurement of the intensity at any moment of the acceleration cycle [25]. The TMS system implementation assumes utilization of existing hardware available on the market (requirement of EU project) whereas intensity measurement needs development of dedicated VME module equipped with BCT calibration pulse generator. Moreover, existing calibration method needs to be upgraded because it does not meet the requirements in terms of accuracy and user friendlies.

5.2 Existing solutions and limitations

The existing intensity measurement system (5.1) consists of a device called "6 turn transformer" and precision DC transformer. The 6-turn measurement utilizes a set of 6 integrators and the VME-based timing generator. The integrators are gated analogue devices, without any offset compensation nor baseline restoration. Figure 5.2 presents typical

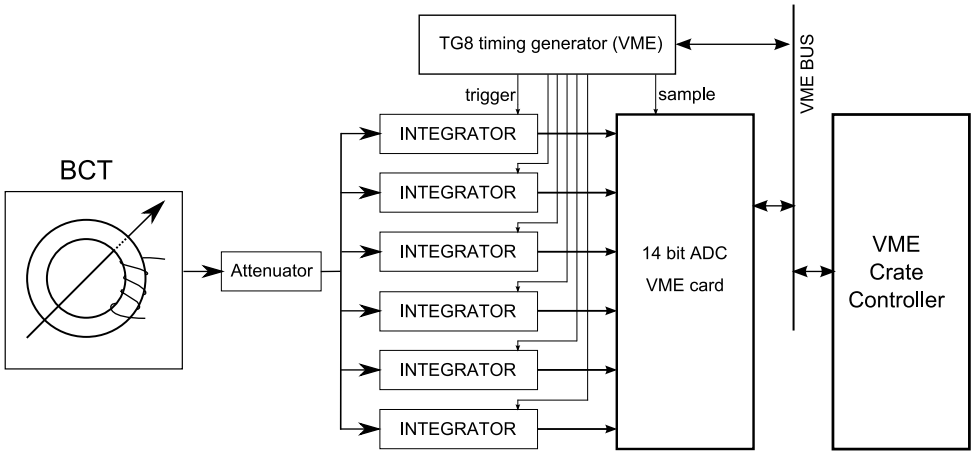

Figure 5.1: Existing 6-turn intensity measurement system

signal from the transformer. Such signal, in existing system, is integrated without the baseline correction which leads to the inaccurate measurements, especially for the first 3..4 turns.

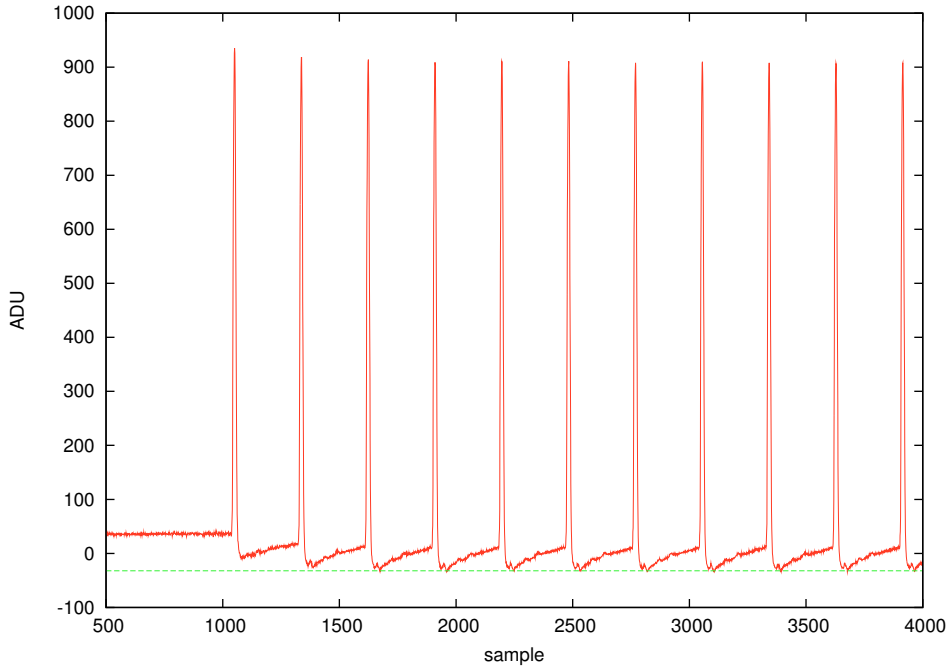

Figure 5.2: 6 turn transformer signal after injection

The idea of precision measurement of the beam intensity using that transformer, assumes that the signal has the baseline restored before the integration. The integration gates would be synchronized and derived directly from the beam signal since there is no precision timing signal which could be used to easily compute all the gates for first

thousand of turns.

5.3 Usage of numerical Phase Lock Loop for tracking of the beam revolution frequency

5.3.1 The synchronization algorithm

Due to the fact that intensity measurement system requires precise adaptation of the algorithm to the beam frequency, and each revolution of each bunch must be undoubtfully identified after the measurements, this implies a method with recovery of the bunch frequency.

Other possible methods based on generation of the integration gates from the signal itself were mentioned in chapter 4.3.

One of the most widely used methods of synchronization of the local generator to an external varying signal source is a Phase Locked Loop (PLL) . Its operation is based on continuous comparison of the phase of the local oscillator (LO) to the phase of the external signal, and such control of the LO frequency to keep the phase difference between them as small as possible. The PLL solution used in case of Intensity measurement system is very similar that one in TMS. The method used for this purpose is described in chapter 4.3. The difference is in the method of generation Gate and BLR pulses.

5.3.2 The BCT signal treatment

The BCT, with its load resistance, yields a high-pass filtered version of the instantaneous beam current(Fig 4.5).

This leads to distortion of the BCT signal baseline. Figure 4.6 presents an example beam current as it is passing through the BCT. Since it is usually non-periodical, its DC components varies significantly compared to the pulse amplitude.

Since the baseline effect is caused by the high pass character of the BCT, the correction can be done using the complementary low-pass filter which would compensate the signal distortion for lower frequencies. Exactly the same method was used in case of PU (chapter

4.3.2). The main difference is the cut-off frequency which is lower resulting in the change of the coefficient value in the low pass filter.

Proper operation of both the integrator and DC offset compensation circuit, require precision reference pulses, which are generated by the numerical PLL block.

5.3.3 Implementation of numerical Phase Lock Loop for tracking of the beam revolution frequency

The algorithm is actually independent on the target hardware used. It has been implemented on 2 different hardware platforms, all of them providing fast 12..14bit ADCs, large field programmable gate arrays (FPGAs) and fast memory.

The first platform, Libera (Fig 4.9) available on the market from Instrumentation Technologies was used mainly for laboratory tests and used to capture real beam data useful during algorithm development. Detailed description of the hardware contains chapter 4.3.3.

The second hardware platform was build as a dedicated VME card to support the BCT-based measurements. The Transformer Integrator Card (TRIC) card (fig.5.3) was originally developed as a digital integrator for PS Booster transfer line transformers [24]. But due to its flexibility it was used for the PS intensity measurement as well. The adaptation required an implementation of the PLL algorithm in the FPGA.

The card is equipped with dual 12 bit, 212MS/s ADC, big FPGA, VME bridge, memory module and dual current/charge calibrator (5.4). It provides an integrated solution for BCT related measurements. Due to the solid state construction of the calibrator, it allows continuous calibration of the measurement chain including the BCT. Existing high-current calibrators contain relays which have limited lifetime and are hardly able to sustain a few millions of cycles. The calibrator is capable of generating signals reaching 4A at 200V. To increase the accuracy, the current which is being injected to the BCT is additionally measured using a 12 bit ADC. To simplify the power supply of the card, an embedded high voltage DC/DC converter was integrated as well. A next version of the card, equipped with 4 ADC channels is under development. It will allow direct processing of the position pickup signals. In order to enable remote FPGA firmware update, the TRIC card was equipped with a CPLD bridge that translates VME bus requests to the

local bus transfers. It also configures the FPGA and provides a serial link for debugging purposes.

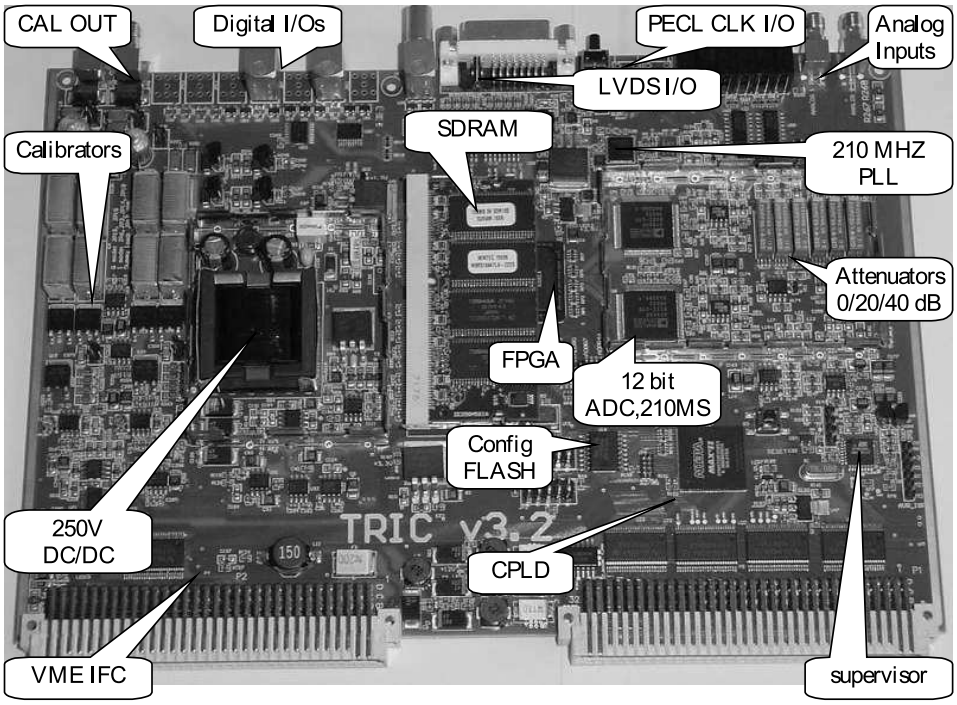

Figure 5.3: The TRIC acquisition card

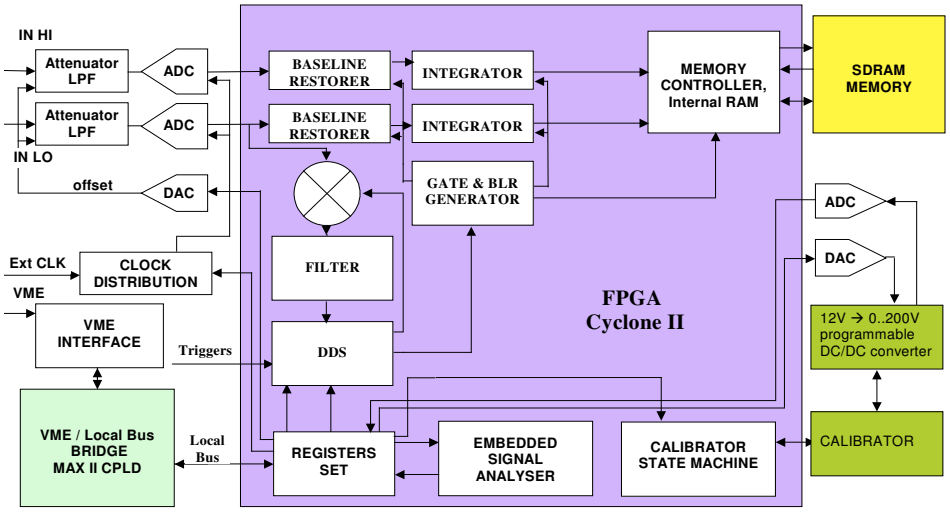

Figure 5.4: The TRIC acquisition card block schematic

In order to enable easy migration of the algorithm between different hardware platforms, the signal processing was implemented in VHDL using general adders/ register, without using vendor dedicated FPGA resources like multipliers, shifters or DSP blocks.

The ADCs and all the processing logic run at 112.5MHz clock rate and the FPGA internal data bus is 24 bits wide. They are driven by a low-jitter clock generator. More information about ADC clock requirements contains chapter 4.3.3. The TRIC card is equipped with dedicated, programmable low jitter clock generator. The generator is freely programmable, so the frequency and phase of the ADC clocks can be easily changed. This opens possibility of paralleling input channels in order to work in the interleaved mode resulting in twice higher effective sampling rate.

A timing reference to produce the Gate and BLR signals must be derived from the Σ signal by locking to it with a locally produced frequency, using a numerical Phase Locked Loop (PLL). The PLL used is very similar as in case ot the TMS. The main difference is absence of the phase table.

In case of the intensity measurement, a slightly different approach was used. Since during first 1000 turns the harmonic number does not change and the revolution frequency is practically constant, the PLL can run at the bunch frequency instead of the revolution frequency. This simplifies the generation of Gate, BLR and LO signals. Instead of the phase table, a simple comparator and the timer can be used for BLR and Gate. As the LO signal, the MSB of the phase accumulator can be used (Fig 5.5).

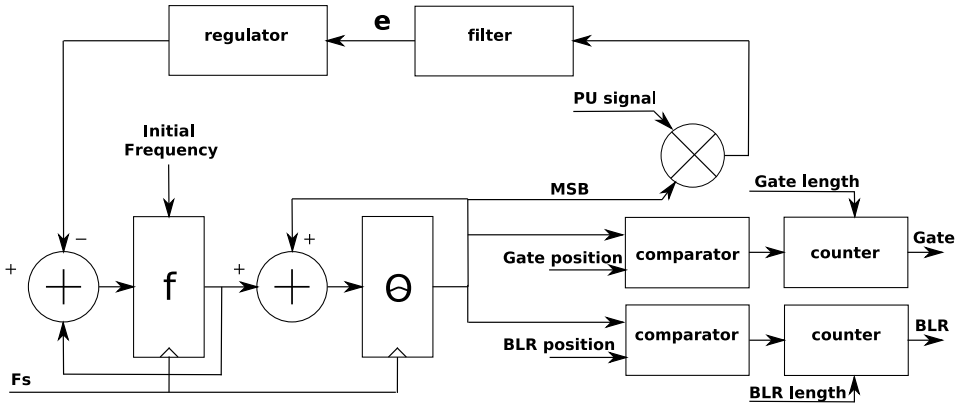

Figure 5.5: Reference frequency generation principle for intensity measurement

The Gate and BLR pulse generation with utilization of counters has an advantage - the pulses lengths are always the same. In case of the phase table generation method used in TMS, their length varies by one clock cycle in random way. It is caused by the fact that phase table is incremented by a non-constant value stored in the frequency accumulator.

This inherently introduces additional measurement noise.

In case of the position measurement, the same gate length (and jitter) is applied to the Σ and Δ signals. So such generated noise in all the channels is correlated. Due to the correlated character of the noise, its value in position result is suppressed. In case of the intensity measurement, there is only one integration channel used, so all the methods which are able to limit the readout noise are very welcome.

The BCT signal has a LF cut-off frequency of 100 kHz, resulting in a baseline that is not at zero potential. In order to get an accurate integral, the baseline must first be restored. This is done by passing the samples through a numerical low-pass filter with a characteristic that is complementary to the high-pass response of the analogue channel, extending the lower cut-off frequency down to DC. The signal treatment is described in chapter 4.3.2.

The input signal, after baseline restoration, is fed into one numerical integrator which calculates the sum. The results are stored in 8192-entry SRAM memory. Depth of the SRAM allows storage up to 8192 turns. In case where harmonic number is higher than 1, there are stored 8192/h turns.

The results from the SRAM buffer are then read out on user request and processed further in software running on a remote machine. Since there is no way to pre-calculate the exact phasing of the beam signal with respect to the externally applied $TRIG$, it is necessary to align the phases of the LO, the $Gate$ and BLR signals manually during system setup. It was also necessary to inspect the phase error and the frequency to make sure the loop locks reliably. This is a task for data logger (signal analyzer) There also are diagnostic facilities that provide remote access to recordings of critical algorithm signals. Users can set triggers, choose delay times and signals to be recorded. It allows capturing the chosen signals on different time scales (fig 4.17). It is controlled by FESA advanced user tab.

The integral over the length of each bunch is found simply by adding together the samples belonging to a given bunch. Attempts were made to implement a more sophisticated integration like the triangle method. But the difference of results in terms of accuracy and measurement noise were negligible. The synchronization system tells which samples are to be taken as part of a bunch, using a Gate signal. The length of the Gate

signal is not very critical, because it starts and ends when the beam signals are near zero. Integration is also applied to both signals.

5.3.4 Intensity measurement system control software

In case of beam intensity measurement system, the dedicated FESA application was created in order to display debugging informations and measurement results. This application is part of CERN control system. FESA provides both driver which communicates with the hardware, an application that runs on the VME crate controller and provides synchronization of the card with accelerator timing system, and GUI written in Java which displays results and provides interaction with the user (fig.5.15, fig.5.17). The crate controller is connected to CERN control network, a dedicated trusted network which transfers only instrumentation data.

5.3.5 Calibration of the measurement system

Existing calibration system

To enable precision intensity measurement, the signal chain needs to be calibrated. The existing solution uses a manually triggered and adjusted calibrator with a mechanical switch. A known capacitor charged to known voltage is used as a reference which gets discharged to the calibration turn (fig 5.6). Rt is used to match the transformer impedance to the cable.

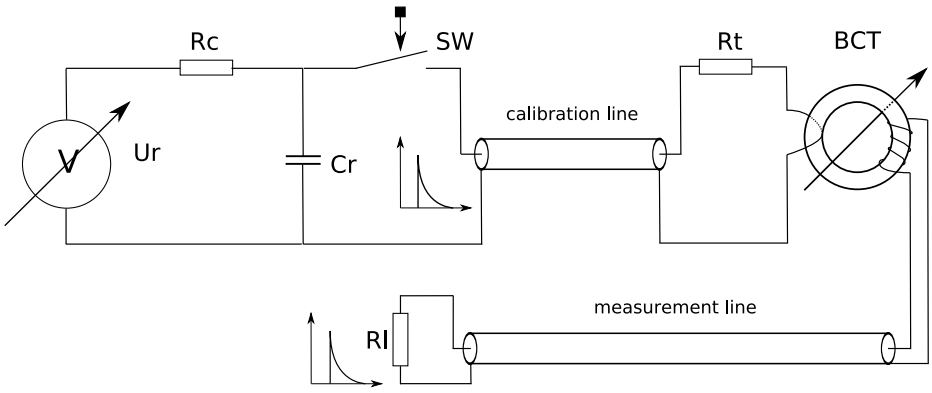

Figure 5.6: existing BCT calibration scheme

Main limitation of the method used is the mechanical relay SW which has limited life-time. Moreover it introduces a delay which is variable with temperature and time. It needs to be evaluated if the calibration cable attenuation, represented as resistive losses, does have an influence on the calibration accuracy.

The charge collected in the Cr capacitor is:

$$Q_c = C_r \cdot U_r \tag{5.1}$$

The amount of the charge injected into the transformer

$$Q_{inj} = \int_{t_0}^{t_f} i dt = \int_{t_0}^{t_f} \frac{u_c}{R_t} dt \tag{5.2}$$

The function of the current in time is exponential, with an $R_t \cdot C_r$ time constant, so the capacitor voltage is:

$$u_c = U_c \cdot e^{(-t/R_t \cdot C_r)} \tag{5.3}$$

Since the total charge injected to BCT needs to be obtained: $t_0 = 0$, $t_f = \infty$:

$$Q_{inj} = \int_0^{\infty} e^{(-t/R_t \cdot C_r)} dt = \frac{U_c}{R_t} \int_0^{\infty} e^{(-t/R_t \cdot C_r)} dt = \frac{U_c}{R_t} (R_t \cdot C_r \cdot e^{-t})|_0^{\infty} = \frac{U_c}{R_t} \cdot R_t \cdot C_r = U_c \cdot C_r \tag{5.4}$$

So the calibration result theoretically should not depend on the resistive loses in the calibration cable as well as value of R_t.

Taking into account the drawbacks of the existing calibration system, the new one should be completely solid-state design, possibly with a high precision current source. The calibrator needs to simulate beam intensity varying from $10^{10}..10^{13}$ particles. Assuming a length of the calibration pulse to be approximately $0.5\mu s$, this corresponds to the maximum peak current (5.5):

$$i = \frac{q}{t} = \frac{N_p \cdot e}{t} = \frac{10^{13} \cdot 1.602 \cdot 10^{-19} C}{0.6 \cdot 10^{-6} s} = 3.204 A \tag{5.5}$$

where e is an elementary charge, N_p is a number of charges . Since the BCT termination resistance is 50Ω this corresponds to the maximum peak voltage (5.6):

$$u = R \cdot i = 50\Omega \cdot 3.204A = 160.2V \tag{5.6}$$

So the practical implementation of the current calibrator should deliver about 4A of pulse current at 200V to the 50Ω load to cover additional loses of the cable.

New calibration system

To satisfy requirements on the precision of beam intensity measurements, the whole system needs to be calibrated. Due to the requirements for current ranges for BCT exceeding 3A at 200V the standard approach with linear current source cannot be used. The losses on active components would be unacceptable. Two calibrator circuits were implemented: the charge calibrator and the constant current calibrator. Both solutions are able to deliver pulses simulating the maximum beam intensity.

The charge calibrator, which utilizes capacitor with precisely known capacity charged to a known voltage, has very high requirements for precise impedance matching to the calibration turn of the BCT. In some cases, specially of old transformers such a calibration method generates oscillations and reflections, which affect the calibration accuracy. This was one of the reasons, why an alternative method was developed. The current source method allows injection of relatively long current pulses. The integration gate can be opened after the transients and oscillations calm down and closed before the calibration pulse is switched off.

The charge calibrator utilizes similar approach as existing one (fig 5.6). The main difference is the type of the switch used. Due to the limitation of mechanical switches, a solid-state high voltage MOSFET was used. Since the measurement system accepts both negative and positive signals, it was more convenient to build the calibrator delivering negative pulses. Their polarity can be easily changed by swapping the BCT calibration turn connections. Moreover, the new calibrator is remotely controlled due to the fact that it is embedded into the intensity measurement system VME board. The calibration voltage as well as the trigger can be easily adjusted remotely.

As it was shown in equation 5.4, the charge is conserved even in case of calibration cable resistive losses. Since the measurement result is usually presented in form of number of elementary charges, the calibration factor can be obtained in the following way:

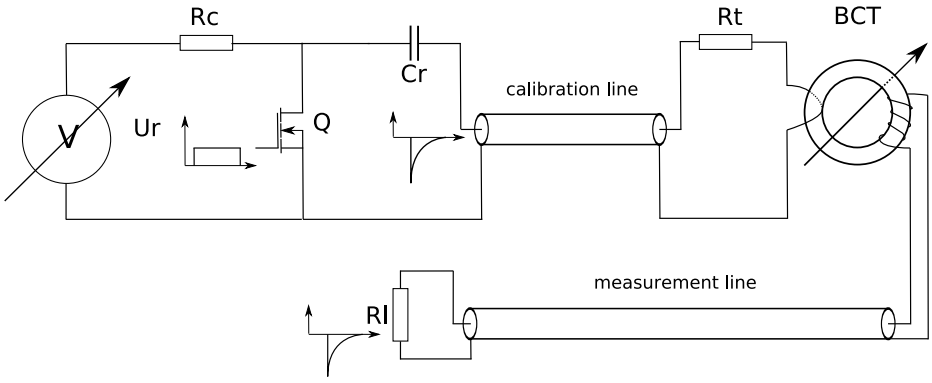

Figure 5.7: New charge calibrator

The number of charges N_c that corresponds to the charge of capacitor C_r charged to V_r is:

$$N_c = \frac{C_r \cdot U_r}{e} \tag{5.7}$$

This value corresponds to the integral of the calibration pulse measured. Since the measurement system has a discrete time, the integral of the pulse is represented by the sum.

$$I_c = \sum_{n=0}^{Gate} S_i(n) \tag{5.8}$$

where I is an integral, $Gate$ is the last sample of the input pulse, S_i is the input signal.

In order to know the relationship between the integral of the pulse and real number of charges, the integral needs to be multiplied by the calibration factor. The factor k is calculated from formula:

$$k = \frac{I_c}{N_c} \tag{5.9}$$

where I_c is an integral of calibration pulse, N_c is equivalent number of charges of stored in calibrator capacitor.

So, the measurement result expressed as number of charges N_p can be expressed by:

$$N_p = \frac{I_m}{k} = I_m \frac{N_c}{I_c} = I_m \frac{C_r \cdot U_r}{I_c \cdot e} \tag{5.10}$$

where:

C_r is a calibrator reference capacitor,

U_r - capacitor voltage,

I_m - measurement signal integral,

I_c - calibration pulse integral,

e - elementary charge.

The measurement system optionally performs the calibration after each measurement. The calibration factor can be updated on request.

The constant current calibrator (fig 5.8) uses a high current programmable current source (Q3). Its current is defined by a DAC. To limit the losses to a reasonable level, the current source operates in switched mode. The operational amplifier based precision current source requires some settling time after connection to the load. To get rid of the transients, a differential switch (Q_1, Q_2) was added. The Q1 is switched on for about 500ns to connect a dummy load (R_l) to the source. After the current reaches its desired value, Q_1 is switched off and Q_2 is switched on to enable the current flow to the BCT. The diodes prevent the current that charges the output capacitor against flowing through the load. The amount of the current injected into the transformer is directly measured using an ADC connected to the reference resistor R_r. This also compensates an offset of the high speed amplifier (OA).

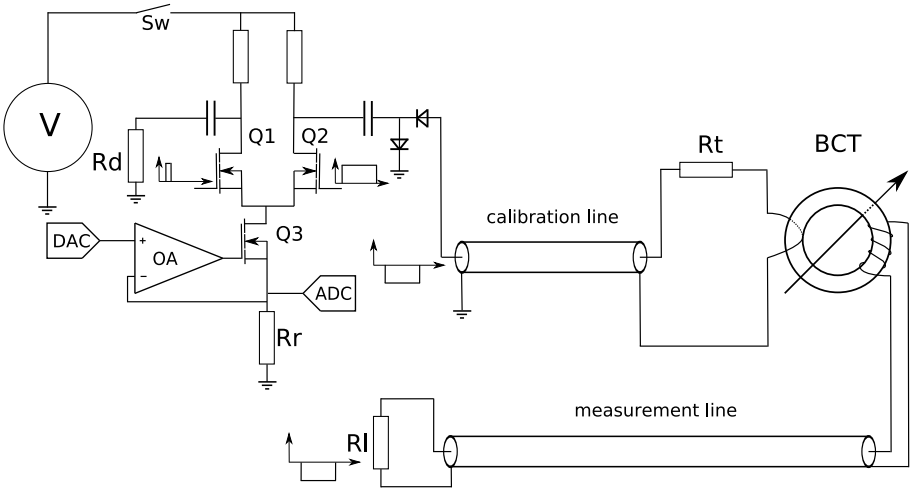

Figure 5.8: The current calibrator

5.4 The limitations of used method, alternative solutions

The PLL- based approach of the beam frequency estimation copes well with slowly varying beam frequency, as well as high dynamic range of the input signal. But it still may have problems with locking to the signal when the initial frequency or phase is not set precisely. Another problem was identified: at high harmonic numbers, i.e. 8 or 16, the bandwidth of the transformer does not allow to clearly distinguish bunches from neighboring ones. This is critical for the Baseline Restoration Circuit. Since the reference levels are not clearly defined, the input signal has some DC component and integration results are erroneous. This issue was solved by parallel operation of a second channel of the TRIC module, connected to the Wall Current Monitor (WCM). Since the WCM has a bandwidth of a few GHz, the pulses can be clearly distinguished even in case of high harmonic numbers. Unlike BCM, the WCM does not possess any calibration capability. This drawback can be solved by cross-calibration with the BCT.

5.5 Usefulness for other accelerators of the method and hardware developed

The intensity system can be used to measure the position of the beam in virtually any circular accelerator. The only requirement is standard VME crate and trigger signal. In GSI, Germany there are tests of complete intensity measurement system based on TRIC and attempts to adopt it to the requirements of their control system.

The custom TRIC module is also used with a much simpler algorithm to measure intensities at the PS Booster transfer lines, as well as at nTOF * experiment. Since the timing structure of the incoming BCT pulses are known in advance, it was possible to eliminate the complicated PLL algorithm. The gate pulses are generated using block a of

*nTOF - Neutron time-of-flight measurements. The goal of the nTOF is to provide unprecedented precision in neutron kinetic energy determination, which will in turn bring much-needed precision in neutron-induced cross-section measurements. Such measurements are vital for a range of studies in fields as diverse as nuclear technology, astrophysics and fundamental nuclear physics. The nTOF will provide neutron rates some three orders of magnitude higher than existing facilities, allowing measurements to be made more precisely and more rapidly than in the past.

programmable timers shown in 5.9. The Settings RAM stores gate length and position for all the cycles present in the machine. Up to 32 cycles can be stored. The result RAM is organized in cycle-based order as well. This allows readout of the measurements and update of the settings once per super-cycle. Some measurement results are described in chapter5.

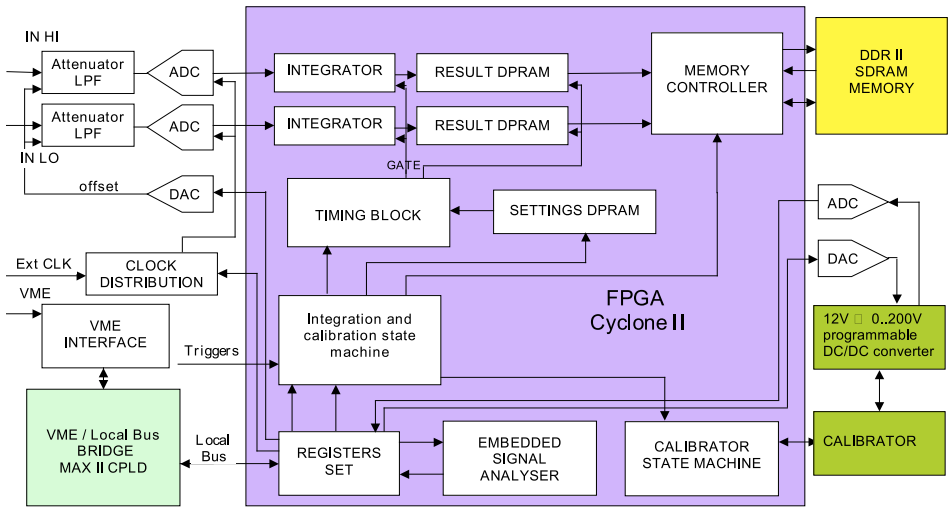

Figure 5.9: TRIC card block schematic for PS Booster intensity measurement

The measurement method assumes a precise position of the Trigger signal with respect to the BCT pulse signal (5.10). After the programmable delay t1 the integration of the BCT pulse starts. The gate is open for t2 ns. Since the BCT signal is usually distributed using an amplifier, an offset is introduced to the signal. Its value varies with time and temperature and is not negligible. To compensate the offset, an additional integration is executed t3 after the measurement. The same length of the gate is used. After the measurement, an optional calibration sequence is applied using embedded charge or current calibrator.

The TRIC is equipped with high speed data link and two of such cards can be connected together to the hardware watchdog which monitors level of the beam losses in the beam transfer line and stops the beam when it is exceeded. Such device called Isolde Watchdog is under development.

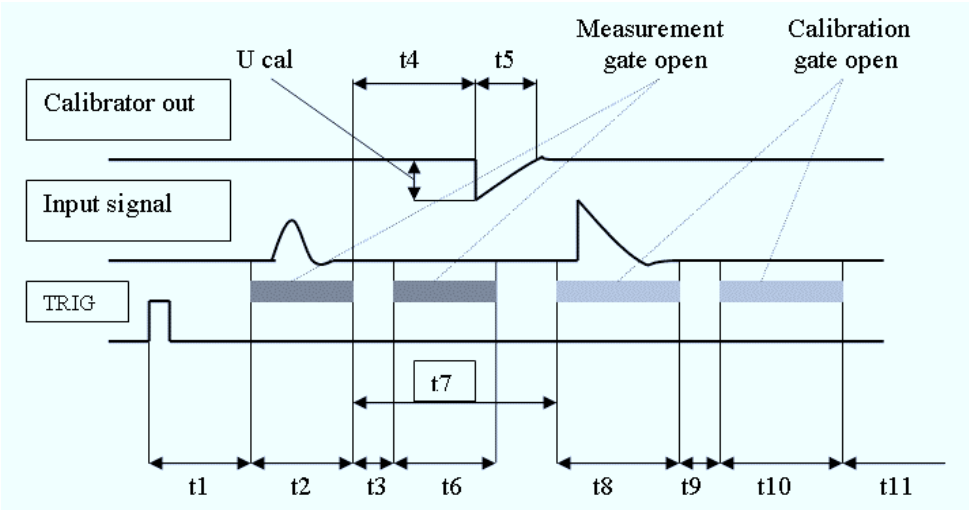

Figure 5.10: TRIC card timings for the PS Booster transfer lines intensity measurement

5.6 Measurements and tests

5.6.1 Laboratory tests

First tests of the TRIC module were performed in the lab. The DDS generator was used as the signal source. The train of triangle pulses simulated the beam signal. All the settings were done using dedicated console based program running on the VME crate controller under LynxOs operating system. Measurement data were captured and written into the text file. A JTAG debugger (Altera USB Blaster) was used to directly analyze signals inside the FPGA circuit(fig.5.11) using the SignalTap analyzer. The SignalTap, developed by Altera, uses FPGA resources to create freely customizable logic analyzer. This is very versatile tool which enables real-time preview of all the signals inside the FPGA chip. It is useful during all the stages of the project, because it mostly does not interfere with rest of the project because it operates in parallel.

The only drawback of this solution is interface - it must be connected to the PC using USB and thus has limited cable length. In order to enable continuous preview of important signals, an embedded analyzer (fig.4.17) was created together with dedicated FESA software (fig. 5.12). The analyzer was described in chapter 4.3.3 First picture present Local Oscillator, Gate, BLR signals locked to the input signal - the center of the input pulse is located at the rising edge of the LO signal.

Figure 5.12 presents the FESA application showing the PLL locked to the triangle

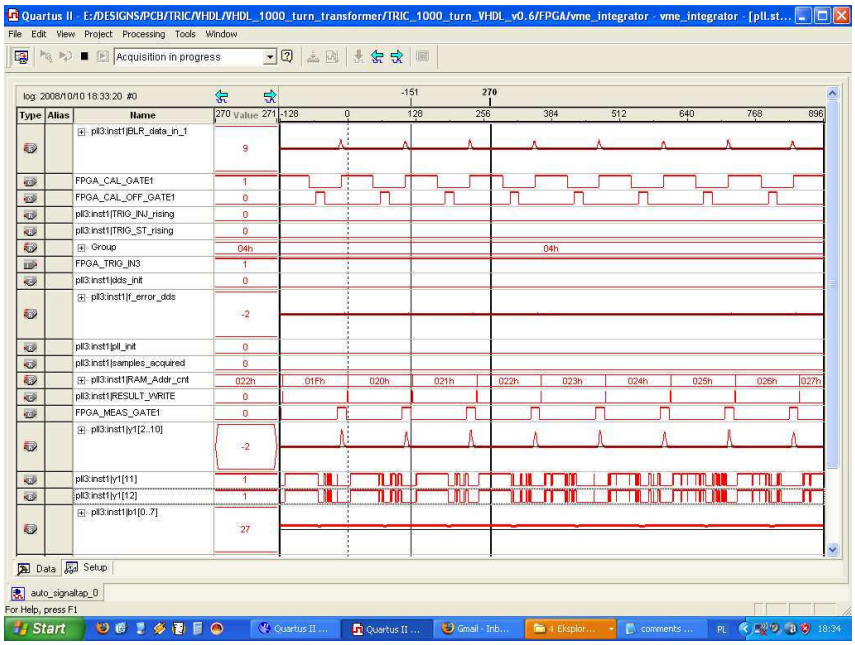

Figure 5.11: TRIC Signal Tap data

pulse generator which simulates the real PU signal. The simulated harmonic number is 2, with only one bucket filled. There are visible from top:

- LO signal,
- Gate,
- BLR,
- input signal.

In second window:

- LO,
- error,
- multiplier output,
- input signal.

The same FESA application (different tab) displays measurement results (fig. 5.13). The generator simulated two bunches, one with zero value. On the plot they are clearly visible as two traces.

Figure 5.12: FESA analyzer signals

5.6.2 Real beam signal tests

The TRIC module was installed in dedicated VME crate (fig.5.14) and connected to the PS beam current transformer and WCM through 20dB attenuator. The trigger signal was taken from original 6-turn measurement system, provided by the TG8 module. After the configuration using FESA expert setting tab (fig.5.15), the measurements were performed.

The FESA control GUI allows subscription to one of the user beams. All the user beams are registered, but only one selected is displayed. This allows simultaneous operation of many GUI applications.

Figure 5.16 presents result of bunch-by-bunch TOF beam intensity measurement. There is clearly visible, that some losses (about 3%) occur during first 250 turns. They are probably responsible for excessive losses which were detected by radiation monitors. This case requires further investigation but shows the possibilities of the measurement device. The scale is in 10^10 protons. Since TOF beam has harmonic number 1, 8192 turns could be acquired.

In case of the EASTB beam, harmonic number is 4, so only 2048 samples could be acquired (fig. 5.17). The figure presents 4 plots which correspond to 4 bunches in each

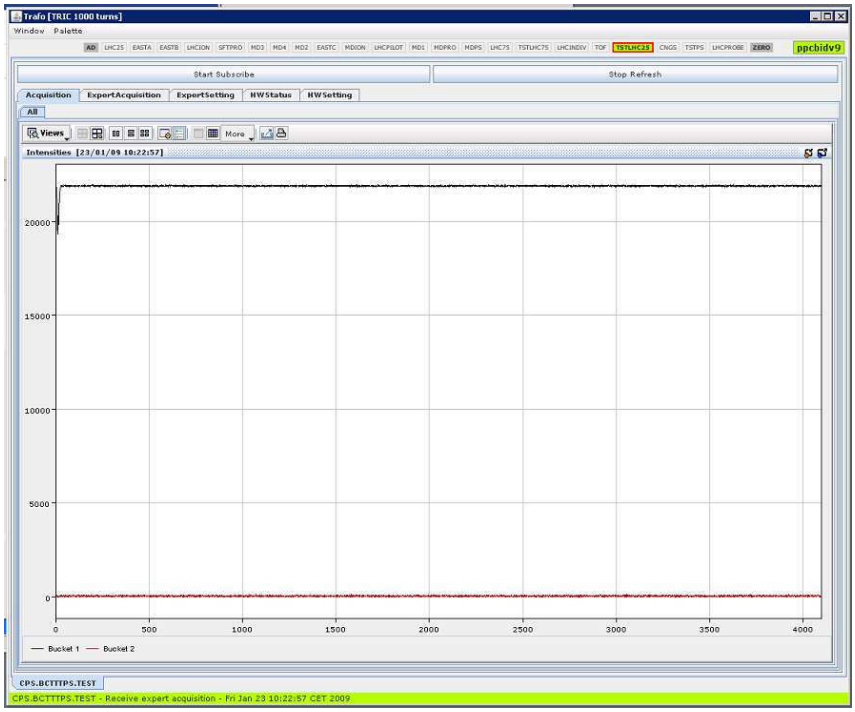

Figure 5.13: FESA application measurement results

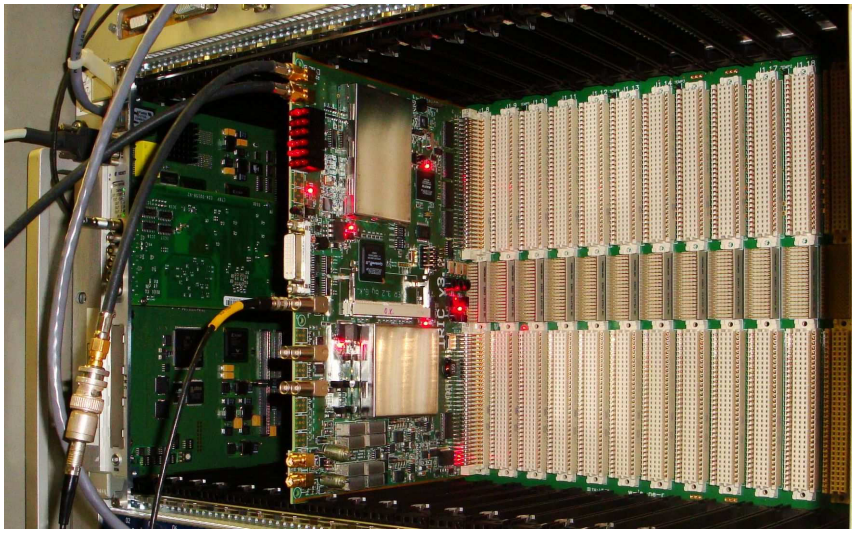

Figure 5.14: TRIC Card in the VME Crate

turn. Interesting thing is a bump observed at the lowest one. Theoretically the beam cannot increase its intensity. Identical phenomena was registered using DC transformer and TMS system - one of the bunches in turn has for unknown reason variable amplitude. The embedded analyzer was used to verify position of the gate and BLR pulse, but they were correct. There are assumptions, that some interference from RF system may case this effect since it is synchronous to the revolution frequency and observable using two

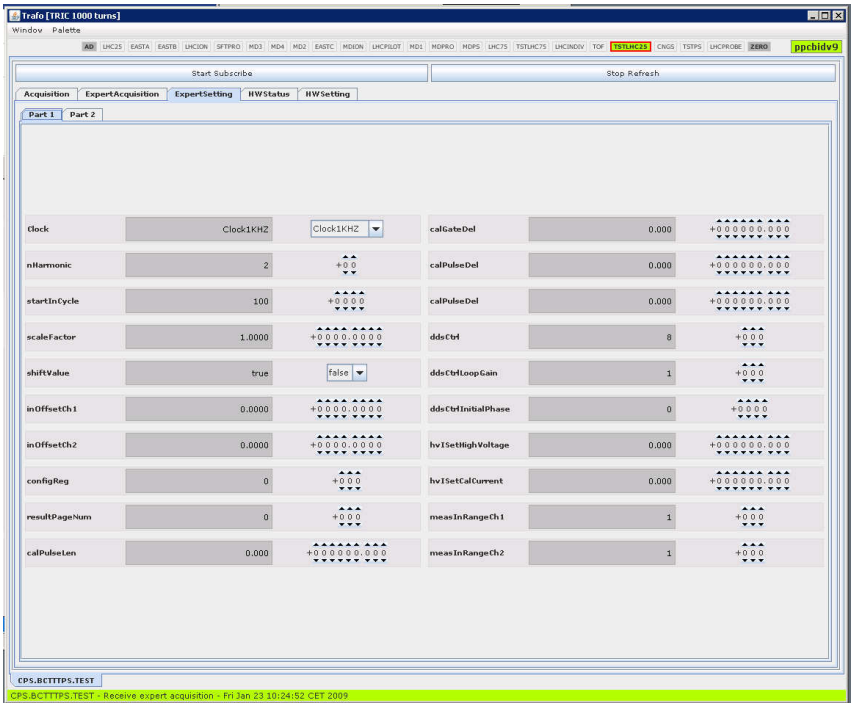

Figure 5.15: FESA advanced settings tab

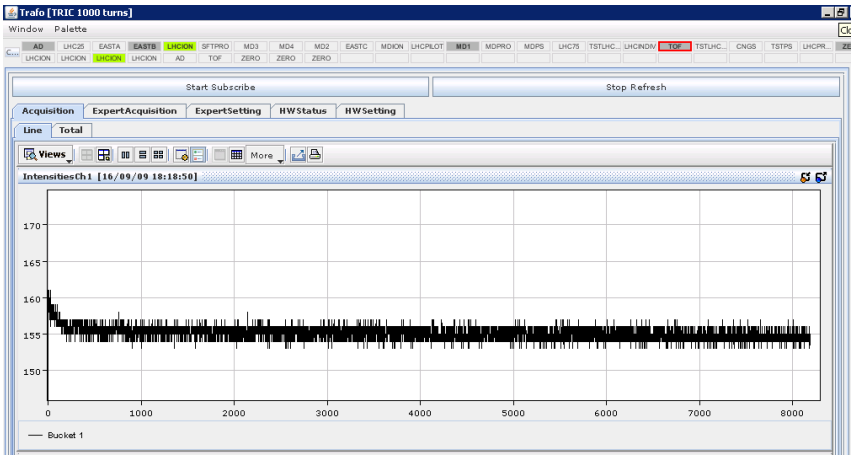

Figure 5.16: TOF beam results

independent measurement systems.

Construction of new intensity measurement system enabled further investigation and correction of accelerator problems. It supplements operation of the DC transformer which was not operational for first hundreds of turns after injection due to high settling time. Short comparison of new and old systems is presented in table 5.1.

The hardware, FPGA firmware and control software can be used to measure intensity of virtually any accelerator. The only signals required for operation are BCT and trigger.

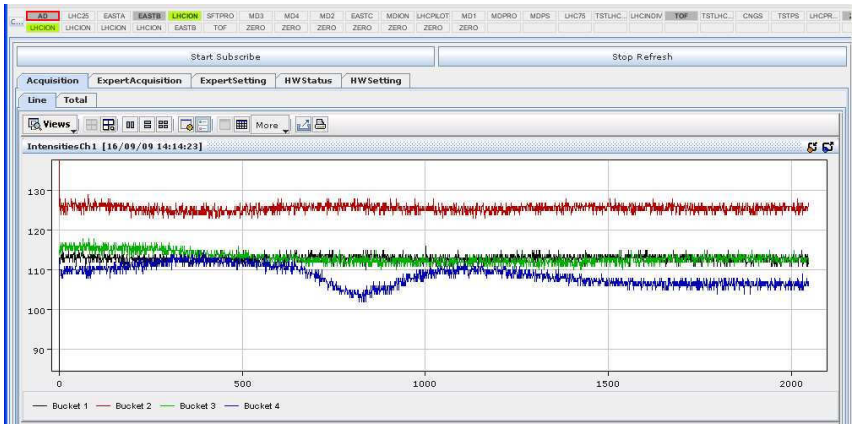

Figure 5.17: EASTB beam results

Parameter	Old system (6 turn)	New system (TRIC)
Accuracy	10%	2%
Number of tracked bunches	1	all
Number of tracked turns	6	1000
Baseline correction	no	yes
Occupied space	1 rack	1 VME card
Calibration	no	yes

Table 5.1: Intensity measurement system summary

There are no cards available from the market, that posses on one board both acquisition system, high voltage supply and the calibrator. Universal character of the hardware built enables its wide application in many accelerator related applications and is used in a few different measurement systems at CERN.

Chapter 6

Closing remarks

The CERN Proton Synchrotron has been fitted with a new trajectory measurement system. Analogue signals from forty beam position monitors are digitized and then further treated entirely in the digital domain to derive the positions of all individual particle bunches on the fly. Large FPGAs handle all digital processing. Data are stored in circular buffers of large enough size to keep a fewseconds-worth of position data. Multiple clients can then request selected portions of the data, possibly representing many thousands of consecutive turns, for display on operator consoles. The system uses digital phase-locked loops to derive its beamlocked timing reference. The possibility of the TMS to acquire over many, many turns is very useful for injection and ejection studies. The system will also deliver data to the Automatic Beam Steering (ABS), which calculates field corrections in order to optimize the beam injection trajectory. The new trajectory measurement system delivers both individual bunch trajectories and averaged orbits, over a large number of consecutive turns. It advantageously replaces the old CODD trajectory measurement system, which could only measure a single two-turn trajectory every 5ms, and which was blind during bunch splitting

The design is sufficiently flexible to follow all present and known future RF gymnastics in the PS. The same design has been shown to be usable for other p+ or ion synchrotron, the GSI SIS18.

The hardware and FPGA algorithms developed for intensity measurement can be applicable to virtually any accelerator. The system was shown to properly acquire intensity

of up to 8000 bunches after the injection. This number can be easily extended by installation of additional memory in a VME card slot. This is far more than 6 turns of the old system and enables precise diagnostic and measurement of the beam properties. During first test it was shown that there are unacceptable losses just after injection, that were not recorded by any other beam instrumentation. Only radiation monitors showed abnormal level in proximity of the transfer line.

The thesis presents subnational progress in development of beam methodology for hadron accelerators.

The work proves that there exists an efficient method with which it is possible to synchronize to the beam and follow the changes of its frequency in order to precisely estimate its intensity and position. The method bases on extension of the measurement circuits and digital analysis of the measurement results with the usage of advanced FPGA hardware and relevant algorithms.

Bibliography

[1] Technical report. [cited at p. 31, 32, 117]

[2] A high stability intensity monitoring system for the ISIS extracted proton beam. http://accelconf.web.cern.ch/accelconf/e96/PAPERS/TUPL/TUP079L.PDF. [cited at p. 27, 117]

[3] Alpha Data CERN support web page. http://portal.beam.ltd.uk/support/cern/doc/. [cited at p. 76]

[4] Alpha Data web page. http://www.alpha-data.com/acp-fx-n2.html. [cited at p. 59, 60, 118]

[5] CERN accelerators complex - LHC machine outreach. http://lhc-machine-outreach.web.cern.ch/lhc-machine-outreach/. [cited at p. 17, 117]

[6] Instrumentation Technologies web page. http://www.i-tech.si/index.php. [cited at p. 58, 118]

[7] Introduction to Particle Accelerators - Longitudinal motion. https://espace.cern.ch/be-dep/Lists/AXELongitudinal_motion.ppt. [cited at p. 25, 117]

[8] Maxim application note - design a low-jitter clock for high-speed data converters. http://www.maxim-ic.com.cn/appnotes.cfm?an_pk=800. [cited at p. 61]

[9] Official GSI webpage. http://. [cited at p. 76]

[10] Technical Specification for a new trajectory measurement system for the CERN PS. http://portal.beam.ltd.uk/support/cern/tenderInfo/IT3384Specification.pdf. [cited at p. 35, 68, 69, 73, 75, 118, 120]

[11] Wikipedia - accelerator. http://en.wikipedia.org/wiki/Particle_accelerator. [cited at p. 14, 23]

[12] Wikipedia - Beam emittance. http://en.wikipedia.org/wiki/Beam_emittance. [cited at p. 24]

[13] Wikipedia - Cyclotron. http://en.wikipedia.org/wiki/Cyclotron. [cited at p. 21]

[14] Wikipedia - GSI. http://en.wikipedia.org/wiki/Gesellschaft_f. [cited at p. 17]

[15] Wikipedia - Luminosity. http://en.wikipedia.org/wiki/Luminosity. [cited at p. 23]

[16] Wikipedia, the free encyclopedia - Constant Fracion Discriminator. http://en.wikipedia.org/wiki/Constant_fraction_discriminator. [cited at p. 52]

[17] Wikipedia, the free encyclopedia - Direct digital synthesis. http://en.wikipedia.org/wiki/Direct_digital_synthesis. [cited at p. 53]

[18] Wikipedia, the free encyclopedia - Numerically-controlled oscillator. http://en.wikipedia.org/wiki/Numerically-controlled_oscillator. [cited at p. 53]

[19] J.M. Belleman. A new trajectory measurement system for the cern proton synchrotron. *Proceedings of DIPAC 2005, Lyon, France*, 2005. [cited at p. 78, 118]

[20] CERN. Official CERN webpage - fundamental science . Website. http://public.web.cern.ch/public/en/About/Fundamental-en.html. [cited at p. 13, 22, 117]

[21] CERN. SPS the Super Proton Synchrotron. Website. http://public.web.cern.ch/Public/en/Research/SPS-en.html. [cited at p. 21]

[22] CERN. The TG8 Timing Module Hardware Description. Website. http://sl-timing.web.cern.ch/sl-timing/notes/sl-97-031.pdf. [cited at p. 49]

[23] OP. Odier S. Thoulet D. B. Belohrad, S. Longo. Mechanical design of the intensity measurement devices for the lhc. *Proceedings of DIPAC 2007*, 2007. [cited at p. 29]

[24] Grzegorz Kasprowicz David Belohrad. Beam intensity measurement system for proton synchrotron booster. *Proceedings of SPIE, the International Society for Optical Engineering*, 2006. [cited at p. 29, 40, 92, 117]

[25] M. Chanel M. Ludwig E. Metral G. Metral J.P Potier U. Raich R Scrivens R. Steerenberg E. Bravin, J. Belleman. Specification of the beam position measurement in the ps machine. *AB-Note-2004-001-ABP*, 2005. [cited at p. 89]

[26] M.Chanel M.Ludwig E.Metral G.Metral J-P.Potier U.Raich R.Scrivens R.Steerenberg E.Bravin, J.Belleman. Specification of the beam position measurement in the ps machine, ab-note-2004-001. Technical report, CERN, 2004. [cited at p. 47]

[27] A. Galatis et al. Beam position monitor system development for fair. *GSI Scientific Report*, 2005. [cited at p. 52]

[28] A. Galatis et al. Digital techniques in bpm measurements at gsi-sis. *Proceedings of EPAC'06*, 2006. [cited at p. 52]

[29] A. Galatis et al. Beam parameter estimation for beam position measurements at the sis18 accelerator. *Proceedings of SSP'07*, 2007. [cited at p. 52]

[30] A. Galatis et al. First tests with the sis18 digital bpm system. *Proceedings of DIPAC'07*, 2007. [cited at p. 77]

[31] A. Guerrero et al. Cern front-end software architecture for accelerator controls. *Proceedings of ICALEPC S2003*, 2003. [cited at p. 82]

[32] Peter Forck. Lecture notes on beam instrumentation and diagnostics. *Joint University Accelerator SchoolC*, 2009. [cited at p. 33, 34, 117]

[33] U.Raich G.Kasprowicz, J.M.Belleman. Digital beam trajectory and orbit system, for the cern proton synchrotron. *Proceedings of DIPAC 2007, Venice, Italy*, 2007. [cited at p. 53, 117]

[34] R. Jones J.J. Savioz H. Jakob, L. Jensen. A 40mhz bunch by bunch intensity measurement for the cern sps and lhc. *Proceedings of DIPAC*, 2003. [cited at p. 27, 117]

[35] C. Gruber J.M. Belleman, J.L. Gonzalez. Vme gate & blr generator, ps/bd/ note 98-07. Technical report, CERN, `http://jeroen.web.cern.ch/jeroen/reports/blr_gate.pdf`, 1998. [cited at p. 49]

[36] C. Gruber J.M. Belleman, J.L. Gonzalez. Vme rf-mux and synchroniser, ps/bd/ note 98-08. Technical report, CERN, `http://jeroen.web.cern.ch/jeroen/reports/rfmux.pdf`, 1998. [cited at p. 51]

[37] Richard G. Lyons. *Understanding Digital Signal Processing*. Prentice Hall PTR, 2004. [cited at p. 63]

[38] Uwe Meyer-Baese. *Digital Signal Processing with Field Programmable Gate Arraysg*. Springer, 2007. [cited at p. 64]

[39] Didcot United Kingdom Michael A. Clarke-Gayther, RAL. Drift TUbe Linac principle. `http://www.fnrf.science.cmu.ac.th/theory/linac/LinacBasicConcepts.html`. [cited at p. 20, 117]

[40] Switzerland P.Odier CERN, Geneva. A new wide band wall current monitor. *Proceedings of DIPAC, Mainz, Germany*, 2003. [cited at p. 29, 30, 31, 117]

[41] Peter Strehl. *Beam Instrumentation and Diagnostics*. Birkhuser, 2006. [cited at p. 28]

[42] Fang Zhigao Wang jihong Zhao Feng Tao Xiaoping Liu Guangjun Li Guangyeng Fang Lei Wang Guicheng, Leng Yongbin. Development of film-mode wall current monitor and its application in hls. *Proceedings of the 1999 Particle Accelerator Conference,New York*, 1999. [cited at p. 30, 117]

List of Symbols and Abbreviations

Abbreviation	Description	Definition
AD	Antiproton Decelerator	16
ARM	Advanced RISC Machine	58
BCT	Beam Current Transformer	39
BLR	BaseLine Removal	55
BPM	Beam Position Monitor	76
CAL	Calibration	69
CERN	European Organization for Nuclear Research	13
CFD	Constant Fraction Discriminator	52
CPLD	Complex Programmable Logic Device	92
CRT	Cathode Ray Tube	19
DDR	Double Data Rate	58
DDS	Direct Digital Synthesis	53
DESY	Deutsches Elektronen-Synchrotron	13
DTL	Drift Tube Linac	19
ELFT	(End of Last Flat Top)	69
EOC	is End Of Cycle	69
FEL	Free Electron Laser	15
FESA	The Front-End Software Architecture	81
FPGA	Field Programmable Gate Array	93
LAN	Local Area Network	74

Abbreviation	Description	Definition
LEP	Large Electron Positron Collider	21
LHC	Large Hadron Collider	43
LO	Local Oscillator	94
MOSFET	Metal Oxide Field Effect Transistor	98
MUX	Multiplexer	48
MRP	Mean (arithmetic) Radial Position of the beam all around the machine	48
NCO	Numerically Controlled Oscillator	53
nTOF	Neutron time-of-flight measurements	101
PET	Positron emission tomography	14
PLL	Phase Locked Loop	91
PS	Proton Synchrotron	49
RF	Radio Frequency	76
RMS	Root Mean Square	78
SBC	Single Board Computer	58
SDRAM	Synchronous Dynamic Random Access Memory	58
SLAC	SLAC National Accelerator Laboratory	19
SNR	Signal to Noise Ratio	60
SPS	The Super Proton Synchrotron	21
TG8	Timing receiver and pulse generator module	49
TMS	Trajectory Measurement System	57
TRIC	Transformer Integrator Card	102
VCO	Voltage Controller Oscillator	52
VHDL	Very High Speed Integrated Circuits Hardware Description Language	93
WCM	Wall Current Monitor	101

List of Figures

List of Tables

Index